BIO-FUNCTIONALIZATION OF ELECTROSPUN NANOFIBRE SCAFFOLDS FOR CELL CULTURE APPLICATIONS

CHUA KIAN NGIAP

B. Eng. (Hons.), NUS

A THESIS SUBMITTED

FOR THE DEGREE OF DOCTOR OF PHILOSOPHY

GRADUATE PROGRAMME IN BIOENGINEERING

NATIONAL UNIVERSITY OF SINGAPORE

2006

ACKNOWLEDGMENTS

First of all, I would like to thank my project supervisors Professor Seeram Ramakrishna, Professor Kam W. Leong and Assistant Professor Hai-Quan Mao for their constant support and guidance, and for all the opportunities that they have given me in my education and research. I have learnt to become a better researcher and also a better person. A simple “thank you” will not be enough to express my gratitude.

I would like to thank all my colleagues at the Tissue and Therapeutic Engineering Laboratory, Division of Johns Hopkins in Singapore for all the assistance that they provide for the completion of this thesis. My special thanks to Dr. Chou Chai, Dr. Hong-Fang Lu, Dr. Xue-Song Jiang and Dr. Chao Yin for imparting me with their skills and knowledge. My sincere appreciation is also given to Mr. Peng-Chou Lee, Ms. Yen-Ni Tang, Mr. Wei-Seng Lim, Ms. Chai-Hoon Quek, Dr. Peng-Chi Zhang, Mr. Justin Gorham, Ms. Ai-Cheng Tan and Mr. Teck-Jin Tan for all the precious technical support that they have provided through these years.

I would also like to thank all my colleagues in the Nanobioengineering Laboratory, NUSNNI and Graduate Programme in Bioengineering. I express my deepest gratitude to Dr. Kazutoshi Fujihara, Dr. Joon-Kin Yong, Ms. Satinderpal Kaur, Ms. Yan-Ping Wang, Mr. Daniel Wong, Mr. Ramakrishnan Ramaseshan, Mr. Chun-Wai Ng, Ms. Puay-Joo Low, Ms. Siew-Teng Yeo and Ms. Soo-Hoon Pang for all the assistance that they have given me in many different ways.

Finally, I am greatly indebted to my family for their constant support and encouragement throughout these long thesis years.

TABLE OF CONTENTS

SUMMARY

This thesis presents the studies of bio-functionalization of electrospun nanofibers, which can serve as cell culture scaffolds that can promote cell-substrate interactions and are bioactive in soliciting favorable cellular responses like cell adhesion, cell morphological reorganization, cell differentiated functions or cell proliferation.

The general strategy of scaffold development involves nanofiber scaffold fabrication via the electrospinning technique, followed by nanofiber bio-functionalization. The bio-functionalization process involves the initial functionalization of the nanofiber surface with carboxylic acid groups using UV-initiated poly(acrylic acid) grafting method. This is followed by conjugation of bioactive molecules onto the functionalized nanofiber surfaces. We then tested the efficacy of this nanofiber bio-functionalization strategy on hepatocyte scaffold cultures and hematopoietic stem cell expansion culture systems.

Through galactose bio-functionalization, we have developed galactosylated nanofiber scaffolds that can support the hepatic functions (albumin secretion, ammonia removal and cytochrome P450 activity) of cultured primary hepatocytes. Interestingly, the nanofiber topography and the surface-immobilized galactose ligand synergistically enhance the hepatocyte-nanofiber interaction, and the galactosylated nanofiber scaffolds exhibit the unique property of promoting hepatocyte aggregates and cell infiltration within the mesh and around the fibers, forming an integrated spheroid-nanofiber construct. Subsequently, we have also demonstrated that hepatocyte cytochrome P450 activity enhancement can be brought about through further 3-Mc bio-functionalization of this galactosylated nanofiber scaffold.

Through amine molecule bio-functionalization, we have developed aminated nanofiber scaffolds that can support *ex vivo* hematopoietic stem / progenitor cell (HSPC) expansion. We have shown that aminated nanofiber meshes supported a high degree of cell adhesion, percentage of $CD34^{+}CD45^{+}$ cells and expansion of CFU-GEMM forming progenitor cells. SEM imaging also revealed discrete colonies of cells proliferating and interacting with the aminated nanofibers. In addition, we have shown that nanofiber scaffolds immobilized with amine functional groups of different carbon spacer chain lengths could further modulate HSPC proliferation and phenotype maintenance, resulting in different HSPC proliferation kinetics, cell population phenotypic expression, mouse engraftment potential and also colony-forming ability. The adherent hematopoietic cell populations on the aminated nanofiber scaffolds also showed enrichment of $CD34^{+}CD45^{+}$ cells compared with the non-adherent cell population, and indicated significant commitment towards the myeloblast / monoblast lineage, while the non-adherent population showed skewed commitment towards the erythroid lineage. These observations suggested the importance of nanofiber topography and amino functional group mediated cell-scaffold interactions in regulating HSPC proliferation and self-renewal. In addition, they also highlight the importance of cell-scaffold interactions as a new approach in modulating HSPC multipotency maintenance and lineage commitment.

In conclusion, this thesis has:

(1) Presented a nanofiber bio-functionalized strategy to develop polymeric nanofiber constructs that can serve as cell culture scaffolds.

(2) Demonstrated through primary hepatocyte cultures and HSPC expansion cultures that these scaffolds can promote cell-substrate interactions and are

bioactive in regulating cellular responses like cell adhesion, cell morphological reorganization, cell differentiated functions, cell proliferation or cell phenotype maintenance.

(3) Demonstrated the synergistic effects that both nanofiber topography and surface immobilized biochemical cues play in enhancing these cell-scaffold interactions and regulation of cellular functions.

LIST OF PUBLICATIONS

1. **Chua KN**, Lim WS, Zhang PC, Lu HF, Wen J, Ramakrishna S, Leong KW, Mao HQ. Stable Immobilization of Rat Hepatocyte Spheroids on Galactosylated Nanofiber Scaffold. Biomaterials 2005; 26(15):2537-2547.

2. Lu HF, **Chua KN**, Zhang PC, Lim WS, Ramakrishna S, Leong KW, Mao HQ. Three-Dimensional Co-Culture of Rat Hepatocyte Spheroids and NIH/3T3 Fibroblasts Enhances Hepatocyte Functional Maintenance. Acta Biomaterialia 2005; 1(4):399-410.

3. Luong-Van E, Grondahl L, **Chua KN**, Leong KW, Nurcombe V, Cool SM. Controlled Release of Heparin from Poly(epsilon-caprolactone) Electrospun Fibers. Biomaterials 2006; 27(9):2042-2050.

4. **Chua KN**, Chai C, Lee PC, Tang YN, Ramakrishna S, Leong KW, Mao HQ. Surface-Aminated Electrospun Nanofibers Enhance Adhesion and Expansion of Human Umbilical Cord Blood Hematopoietic Stem/Progenitor Cells. Biomaterials 2006; 27(36):6043-6051.

5. **Chua KN**, Chai C, Lee PC, Ramakrishna S, Leong KW, Mao HQ. Functional Nanofiber Scaffolds with Different Spacers Modulate Adhesion and Expansion of Cryopreserved Umbilical Cord Blood Hematopoietic Stem/Progenitor Cells. Experimental Hematology (In Press).

LIST OF FIGURES

LIST OF TABLES

CHAPTER ONE

General Overview

1.1 Background

Biomaterials play central roles in modern strategies in cell culture as designable biophysical and biochemical milieus that direct cellular behavior and function [1,2]. In most approaches, the Biomaterial is engineered into a scaffold which provides a niche for cells to proliferate and differentiate.

The intended uses for scaffold-based cell cultures are vast: In some applications, the cells develop into tissues that are suitable for implantation, or applied as part of a cell-based artificial organ [2-6] (e.g. bioartificial pancreas, bioartificial liver). In other applications, the cells are harvested after being expanded on proliferation-inductive scaffolds, for use in cell-based therapies [2-6] (e.g. stem cell therapy). In all cases, a scaffold that can interact and influence the cellular behavior is the crucial component.

The success of scaffold-based cell cultures largely depends on the optimal events of attachment, proliferation, differentiation, and phenotypic maintenance, which in turn are governed by a host of signals provided by the cell-scaffold microenvironment. These signals include: (1) homotypic / heterotypic cell-cell interaction; (2) soluble signaling molecules; and (3) cell-substrate interaction signals which consists of substrate-bound signaling molecules, scaffold topographical cues and scaffold biomechanical properties (Fig. 1.1). Therefore, an ideal scaffold culture system should include all these interactive components [1,2,7,8].

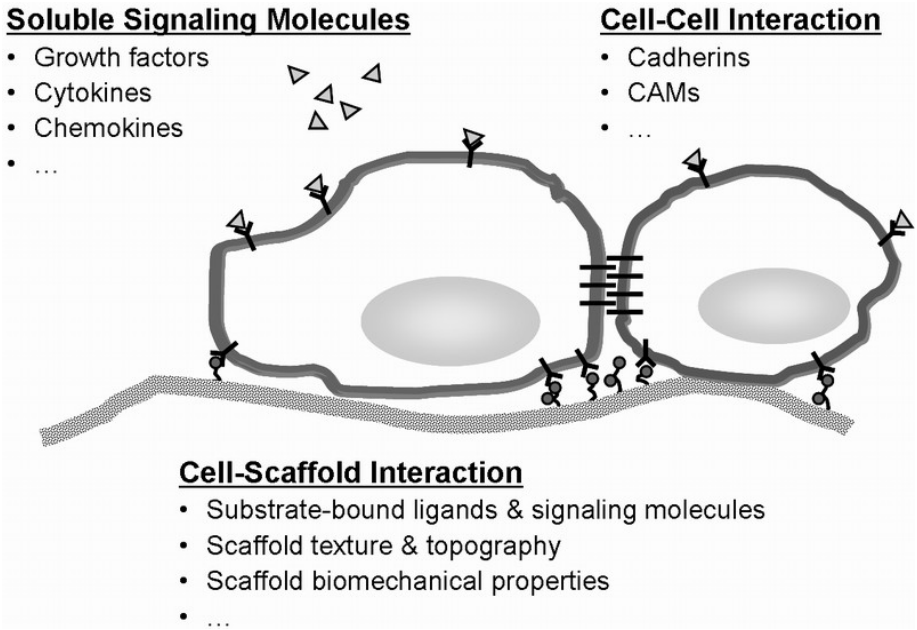

Figure 1.1: The cellular microenvironment. The behavior of individual cells and the dynamic state of multicellular tissues is regulated by intricate reciprocal molecular interactions between cells and their surroundings.

In recent years, scaffolds based on electrospun nanofibers have been investigated intensively [9-27]. This is largely due to the unique nano-topographical cues that the nanofiber scaffold provides as compared to 2-dimensional substrates, micro-porous and micro-fiber scaffolds and hydrogels traditionally used in cell cultures. Indeed, morphological and cytoskeletal reorganization of cells induced by the nanofiber topographical cues has been clearly demonstrated in many literatures [14-27].

Though several nanofiber scaffolds of unique topographical textures (aligned fiber scaffold, multilayered fiber scaffold, etc.) have been designed through manipulation of the electrospinning process [9-13,28-29], the nanofiber scaffolds used in current literature are mainly pristine and lack of substrate-bound signaling molecules [14-27]. In contrast, abundant research on the traditional film, micro-fiber or gel scaffolds have shown that scaffold functionalization (surface immobilization or entrapment) with bioactive molecules (e.g. proteins, peptides, drugs, simple chemical groups, etc.) are necessary in soliciting favorable cellular responses like cell adhesion

and proliferation responses [30-36]; and electrospun nanofiber scaffolds should not be the exception. Therefore, the design of a nanofiber scaffold modified with at least one bioactive molecule would be important in enhancing cell-substrate interaction, with the eventual goal of mimicking the cell's native microenvironment.

Due to the similarities in the materials used, the common modification methods for bio-functionalizing the traditional scaffolds can also be directly imported to modify the nanofibers. In this thesis, we present a comprehensive approach to systematically incorporate various types of biochemical cues into nanofiber scaffolds that are critical for hepatocyte functional maintenance as well as for hematopoietic stem cell proliferation and primitive maintenance.

1.2 Thesis Objectives

The overall objective of this thesis is to develop polymeric nanofiber constructs that can serve as cell culture scaffolds, which can promote cell-substrate interactions and are bioactive in soliciting favorable cellular responses. We believe that although the topographical cues on a pristine nanofiber scaffolds are able to induce morphological and cytoskeletal reorganization in cells [14-27], they are insufficient in providing optimal regulation of cell behavior.

We therefore hypothesize that the development of nanofiber scaffolds that present bioactive molecules is important in mimicking the native cellular microenvironment, as these bioactive scaffolds can actively engage with cells and consequently regulate their cellular activities.

We also hypothesize that a combination of nanofiber topographical cues and surface biochemical cues will synergistically enhance the cell-substrate interactions

and consequently induce further favorable cellular responses like cell adhesion, cell morphological reorganization, cell differentiated functions and/or cell proliferation.

Through the systematic testing of unmodified and bioactive molecule-conjugated films and nanofiber scaffolds in different primary cell culture models, we will be able to demonstrate these synergistic cell-substrate interactions. In addition, we hope to demonstrate the versatility of our nanofiber bio-functionalization strategy for cell culture applications through applying it in different cell culture models.

1.3 Thesis Scope

The general strategy of scaffold development involves nanofiber scaffold fabrication via the electrospinning technique, followed by nanofiber bio-functionalization. The bio-functionalization process involves the initial functionalization of the nanofiber surface with carboxylic acid groups using UV-initiated poly(acrylic acid) grafting method. This is followed by conjugation of bioactive molecules onto the functionalized nanofiber surfaces.

In this thesis, we will test the efficacy of this nanofiber bio-functionalization strategy on two cell culture systems: (1) hepatocyte scaffold cultures and, (2) hematopoietic stem cell expansion cultures. The effect of immobilized bioactive molecules in promoting cell-substrate interactions will be investigated. In addition, we will also be focusing on the effect of nanofiber topography in synergistically enhancing these cell-substrate interactions, as outlined in the thesis objectives.

We first describe the galactose bio-functionalization of electrospun poly(caprolactone-*co*-ethyl ethylene phosphate) nanofibers for liver cell culture. Prior to this study, nanofiber bio-functionalization strategies have never been demonstrated in literature before. Using the bio-functionalization strategy described above, we have

developed a nanofiber scaffold culture that can sustain primary hepatocyte viability as well as maintain the differentiated functions of the hepatocytes. The importance of scaffold topographical cues and immobilized galactose biochemical cues on hepatocyte morphological reorganization and function maintenance are investigated. In addition, efforts to further enhance the hepatocyte functions through additional nanofiber scaffold modification (3-methylcholanthrene incorporation) are presented.

Subsequently, we describe the amine bio-functionalization of electrospun polyethersulfone nanofibers for *ex vivo* hematopoietic stem / progenitor cells (HSPCs) expansion. HSPC expansion is commonly performed in a suspension culture format where the importance of cell-substrate interactions has been undermined. Throughout the course of this thesis research, we have discovered the significant roles that surface immobilized amine molecules play in providing cell-substrate interactions to the HSPCs. Using the same bio-functionalization strategy as described above, we have developed an aminated nanofiber scaffold culture that can promote HSPC growth while preserving the primitive HSPC multipotency. The importance of scaffold topographical cues, immobilized amine biochemical cues and amine spacer lengths on regulating cellular responses like HSPC adhesion, proliferation and primitive maintenance are also systematically investigated and presented.

CHAPTER TWO

Literature Review

2.1 Electrospun Nanofibers

Over the past decade, several techniques have been developed to fabricate polymeric nanofibers. These techniques include electrospinning, drawing, phase separation, self-assembly, and template synthesis [9-13,28-29]. Among them, electrospinning, a technique that can produce continuous fibers with diameters ranging from tens of nanometers to a few microns, is by far the most popular technique because of its relative simplicity and scalability for industrial level manufacturing and applications [9-13,28-29].

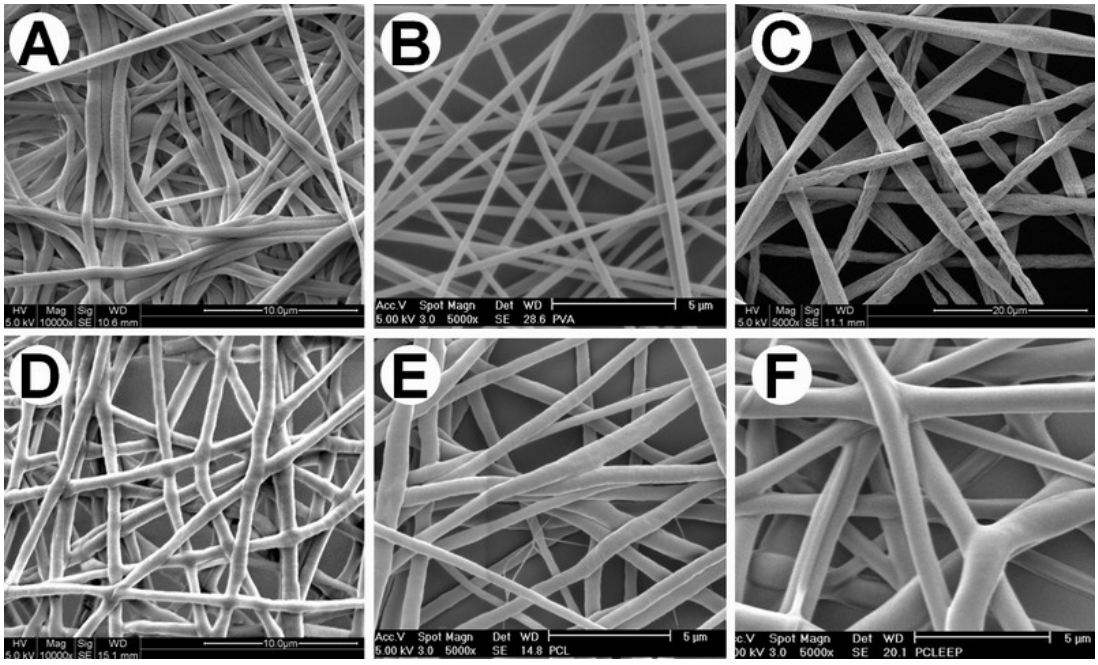

Figure 2.1: SEM images of fibers prepared by electrospinning of non-degradable (A-C) and degradable polymers (D-F): (A) polyethersulfone (PES); (B) polyvinyl alcohol; (C) poly(bisphenol A carbonate); (D) polyhydroxybutyrate; (E) polycaprolactone; and (F) poly(caprolactone-*co*-ethyl ethylene phosphate) (PCLEEP).

Electrospinning can be applied to spinning of a wide range of polymers (some examples shown in Fig. 2.1), and the list of synthetic and natural polymers (both biodegradable and non-degradable) that can be electrospun into nanofibers has been expanding rapidly [10-13]. Due to its simplicity and versatility in nanofiber fabrication, the electrospinning technique has generated great interest in many potential applications like nano-sensors, military protective clothing, media filtration and life science applications [9-11].

2.1.1 Principles and Mechanisms

A typical laboratory electrospinning setup is schematically shown in Fig. 2.2. The major components include: (1) a polymer solution feed unit (e.g. syringe pump); (2) a spinneret unit (e.g. syringe needle); (3) a high voltage power generator; and (4) a grounded collector.

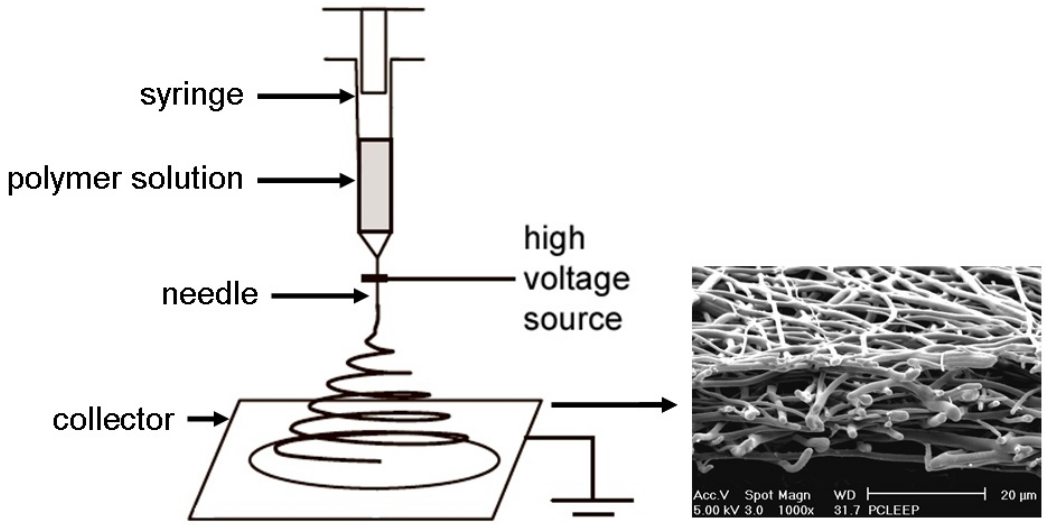

Figure 2.2: Schematic illustration of an electrospinning setup. The inserts show a drawing of the electrified Taylor cone and a typical SEM image of nanofibers deposited onto the collector.

The process of electrospinning is driven by electrical forces on free charges on the surface or inside a polymeric liquid. In a typical electrospinning process, when a large electric potential is applied between the collector and the spinneret, an electrical

field is simultaneously induced. The polymer solution ball-shape drop pendent on the nozzle exit is then deformed, as a consequence of the force interactions between the coulombic force (exerted by the external electric field) and the surface tension of the polymer solution, into a conical shaped Taylor Cone [28,29,37-39]. At sufficiently high electric potentials (typically 6 – 30 kV, depending on the surface tension of polymeric solutions), the electric field strength reaches a threshold value, and the electrostatic force overcomes the surface tension, resulting in an ejection of a polymer liquid jet. This jet is then subjected to an extremely high ratio of stretching through whipping[1] [28,29,37-39] and rapid evaporation of solvent, leading to the formation of sub-micron sized nanofibers, which were then attracted and gathered into a mesh at the collector.

2.1.2 Parameters that Control the Electrospinning Process

Although electrospinning is said to be a relatively simple fiber fabrication technique, there are surprisingly many parameters that govern this process, and it is through control variations of these parameters that result in generation of many interesting nanofiber morphologies and structures as briefly discussed in the following subsections.

---

[1] The formation of nanofibers by electrospinning was previously attributed to the splitting or splaying of the electrified jet as a result of repulsion between surface charges. It appears that the cone shaped, instability region is composed of multiple jets [29].

However, recent experimental observations demonstrated that the thinning of a jet during electrospinning is mainly caused by the bending instability associated with the electrified jet. It appears that the conical envelop contains only a single, rapidly bending or whipping thread. The frequency of whipping is so high that conventional photography cannot properly resolve it, giving the impression that the original liquid jet splits into multiple branches as it moves towards the collector [29].

In some cases, splaying of the electrified jet might also be observed, though it was never a dominant process during electrospinning.

Electrospinning parameters in general can be classified under 2 categories:

(1) Parameters which control the resultant fiber morphology (e.g. shape, size, uniformity, defects, etc.); and

(2) Parameters which control the resultant fiber mesh morphology (e.g. random, aligned, composite structures, etc.).

Among them, the four parameters presented in the following subsections are found to be the more dominant control factors, as reported frequently in literature.

2.1.2.1 Effect of Polymer Concentration in Electrospinning Solution

The polymer solution concentration is an important parameter that affects the diameter, shape and the uniformity of the resultant fiber. The solution concentration decides the limiting boundaries for the formation of electrospun nanofibers due to variations in the viscosity and surface tension [12,40].

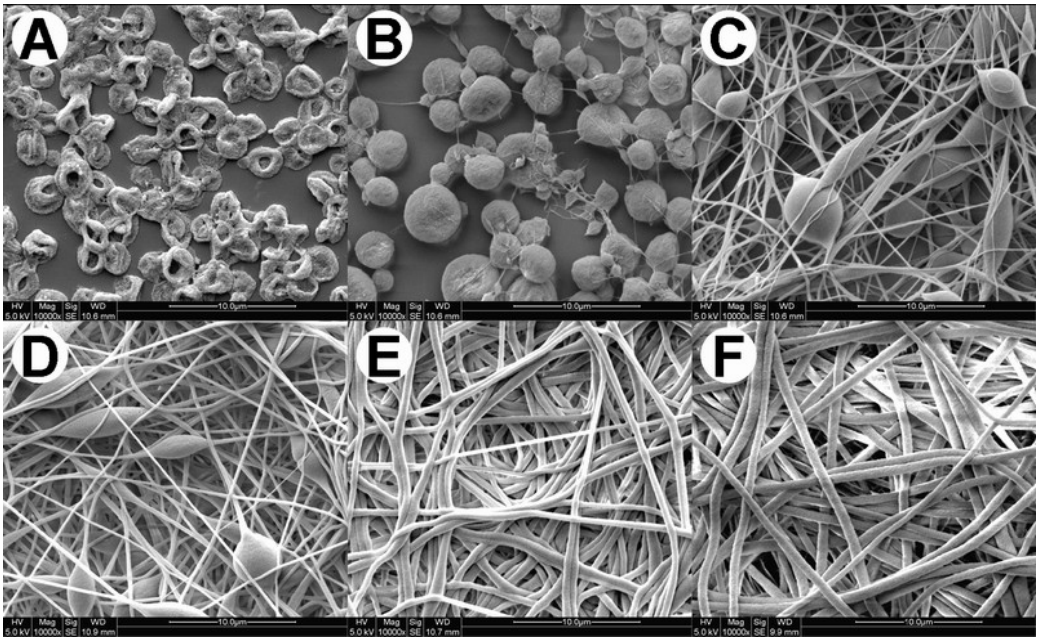

Figure 2.3: SEM images of electrospun PES with increasing concentrations in dimethylsulfoxide solvent (w/w). (A) 5%; (B) 10%; (C) 15%; (D) 18%; (E) 20%; and (F) 25%. The polymer solutions are fed at a rate of 0.3 mL/h, electrospun at 13 kV, and fibers or beads are collected onto a grounded surface 160 mm away from the spinneret.

In general, low concentration solution forms droplets due to the influence of surface tension, while higher concentration prohibits fiber formation due to higher viscosity [40]: When the solution concentration increases, the resultant polymer morphology shifts from polymer droplets, to beaded nanofibers, to uniform nanofibers of increasing diameters; until the solution becomes too viscous for fiber formation, as shown in Fig. 2.3.

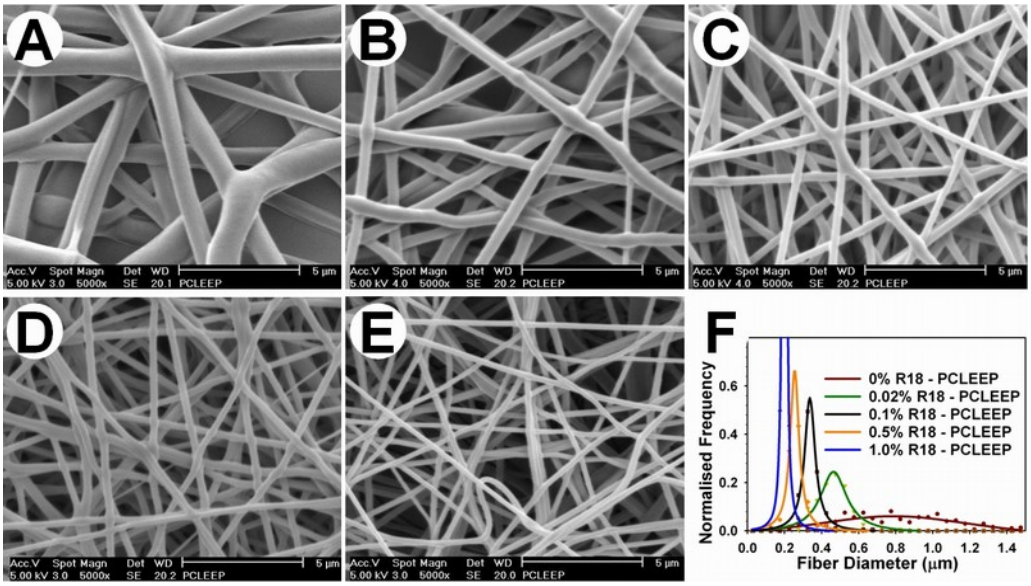

Figure 2.4: SEM images of PCLEEP fibers co-electrospun with increasing concentrations of R18 in PCLEEP (w/w). (A) 0%; (B) 0.02%; (C) 0.1%; (D) 0.5%; (E) 1.0%; and (F) PCLEEP, R18 loading – PCLEEP fiber diameter relationship. PCLEEP and R18 are dissolved in 8:2 dichloromethane / methanol solvent mixture The polymer solutions are fed at a rate of 0.3 mL/h, electrospun at 12 kV, and the fibers or beads are collected onto a grounded surface 60 mm away from the spinneret.

2.1.2.2 Effect of Ionic Additives in Electrospinning Solution

Fiber diameter can also be controlled via the doping of ionic additives into the polymer solution. Charged ions in the polymer solution are highly influential in jet formation. The ions increase the charge carrying capacity (electro-conductivity) of the jet, thereby subjecting it to higher tension with the applied electric field [12,41]. Also,

the polymer solution jet radius has been demonstrated to vary inversely to the cube root of the electrical conductivity of the solution [12]. The resultant effect is reduction in bead formation or significant reduction in fiber diameters. To date, several reports have successfully employed ionic additives like sodium chloride [41,42], heparin [43], octadecyl rhodamine B chloride (R18, Fig 2.4), pyridine [44], ammonium acetate, etc., to control nanofiber diameter and morphology.

2.1.2.3 Collector Design

Electrospun nanofibers are usually deposited on the surface of the collector (often a flat piece of conductive substrate) as randomly oriented nonwoven mesh, because of the bending instability associated with the spinning jet (Fig. 2.2). However, in recent years, new collector designs have been developed that were able to collect electrospun nanofibers as uniaxially aligned arrays. The collector designs work mainly by modifying the polymer jet movement via controlling the distribution of electric field between the spinneret and the collector [45-49], aligning the fibers towards the sharp edges or corners of the collectors. Some of these designs include the use of a pair of split electrodes [45-47] or a rotating drum, frame or wheel [48,49] as the collector and they have all successfully demonstrated aligned nanofiber mesh collection.

2.1.2.4 Spinneret Design

The most recent addition to electrospinning process control that can significantly influence both the fiber and fiber mesh morphology is spinneret design. In particular, the fabrication of core-sheath nanofibers is a hallmark of the spinneret design parameter [50-52]. Core-sheath nanofibers are fabricated by co-electrospinning two different polymer solutions through a spinneret comprising of two coaxial capillaries. As the electrospinning process took place very quickly, there would not be enough

time for the polymer chains from the two different polymer solutions to be mixed before solidification. The resultant nanofiber core will have a material composition that is different from its outer shell. Though the coaxial electrospinning technique is still at its early development stages, recent papers have demonstrated that the nanofiber core can be used as a storage reservoir for proteins and drugs and that this fiber system has potential in drug / protein delivery applications [50-52].

Another unrelated spinneret design is electrospinning using multiple spinnerets [53,54]. In this design, different polymer solutions are fed into two or more separate spinnerets. Electrospinning using these spinnerets are then performed either sequentially or simultaneously over the same collector, and thus multilayering electrospinning or mixing electrospinning can be performed respectively. This design has demonstrated the fabrication of multilayered nanofiber mesh as well as nanofiber mesh with different polymer fibers that are intertwined or woven together.

2.1.2.5 Other Parameters

Other processing parameters include spinneret–collector gap distance, temperature, humidity, air-flow, applied electric field strength, solution feed rate, solvent characteristics and composition[2], etc. These parameters generally function as "fine-tuning" factors, affecting the fiber uniformity and reproducibility of the electrospinning process. Although their roles have been discussed in literature [9-13,28-29], their influence in determining the fiber and fiber mesh morphology is not as drastic as the four parameters previously discussed. However, we stress that future

[2] The intrinsic conductivity of the solvent will also contribute to the charge carrying capacity of the polymer solution and will therefore determine the resultant fiber diameter range during electrospinning. However, since the range of solvents with different conductivities is very limited for any given polymer, the control of fiber diameters via different solvents compositions generally does not yield significant differences.

industrial electrospinning applications may still need to precisely control these parameters in order to achieve high quality standards and reliability.

2.1.3 Electrospun Nanofibers in Cell Culture Applications

As discussed earlier, the relative versatility and simplicity of electrospinning in fabricating nanofibers of various morphologies and structures has led to keen interest in various research fields [9-13,28-29]. In particular, the potential applications of nanofibers as viable cell culture scaffolds have been intensely investigated in recent years.

The key interest has been mainly the unique fibrous, surface nano-topographical features that a typical nanofiber mesh presents, compared with the smooth, featureless surfaces of tissue-culture plastics commonly used as cell-substrates for *ex vivo* cell processing [3], and several researchers have even compared the topographical morphology of nanofiber mesh to resemble those of extracellular matrix (ECM)[4] in the native cell microenvironment. Indeed, abundant literature exists indicating that a variety of cell types, including fibroblasts, endothelial cells, muscle cells and stem cells responded differently to the nano-featured surface topography as compared to their smooth film counterparts, with or without the influence of additional physical or biochemical cues [55-59].

It has long been recognized that the *in vivo* extracellular matrix, which provides a rich context to the residing cells, includes topographical cue at the nanoscale [60-62].

---

[3] Examples of tissue-culture plastics include polystyrene for culture flasks and plates, and polytetrafluoroethylene for culture bags. These cultures surfaces are usually gas plasma treated, to provide an optimal growth surface for the matrix-dependent tissue cultures.

[4] Tissues are assemblies of one or more types of cells and their associated intercellular materials called the extracellular matrix. For vertebrate animals, the ECM is made of a complex mixture of proteins and carbohydrates, which are produced and maintained by the cells embedded in the network.

A typical example is the basal lamina (basement membrane) that can be found in many tissues. Inspired by the hypothesis that such a nanoscale feature may exert unique interaction with cells, several groups have been investigating the role of nanostructures on cell adhesion, proliferation, differentiation and migration [14-27,55-59]. For example, the Curtis et al. has shown that nano-featured substrates mediate different responses in epithelial fibroblasts, endothelial cells, smooth muscle cells, and peripheral blood mononuclear cells compared to smooth film surfaces [57-59]. The nano-featured substrates induce faster cytoskeleton organization, cell adhesion and spreading in cells, accompanied by clearer and smaller focal adhesion plaques, and a larger number of filopodia interactions with growth substrate.

Several groups investigating on cellular responses to nanofiber substrates have also shown that these nanofiber substrates generally lead to differences in morphological organization, gene expression, proliferation and differentiation responses in fibroblasts, smooth muscle cells, endothelial cells, chondrocytes, cardiomyocytes, bone marrow stromal cells, keratinocytes, mesenchymal stem cell, etc. [14-27]. For example, Li et al. demonstrated that seeding mesenchymal stem cells on nanofiber scaffolds facilitated their differentiation into adipogenic, chondrogenic or osteogenic lineages, with corresponding increases in the expression of lineage-specific genes [16,17]. Xu et al. showed that smooth muscle cells cultured on aligned nanofiber scaffolds attached and migrated along the axis of the aligned nanofibers, expressed spindle-like contractile phenotype, and exhibited actin and myosin cytoskeleton organization that are parallel to the direction of the nanofibers [24]. Yang et al. also demonstrated in aligned and nonwoven nanofiber scaffolds that nanometer diameter fibers enhances neurite growth in cerebellum stem cells better than micron-sized fibers [25].

2.1.4 Nanofiber Modification for Cell Culture Applications

At present, the majority of these electrospun nanofiber studies have only examined the effect of pristine nanofiber surface on cell behavior [14-27]. However, we believe that optimal regulation of cell behavior requires more than an "inert" scaffold that only provides topographical cues; and the electrospun nanofiber scaffolds should also present specific binding domains for cells and growth factors and serve many other functions (e.g. modulate growth factor responsiveness) that are critical to the regulation of cell activities. The systematic design and modification of a nanofiber scaffold containing these functional entities (bioactive molecules) would be important in mimicking the cellular microenvironment.

A few groups have suggested electrospinning of pure ECM components or ECM / synthetic polymer blends into nanofiber scaffolds as the alternative to synthetic polymeric nanofiber scaffolds [63-66]. However, this strategy is only limited to fibril-forming proteins like fibrinogen, collagen, gelatin and elastin, and some glycosaminoglycans like hyaluronan. In addition, the fiber morphology is inherently unstable in aqueous medium (the fibers degrade immediately) and additional crosslinking steps (e.g. treatment with glutaraldehyde, 1,6-diisocyanatohexane, poly (ethylene glycol)-diacrylate, etc.) are usually taken to stabilize these scaffolds for cell culture. Therefore, this strategy is not feasible for the presentation and delivery of the majority of other bioactive molecules to cells. Nonetheless, several of these ECM components have been successfully electrospun and stabilized as nanofiber scaffolds, and cells (keratinocytes, fibroblasts, endothelial cells, etc.) cultured on these scaffolds have showed enhancement in cell adhesion and proliferation compared with synthetic polymer scaffolds [63-66].

In general, nanofiber modification methods can be categorized into two different approaches: either modifying the interior or bulk of the fiber, and/or modifying the exterior or surface of the synthetic polymeric nanofiber with bioactive molecules to provide the desired cell responsive properties.

2.1.4.1 Doping of Bioactive Molecules

In this strategy, the nanofiber core is modified through the incorporation of bioactive molecules like drugs or proteins into the polymer fibers, as illustrated in Fig. 2.5. The bioactive molecules are first added into the polymer solution. The doped polymer solution is then electrospun into a nanofiber mesh. The bioactive molecules in the nanofiber mesh are subsequently released and absorbed by cells during culture.

Various bioactive molecules like heparin, nerve growth factor, DNA nanoparticles, drugs and bone morphogenetic protein have been incorporated into the nanofiber [43,67-69]. These doped nanofiber scaffolds were able to provide sustained release of bioactive molecules to the target cells for extended periods of 1 week to 2 months, and the release kinetics of these molecules is dependent on both the bioactive molecule solubility characteristics, as well as the degradation characteristics of the nanofiber scaffold. In general, for non-degradable and slow-degrading scaffolds, the bioactive molecule release kinetics is a function of the molecule diffusibility and solubility [43,67,68], while for fast-degradable scaffolds the release kinetics is also coupled with the scaffold degradation [69].

Luong-Van et al. demonstrated that sustained release of heparin from doped polycaprolactone nanofiber scaffolds prevented the proliferation of vascular smooth muscle cells in culture [43]. Liang et al. showed that controlled release of DNA nanoparticles released from doped poly(D,L-lactic-co-glycolic acid) nanofiber

scaffolds are effective in transfecting 3T3 cells *in vitro* [69]. We also demonstrated in Chapter 4 that galactosylated nanofiber scaffolds doped with 3-methylcholanthrene is also able to induce and regulate cytochrome P450 activity of hepatocytes *in vitro*.

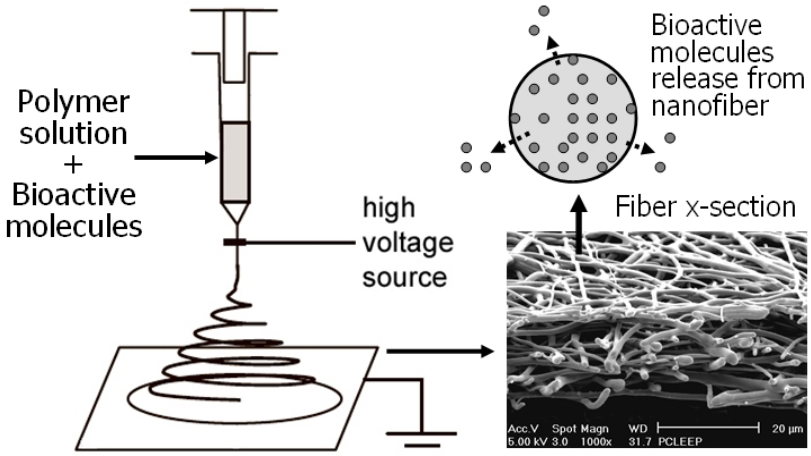

Figure 2.5: Interior modification of electrospun nanofiber scaffolds.

2.1.4.2 Nanofiber Surface Modification

In this strategy, bioactive molecules are chemically immobilized onto the nanofiber surfaces, as illustrated in Fig. 2.6. These immobilized bioactive molecules then serve as ligands which will induce cell responses like adhesion, morphological organization, proliferation or differentiation upon interaction with cells.

Numerous surface modification protocols are available in literature, which describe conjugation of bioactive molecules onto film surfaces [30-36]. Nanofiber surface modification strategies [70-73] have also imported these methods that have worked well with film modification. In general, plasma or UV-initiated grafting treatments, or chemical hydrolysis methods like aminolysis are first employed to functionalize the nanofiber surface with simple functional groups like carboxylic acid, amine, or aldehyde groups. Peptides, proteins, glycosaminoglycans and other ligands are subsequently conjugated onto the functionalized surfaces via chemical crosslinkers (e.g. glutaraldehyde, carbodiimide, etc.) [30-36,70-73].

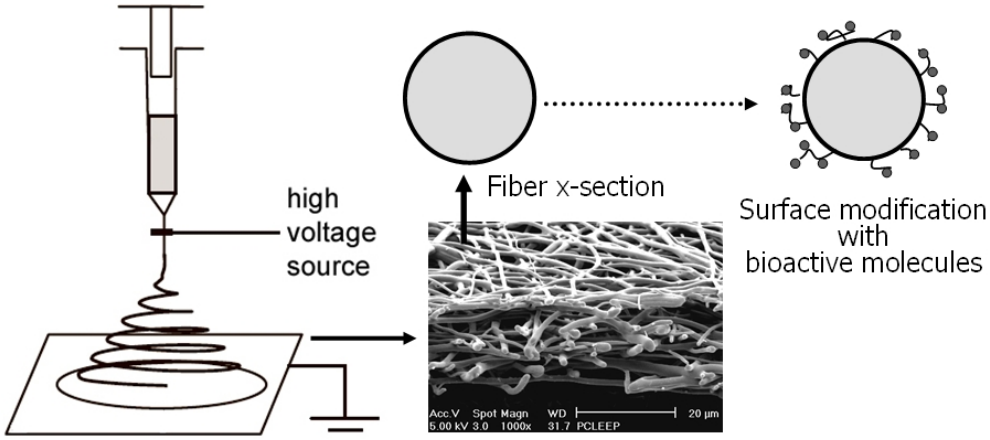

Figure 2.6: Exterior modification of electrospun nanofiber scaffolds.

Kim et al has demonstrated that cell attachment, spreading, and proliferation of 3T3 cells were greatly enhanced in RGD peptide immobilized electrospun poly(D,L-lactic-co-glycolic acid) nanofibers, compared with unmodified nanofibers [73]. Ma et al showed endothelial cells cultured on gelatin immobilized polycaprolactone nanofibers exhibit enhanced spreading, proliferation, and expression of endothelial cell markers [71].

2.2 Biomaterials Design for Primary Hepatocyte Culture

Liver failure has been the cause of death for thousands of people worldwide each year. When liver failure suddenly occurs in healthy individuals with normal livers, it is termed acute liver failure (ALF), while the loss of liver function that complicates chronic liver disease is termed acute-on-chronic liver failure. Both ALF and acute-on-chronic liver failure are curative via immediate liver transplantation [74,75]. Though patient survival after transplantation has improved with advances in both patient management and surgical techniques in recent years, the procedure however, is not always available in a timely fashion due to the problems of organ availability [76].

To alleviate this problem, alternatives to whole liver transplantation organ are currently under active investigation. Some of these methods include extracorporeal bioartificial liver devices (BALs), transgenic xeno-transplantation, isolated cell transplantation, and tissue engineering of implantable constructs (Fig. 2.7) [77-81]. In particular, research on BALs has been widespread as it is seen as a viable form of supportive treatment to liver transplantation. BALs are generally developed as temporary systems to attempt to expedite recovery from acute decompensation, facilitate regeneration in ALF, and serve as a bridge to liver transplantation [77-81].

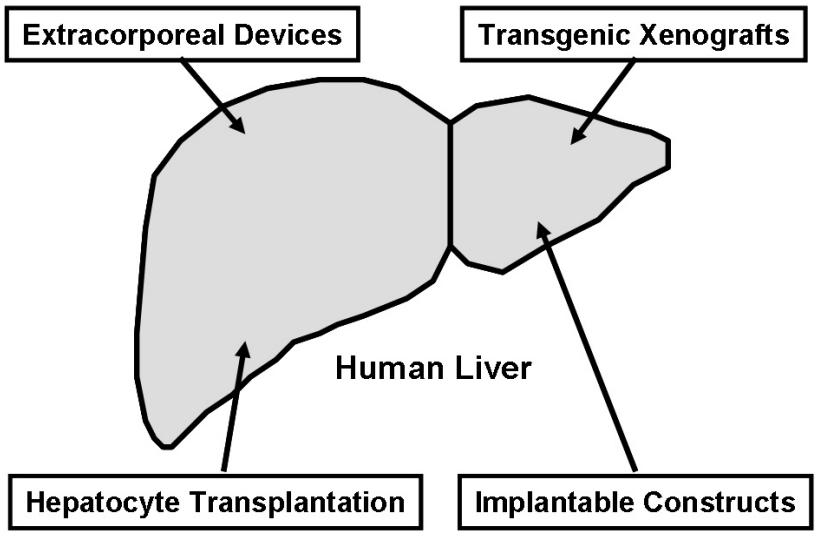

Figure 2.7: Approaches to cellular therapies for the treatment of liver disease. Extracorporeal devices perfuse patient's blood or plasma through bioreactors containing hepatocytes. Hepatocytes are transplanted directly or implanted on scaffolds. Transgenic animals are being raised to harvest a humanized liver.

BALs typically incorporate isolated cells (primary hepatocytes) into bioreactors to simultaneously promote cell survival and function as well as provide for a level of transport seen *in vivo*. The optimal design of a BAL generally spans across several research disciplines. To cell biologists, the design and choice of the BAL cellular component has been a primary focus: Optimization of medium formulations that enhance primary hepatocyte functions and viability [82,83] as well as the design of

immortalized cell-lines (e.g. NKNT-3, HepLiu, etc.) that express hepatic functions have been their key research areas [79,80,84,85].

To BAL engineers, their research focus have been challenges in bioreactor scale-up for effective clinical therapy, as well as challenges in bioreactor designs that provide optimal bi-directional mass transport of oxygen, nutrients, patient's plasma, etc., that is needed to sustain cell viability and allow export of therapeutic cell products [78,79,86].

Lastly, to biomaterials scientists, their key interests have been the design and optimization of biomaterial scaffolds that promote hepatocyte phenotype stabilization *in vitro*. This is because although primary hepatocytes represent the most direct approach to replacing liver function in hepatic failure, they are anchorage-dependent cells and notoriously difficult to maintain *in vitro*: When enzymatically isolated from the liver and cultured in monolayer, scaffold or suspension cultures, the primary hepatocytes rapidly lose adult liver morphology and differentiated functions [77-81].

One approach of hepatocyte phenotype stabilization includes the use of extracellular matrix (ECM) components, which included both variations in composition and topology. For example, surfaces coated with various ECM proteins, such as laminin, fibronectin, and collagen [87-91], or conjugated with cell adhesion peptides, such as RGD and YIGSR [92], have been used for hepatocyte culture. Hepatocytes have been shown to attach well to these substrates [87-92]. An improvement on the ECM culture system is sandwich cultures [89-91] or microencapsulation cultures [93,94] which were designed to mimic the microenvironment of the adult hepatocyte where cells are sandwiched by extracellular matrix in the space of Disse [78-80]. These sandwich or microencapsulation cultures

typically packed hepatocytes closer together at higher densities, thereby promoting homotypic cell-cell interactions. Hepatocytes cultured in this configuration have been shown to stably express many liver-specific functions [89-91,93,94]. However, these "ECM scaffolds" face the same problems as electrospun ECM nanofibers in that they are inherently unstable and attempts to scale-up these culture methods have met with limited success so far.

Nevertheless, the importance of high density cell-packing in promoting homotypic or heterotypic (in the case of hepatocyte cocultures with non-parenchymal cells [95-97]) cell-cell interactions, which in turn stabilizes and maintains hepatocyte liver-specific functions has been well documented [77-81,89-91,93-120], and this has been the basis of culture systems involving hepatocyte spheroid formation [98-120].

2.2.1 Hepatocyte Function Maintenance through Spheroid Formation

Primary hepatocytes, when cultured on certain substrates conditions, will physiologically undergo a series of morphological and functional changes, and eventually self-assemble into spheroids [33,34,98-120].

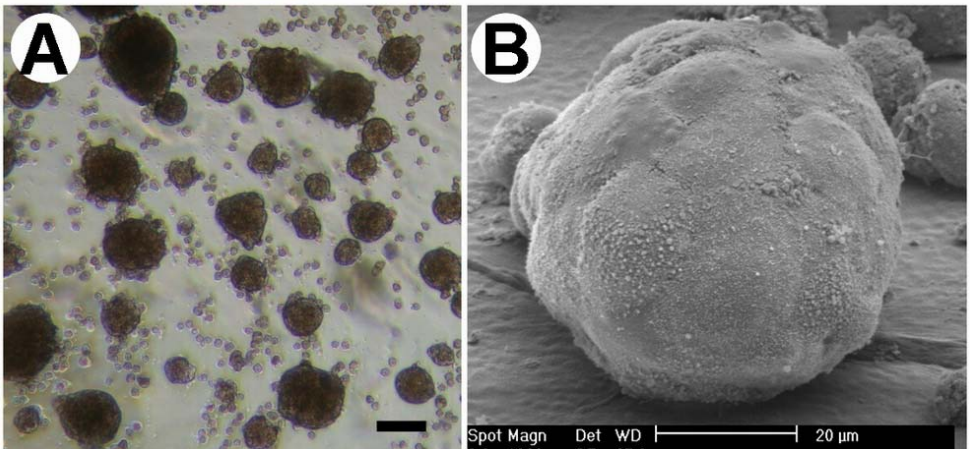

Figure 2.8: Morphology of hepatocyte spheroids. (A) Light microscope image of spheroids after 4 days culture (bar represents 100 μm). (B) SEM imaging shows that the surface of a mature spheroid is relatively smooth and cell-cell contacts are tight.

Hepatocyte spheroids are three-dimensional, compacted multicellular spherical aggregates that exhibit high degrees of cell-cell contacts (Fig. 2.8) [90,98-101]. They show several structural similarities to native liver tissue such as gap junctional complexes and bile canaliculi-like channels [98-101]. Hepatocyte spheroids exhibit prolonged viability and express high levels of liver-specific functions including albumin production, urea synthesis, and cytochrome P450 activity, in contrast to cells cultured as monolayers [102-104]. At present, several different protocols have demonstrated successful in assembling spheroids *in vitro*, they include:

(1) Encapsulating [93,94], sandwich [89-91], or other packing (e.g. polyurethane foam [105-107]) cultures where hepatocytes are physically packed close together to facilitate cell-cell interactions and spheroid assembly;

(2) Positively-charged polystyrene surfaces (Primaria^{TM}, BD Biosciences) [108] or negatively-charged proteoglycan-coated surfaces [109], which induces the formation of non-surface-adherent spheroids;

(3) Rotary suspension cultures, where the swirling motion facilitates cell clustering [110,111]; and,

(4) Hepatocyte cultures on galactose-immobilized substrates, where the hepatocyte-specific galactose ligand attaches hepatocytes and induces spheroid formation along the substrate surface [33,34,112-120]. We shall be using the scaffold galactosylation strategy to bio-functionalize our scaffolds for hepatocyte culture.

2.2.2 Hepatocyte Cultures on Galactosylated Scaffolds

Galactose-conjugated substrates have been proposed as alternatives for hepatocyte culture [33,34,112-120]. These substrates mediate hepatocyte adhesion through the galactose–asialoglycoprotein receptor (ASGPR) interaction, and minimize the involvement of the integrin-mediated signaling pathway, which has been shown to induce the loss of hepatocyte phenotypes [103]. The characteristic attribute of these galactosylated substrates is also the propensity of hepatocytes to form aggregates or spheroids on them, in concomitance with maintaining higher hepatocyte synthetic functions.

At present, several studies have shown that polymeric biomaterial surfaces conjugated with galactose ligands can improve hepatocyte attachment and sustain most of the cellular functions. This has been demonstrated in poly-*N*-*p*-vinylbenzyl-D-lactonamide-coated polystyrene surfaces or foam [113,114] and in galactosylated polyethylene oxide hydrogel or polyacrylamide gel [115,116]. In addition, galactosylated biodegradable polymeric scaffolds, such as alginate/galactosylated chitosan sponge, galactosylated microcapsules, and polylactide-*co*-glycolide foam [117-120], have also been designed for hepatocytes culture.

Recently, galactosylated PET films have also been developed for hepatocyte spheroid culture [33,34]. A galactose ligand called 1-O-(6'-Aminohexyl)-D-galactopyranoside (AHG) was designed for this culture system. This AHG ligand consist of: (1) the galactosyl group; (2) a 6-carbon spacer (~ 0.7 nm) between the galactosyl group and the surface conjugating point to facilitate the conjugation reaction and to increase the accessibility of the ligand to cell surface receptors (ASGPR); and (3) a terminal primary amine group that allowed AHG conjugation to other surfaces via cross-linking chemistry. Details of AHG ligand synthesis are

attached in Appendix I. The AHG ligand is conjugated onto poly(acrylic acid)-grafted PET surface through carbodiimide cross-linking chemistry [33,34]. We shall be using this AHG ligand to bio-functionalize our hepatocyte culture scaffolds.

2.2.3 Bio-functional Nanofiber Scaffolds for Hepatocyte Cultures

Besides the ligand–receptor interaction, the substrate topography in micro-and nanometer ranges has been shown to influence cellular behavior and functions including adhesion, migration, proliferation and gene expression [14-27,55-59]. Hepatocytes cultured on silicon scaffolds with micro-channels or in polyurethane foams [105-107] have also exhibit aggregation behavior and functional maintenance that are dependent upon the pore size of the scaffold. Electrospinning has been increasingly investigated as an interesting technique to produce polymeric fibrous scaffolds for cell culture applications. Several studies have shown that these nanofiber scaffolds effect favorable cellular responses [14-27,70-73]. In this thesis, we would like to extend the investigation to primary rat hepatocytes cultured on nanofiber mesh. We would investigate how nanofiber topography and fiber bio-functionalization can be employed to synergistically enhance cell-substrate interactions and hepatic functions for primary hepatocyte culture systems.

2.3 Biomaterials Design for *Ex Vivo* HSPC Expansion

Ex vivo hematopoietic stem/progenitor cells (HSPCs) expansion is one of the most challenging fields in cell culture. This is a rapidly growing area of tissue engineering with widespread potential applications like gene therapy, immunotherapy, bone marrow transplantation, and the production of mature blood cells for transfusion medicine [132-140].

The importance for HSPC *ex vivo* expansion in medicine is clearly demonstrated in cell transplantation therapy treatments for cancer patients undergoing chemotherapy and radiation therapy. Both chemotherapy and radiation therapy treatment procedures target cells in mitosis, based on the fact that tumor cells are continuously proliferating. As a consequence, all other cells that undergo rapid proliferation are also damaged and this applies especially to the hematopoietic system. In most cases, this leads to total loss of all hematopoietic stem cells, making allogeneic or autologous stem cell transplantation obligatory. Therefore, *ex vivo* HSPC expansion can either increase the number of umbilical cord blood derived cells, making this source also available for adult patients, or reduce the number of leukapheresis procedures necessary for the collection of autologous cells [132-140].

Transplantation of *ex vivo* expanded lineage-restricted progenitor cells are also viable cell therapy treatments [132-140]. For example, expansion of neutrophil granulocytes and megakaryocytes can help to reduce the periods of neutropenia and thrombopenia respectively after chemotherapy. In addition, the expansion of natural killer cells or T-lymphocytes gives access to cell-mediated immunotherapy, while the generation and specific loading of dendritic cells offers possibilities for the *in vivo* induction of antigen-specific immunity. The generation of erythrocytes or thrombocytes can also lead to blood transfusions without a risk of viral contaminants. Finally, hematopoietic stem cells can also serve as a target for somatic gene therapy as they can offer a chance of a lifelong cure from genetic disorders due to their self-renewing capacity.

As hematopoiesis *in vivo* is a highly regulated and complex process, the challenge of *ex vivo* HSPC expansion has always been the optimization of cell cultivation techniques that can control and regulate every step of differentiation of and

maturation of the hematopoietic cell, mimicking that of the cell's native microenvironment. Also, with much progress made in the understanding of the hematopoietic system over the past decades, the cultivation techniques and concepts have also been evolving continuously, in order to expand HSPCs efficiently and effectively.

In the following subsections, we will present and discuss the various knowledge of the hematopoietic system, cell characterization techniques and cell cultivation strategies that have progressively shaped the *ex vivo* HSPC expansion field.

2.3.1 The Hematopoietic System

Hematopoiesis is the process of generating mature blood cells. In the human body, hematopoiesis mainly occurs in the bone marrow, predominantly in the femur, sternum and pelvic bones [137-139]. In the marrow, the hematopoietic cells are embedded in the stromal tissue, which consists of several different cells types (adipocytes, fibroblasts, marcophages, endothelial cells, etc.) responsible for the production of ECM (collagen, laminin, fibronectin, glycosaminoglycans, etc.) as well as providing membrane-bound and soluble growth factors [137-140]. The interactions between hematopoietic cells, stromal cells and ECM controls and regulates the entire hematopoiesis process (Fig. 2.9): Everyday, almost 400 billion hematopoietic cells of different subtypes are produced in an average human to replace the natural loss of cells [137]. Despite this tremendous proliferation, the balance between the different lineages is very efficiently controlled by the bone marrow microenvironment to guarantee the many functions of the blood [137].

Despite enormous research progress over the past decades, the hematopoietic system is still not completely understood. However, it is agreed that all hematopoietic

cells originate from a small population of multipotent hematopoietic stem cells that proliferate and differentiate into the whole spectrum of mature blood cells [132-140]. The hematopoietic stem cells are the only hematopoietic cells that have the capacity to self-renew, while for all other cells, proliferation is inevitably combined with a lineage-specific differentiation and loss of immaturity.

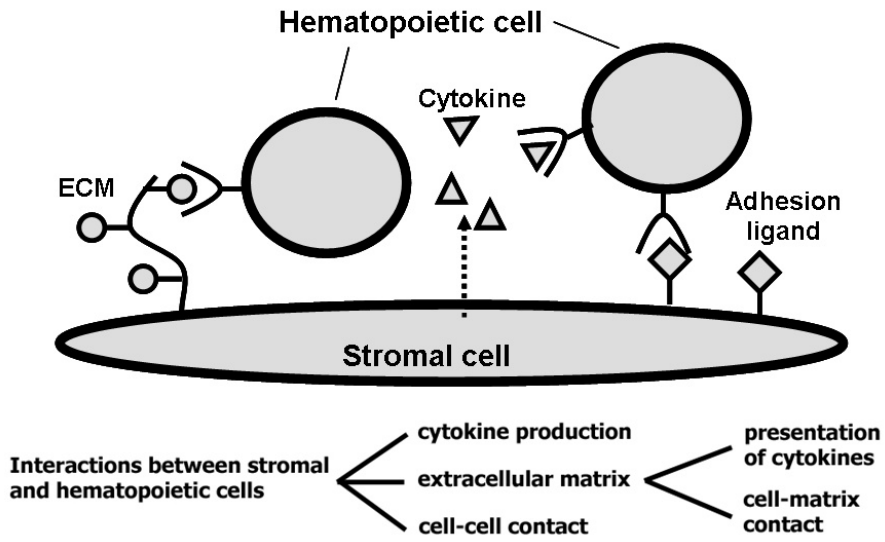

Figure 2.9: Control of hematopoiesis in a bone marrow microenvironment.

2.3.2 Hematopoietic Stem/Progenitor Cell Sources

HSPCs can be harvested from the (1) bone marrow, (2) peripheral blood after stem cell mobilization, or from (3) umbilical cord blood. The bone marrow is a good source of HSPCs and supporting stromal cells as it is the natural site for hematopoiesis. However, the harvesting of cells from bone marrow is an invasive procedure that requires manual extraction under spinal or general anesthesia of the allogeneic donor, so alternative sources are preferred whenever possible [135-137]. HSPCs can also be harvested from peripheral blood after administration of G-CSF or GM-CSF, which mobilizes HSPCs from the bone marrow. Though this is the standard procedure to collect HSPCs from patients for autologous transplantation after high-

dose chemotherapy, it is not applicable to allogeneic transplantation, due to the health risk involved in using HSPC mobilization cytokines [135-137].

Umbilical cord blood is a promising alternative source of HSPCs for both allogeneic and autologous hematopoietic stem cell transplantation, as it contains a significant amount of progenitor cells with high proliferative potential, and the HSPCs are harvested through procedures that are non-invasive for the mother or the neonate [135,139,141,144]. Cord blood sources also contains a lower burden of common viral contaminations like EBV and CMV compared with the other two sources, and as the lymphocytes are more naive, the risk of a graft-versus-host disease is also reduced [135]. However, the main disadvantage of cord blood is the low number of HSPCs obtainable due to the small volume of blood collected from the umbilical cords, so transplantation is limited to pediatric patients of body weight less than 40 kg [141-145]. Nevertheless, it is hoped that through development of efficient *ex vivo* expansion strategies, sufficient quantities of HSPCs can be produced to engraft and sustain long-term hematopoiesis for adult patients.

2.3.3 Hematopoietic Stem/Progenitor Cell Characterization Techniques

HSPC characterization assays are important to *ex vivo* expansion cultures in that they evaluate and identify the primitive HSPC population in the cultures before or after cell expansion have been carried out. They also serve as a means of assessing the effectiveness of an expansion culture technique in producing HSPCs. There are at present a handful of assays used frequently in literature that have demonstrated merits in identifying and evaluating HSPCs, and we will be using most of these assays throughout this thesis to assess our scaffold expansion culture system. The detailed protocols to these characterization methods are described in Chapter 5.3.2 & 6.3.2.

HSPC characterization using flow cytometry techniques has been popular since the discovery of the CD34 cell surface marker [146-149]. The CD34 antigen is frequently used as a marker of stem cells as the $CD34^+$ cell population contains a high amount of CFC, LTC-IC and mouse-repopulating capacity [135-138,143-156]. $CD34^+$ is expressed most strongly on the most primitive cells and is progressively lost as cells differentiate [146-150]. Although recent studies have discovered other stem cell associated markers (e.g. CD133, CXCR-4) [138,157,158] and have also described stem cell subpopulations that are $CD34^-$ [158,159], the CD34 antigen remains a popular marker in identifying HSPCs clinically and in research.

In addition to flow cytometry, a series of *in vitro* assays like colony-forming cell (CFC) assay, cobblestone area-forming cell (CAFC) assay or long term culture-initiating cell (LTC-IC) assay are also used in progenitor cells characterization. In the CFC assay, a small number of cells are cultivated for 2 weeks in cytokine containing semi-solid medium. Colony-forming cells generate distinct colonies of more differentiated cells depending on their lineage specificity. For the detection of more primitive progenitor cells, CAFC or LTC-IC assays are used. Here a small number of cells are placed on a stromal cell layer for 5-8 weeks. During this period the early progenitor CAFC and LTC-IC differentiate and, in the case of CAFC, cobblestone-area-like cells are formed that can be easily identified. In the case of LTC-IC the early progenitor cells differentiate into CFC, which are detected using a subsequent CFC assay [160,161].

Finally, to evaluate the engraftment ability of the expanded HSPCs, *in vivo* assays are used, which measures the potential of these cells in repopulating the hematopoietic system of sub-lethally irradiated immunodeficient mice (NOD/SCID), monkeys or sheep [162,163].

2.3.4 Hematopoietic Stem/Progenitor Cell Expansion Cultures

HSPC expansion culture systems have been evolving continuously (Fig. 2.10), progressing with current knowledge of the hematopoietic system and also with development of new technologies. The first HSPC expansion culture system was described by Dexter et al. in 1977 [164] using stromal cells to support HSPC growth [160,164-172]. The development of human recombinant cytokines in the 1990s has contributed to the widespread popularity of cytokine supplemented HSPC suspension cultures [173-177]. Finally, advancement in micro-fabrication technologies and the progressive understanding and appreciation cell-cell and cell-substrate interactions of the HSPC microenvironment has encouraged development of scaffolds that can support HSPC expansion [178-185]. We will briefly discuss each of these HSPC culture variants in the following subsections.

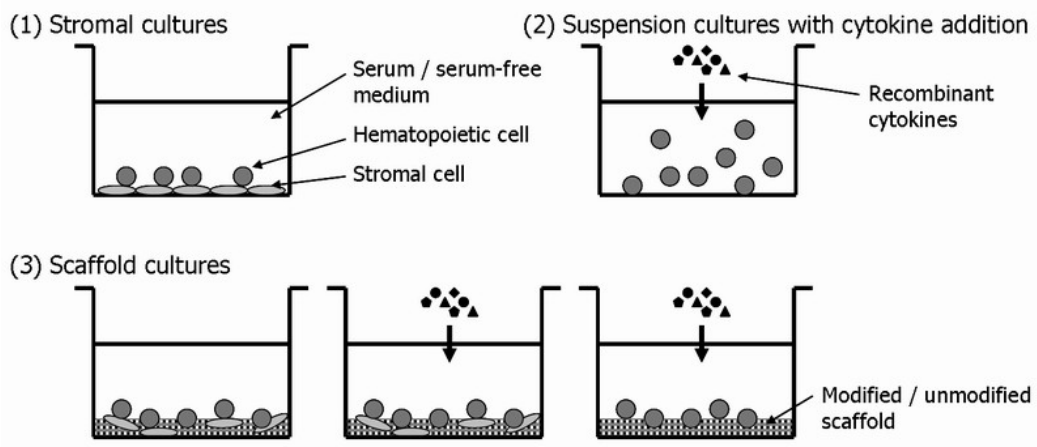

Figure 2.10: Generic HSPC cultivation variants. (1) Stromal cultures; (2) Cytokine supplemented suspension cultures; and (3) HSPC-immobilized scaffold cultures that combine different aspects of the previous two culture variants.

2.3.4.1 HSPC Cultures with Stromal Cells or Conditioned Medium

Before the development of recombinant human cytokines, a feeder layer of stromal cells was essential for HSPC cultivation. Stromal culture of hematopoietic cells is a generic term that covers a variety of cultivation concepts, which includes (1)

direct HSPC – stromal cells co-culture, (2) HSPC culture in stromal-conditioned medium, and (3) partitioned non-contact co-culture.

The first direct co-culture system was demonstrated by Dexter et al. [164]. Since then, several other stromal cells lines have been developed for the HSPC cultivation, though most stable lines are of murine origin. Some examples are HESS-5, M2-10B4, L88/5, hu-ST, etc. [160,164-168]. The main reason that stromal culture provides a superior HSPC cultivation environment is that they appear to mimic the *in vivo* bone marrow environment. The stromal cells provide direct cell-cell interactions as well as cell-matrix interactions through secreting ECM. The stromal cells also secrete numerous different growth factors necessary for the maintenance and expansion of stem and progenitor cells and many of these substances are still unknown [164-169]. However, harvesting and complete separation of expanded HSPCs from the stromal cells is very difficult in such systems.

A variation of direct co-culture is the application of exogenous stromal-conditioned medium [168,169]. This concept enables the application of all bioreactor systems developed for the cultivation of isolated HSPCs and allows the culture to be supplied with (unidentified) growth factors secreted from the stromal cells. The conditioned medium can be produced in large amounts exogenously and stored until application. An improvement of this approach is the in-situ generation of stromal-conditioned medium in a partitioned non-contact co-culture, where HSPCs and stromal cells are physically separated in different compartments using micro-porous membranes [140,170]. This permits active interaction between HSPCs and stromal cells, mediated by secreted molecules, which has been demonstrated to support the expansion of the early progenitor cells more efficiently than the use of exogenous

conditioned medium [140,170]. However, this technique suffers from difficult technical requirements in set-up and process control.

Although the main attraction of stromal cultures is their superior ability for HSPC expansion, clinical realization of these systems has been difficult, if not impossible. The major drawback has been the origin of the stromal support. While the use of autologous stromal cells would be a feasible possibility [171,172], in many cases this is not feasible. Furthermore, the use of cell lines is problematic as all stromal cells have to be removed completely prior to transplantation, a demand which is difficult to fulfill. In the case of murine cell lines a transfer of residue cells into a patient would be a xeno-transplantation, which is faced with extensive regulatory hurdles.

2.3.4.2 HSPC Cultures with Human Recombinant Cytokines

The development of human recombinant cytokines has allowed cultivation and significant expansion of isolated hematopoietic stem and progenitor cells without the use of supporting feeder-layer of stromal cells. The simplicity of these culture systems is their main attraction: The cells are cultivated in chemically defined culture medium containing defined combinations of cytokines [132-139,173-177].

Different kinds of culture set-ups have been devised for cytokine supplemented cultures, but they are generally classified as suspension cultures. The various set-ups include well plates, tissue-culture flasks, gas-permeable culture bags, spinner flasks and stirred vessel bioreactors [132-139]. All these systems have the advantage of being easy to handle, single-use devices, which enable an uncomplicated cell harvest. For the larger culture bag and spinner flask set-ups, cell cultivation on a clinical scale is possible, and these systems have been used clinically [132-139].

The critical element of cytokine supplemented suspension cultures is the cytokine formulation. However, after almost two decades of intensive research of cytokine effects on HSPCs [173-177], the optimal choices and combinations of cytokines for the *ex vivo* expansion of HSPCs has not yet been determined [132-139]. This problem is mainly due to variations in culture conditions (e.g. use of serum or serum-free medium, cell source purity, HSPC sources, etc.) or assays (e.g. LTC-IC, CAFC, mouse-engraftment assay, etc.) employed by the different studies.

Nevertheless, there is consensus among the various research studies, which shows a list of cytokines that can positively regulate HSPC kinetics [173-177]. These cytokines include stem cell factor (SCF), flt3/flt2 ligand (FL), interleukin (IL)-1, IL-3, IL-6, IL-11, IL-12, leukemia inhibitory factor (LIF), granulocyte-macrophage colony-stimulating factor (GM-CSF), granulocyte colony-stimulating factor (G-CSF), thrombopoietin (TPO), and erythropoietin (EPO). In addition, supplementation of two or more cytokines has been repeatedly demonstrated to positively enhance regulation of HSPC kinetics, as compared to single cytokine supplementation [132-139,173-177]. For example, the addition of SCF to a combination of IL-3 and GM-CSF resulted in significant fold increase in cell colony formation [174]. In another study, FL in combination with TPO resulted in extensive expansion with little differentiation of $CD34^+$ cord blood cells cultured under stromal-free conditions [175]. In this thesis, we will be using a cytokine formulation adapted from Miller et al. [173], which consist of SCF, FL, TPO and IL-3. Details of the cytokine formulation and culture conditions are described in Chapter 5.3.2, 6.3.2 & 7.3.2.

Although cytokine supplemented suspension cultures enable better control of the culture conditions, cell processing, and significantly less regulatory hurdles as compared to stromal cultures, important elements in the *in vivo* regulation of

hematopoiesis are missing in this approach: the cell-cell interactions between hematopoietic and stromal cells, and biochemical and topographical cues provided by cell-matrix interactions between hematopoietic cells and the ECM substrate [137-140]. Therefore, it is likely that the cultivation of isolated hematopoietic cells in suspension results in suboptimal HSPC expansion [137,140].

2.3.4.3 HSPC Cultures on Scaffolds

The immobilization of HSPCs into scaffolds is an attempt to imitate the complex topographical microenvironment of the bone marrow. Scaffold topography itself cannot support HSPC survival, so *ex vivo* expansion of HSPCs on scaffolds must always be adapted with addition of other factors like stromal cells, ECM components and/or cytokines [178-185]. The designs of HSPC scaffold culture systems are usually devised to improve the existing stromal culture and cytokine culture systems.

For scaffold cultures with stromal cells, the scaffolds incorporate the 3-D perspective into the culture system, as conventional co-cultures are usually 2-D monolayer cultures. HSPCs and stromal cells have been co-cultured in nonwoven fabrics disks, large pore-size cubes and nylon screens [178-180]. For example, Li et al. have shown that culture in 3-D non-woven polyester matrices enhanced cell–cell and cell–matrix interactions and expansion of stromal and hematopoietic cells [179]. Although high local cell densities can be achieved in these systems, they nevertheless still retain the drawbacks related to the use of stromal cells.

For scaffold cultures with cytokine supplementation, the scaffold topography provides cell anchorage and the possibility of HSPC growth modulation via cell-substrate interactions to the otherwise substrate-less suspension cultures. A growing body of evidence suggests the importance of surface chemistry as well as

topographical features on the rate of HSPC proliferation and $CD34^+$ cell expansion on cytokine supplemented cultures [181-185]. For example, LaIuppa et al. have shown that the type of substrate used in culture, ranging from polymers (polystyrene, polysulfone, polytetrafluoroethylene, cellulose acetate) to metals (titanium, stainless-steel) and glasses, can significantly affect the outcome of *ex vivo* expansion of HSPCs [181]. Leong et al. have also demonstrated that covalent surface immobilization of extracellular matrix proteins (fibronectin) [185] and adhesion peptides (CS-1 and RGD) [184] mediate HSPC adhesion to the scaffold and HSPC expansion.

These results suggest cytokine soluble cues as well as immobilized biochemical and topographical cues could be synergistically involved in dictating the proliferation and differentiation of cultured HSPCs. These observations also prompted us to investigate whether the nano-topographical cues and immobilized biochemical cues on electrospun nanofiber scaffolds could also synergistically influence HSPC adhesion, proliferation and multipotency phenotype maintenance, and we shall demonstrate these effects in this thesis.

2.4 Concluding Remarks

Over the past decade, the understanding of the electrospinning technique has been very progressive: It is possible to control this process and to electrospin almost any polymer material into nanofibers of virtually any size and mesh configuration. The simplicity and versatility of nanofiber fabrication has attracted interests in many research disciplines. In particular, biotechnologists and medical researchers have recently demonstrated the possibilities of electrospun nanofibers as viable cell culture scaffolds. Though the mechanisms in which cells interact with nanofibers remains

largely to be elucidated, we hoped that through nanofiber bio-functionalization, we would be able to understand and control this cell-nanofiber interaction better. Thus, in the following chapters, we will demonstrate how bio-functionalized nanofiber scaffolds can solicit various cellular responses through the synergistic effects of nanofiber topography and immobilized biochemical cues.

We will demonstrate in Chapters 3 & 4 that galactosylated nanofibers can induce hepatocyte morphological reorganization, and enhance attachment, albumin, and cytochrome P450 activity functions. We will also demonstrate in Chapters 5, 6 & 7 that hematopoietic stem / progenitor cell proliferation and phenotype maintenance is enhanced via *ex vivo* cultures on aminated nanofiber scaffolds.

CHAPTER THREE

Stable Immobilization of Hepatocyte Spheroids on Galactosylated Nanofiber Scaffolds for Liver Cell Cultures

3.1 Summary

Primary rat hepatocytes self-assemble into multi-cellular spheroids and maintain differentiated functions when cultured on a two-dimensional (2-D) substrate conjugated with galactose ligand. The aim of this study is to investigate how a functional nanofiber scaffold with surface-galactose ligand influences the attachment, spheroid formation and functional maintenance of rat hepatocytes in culture, as compared with the functional 2-D substrate.

Highly porous nanofiber scaffolds comprising of fibers with an average diameter of 760 nm were prepared by electrospinning of poly(ε-caprolactone-*co*-ethyl ethylene phosphate) (PCLEEP), a novel biodegradable copolymer. Galactose ligand with a density of 66 nmol/cm^2 was achieved on the nanofiber scaffold via covalent conjugation to a poly(acrylic acid) spacer UV- grafted onto the fiber surface.

Hepatocytes cultured on the galactosylated PCLEEP nanofiber scaffold exhibited similar functional profiles in terms of cell attachment, ammonia metabolism, albumin secretion and cytochrome P450 enzymatic activity as those on the functional 2-D substrate, although their morphologies are different. Hepatocytes cultured on galactosylated PCLEEP film formed 50-300 μm spheroids that easily detached from surface upon agitation, whereas hepatocytes cultured on galactosylated nanofiber scaffold formed smaller aggregates of 20-100 μm that engulfed the functional nanofibers, resulting in an integrated spheroid-nanofiber construct.

3.2 Introduction

Primary rat hepatocytes, when cultured on certain culture configurations will self-assemble into spheroids [33,34,98-120]. Hepatocyte spheroids are three-dimensional, compacted multi-cellular spherical aggregates that exhibit high degrees of cell-cell contacts [90,98-101]. In turn, these spheroids sustain viability for extended culture periods and maintain high levels of liver-specific functions including albumin production, urea synthesis, and cytochrome P450 activity, in contrast to cells cultured as monolayers [102-104]. Galactose-conjugated substrates have been proposed as alternatives for hepatocyte culture. These substrates mediate hepatocyte adhesion through the galactose-asialoglycoprotein receptor (ASGPR) interaction, and minimize the involvement of the integrin-mediated signaling pathway, which has been shown to induce the loss of hepatocyte phenotypes. In addition, hepatocytes cultured on galactosylated PET films exhibit spheroid-forming capabilities: hepatocytes attach, then migrate and aggregate on the galactosylated surface, eventually forming surface bound spheroids [33,34].

Besides the ligand-receptor interaction, the substrate topography in micro- and nanometer ranges has been shown to influence cellular behavior and functions including adhesion, migration, proliferation and gene expression [14-27,55-59,105-107]. Electrospinning has been increasingly investigated as an interesting technique to produce polymeric fibrous scaffolds for cell culture applications. Nanofibers ranging from 100 nm to 5 μm can be electrospun into a non-woven or an aligned nanofiber mesh. Several studies have shown that these nanofiber scaffolds effect favorable cellular responses [14-27,70-73]. We would like to extend the investigation to primary rat hepatocytes cultured on nanofiber mesh composed of poly(ε-caprolactone-co-ethyl ethylene phosphate) copolymer (PCLEEP). PCLEEP is a

recently developed biodegradable polymer [121]. With ester and phosphate linkages in the backbone, PCLEEP shows an intermediate degradation rate between poly(ε-caprolactone) and poly(ethyl ethylene phosphate) with a relatively linear degradation profile. PCLEEP is soluble in several solvents and therefore confers good processibility for the electrospinning process. It has also shown good tissue compatibility and low cytotoxicity [67,121-123]. Initial studies also shows that unmodified PCLEEP confers better hepatocyte adhesion properties compared to other polymers such as poly(ε-caprolactone).

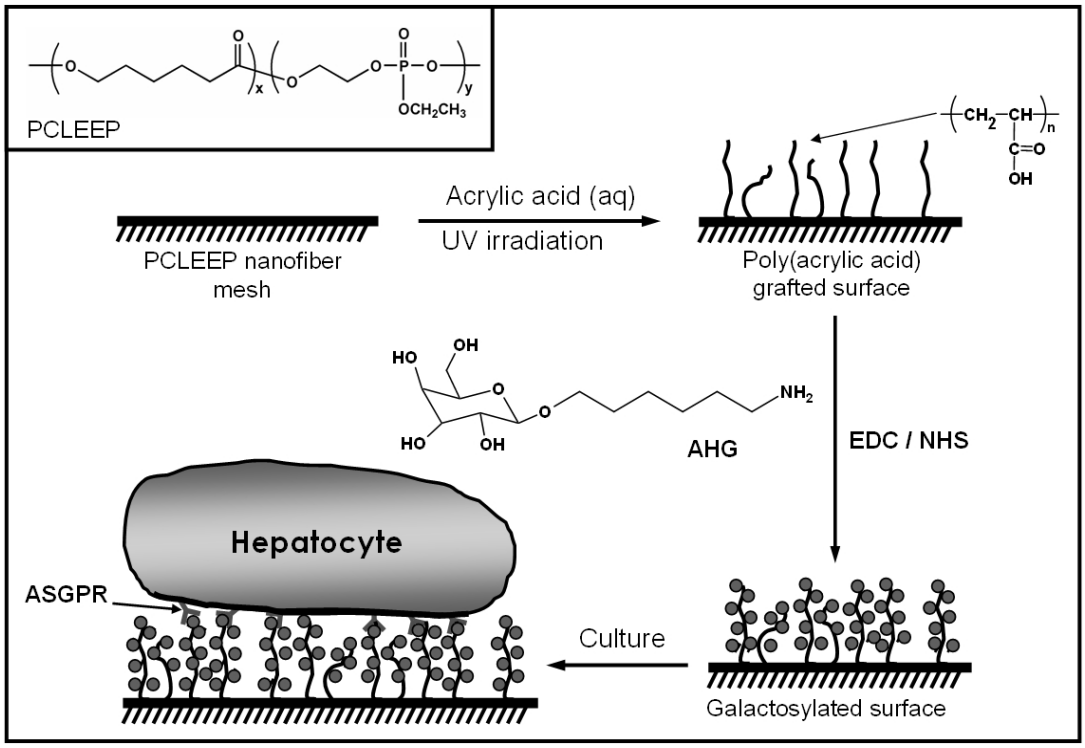

Figure 3.1: Surface modification scheme for galactose conjugation to PCLEEP nanofiber mesh. Insert: PCLEEP copolymer chemical structure.

In this study, we present the development of a biofunctional PCLEEP nanofiber construct for hepatocyte culture (Fig. 3.1). This was achieved by conjugating hepatocyte-specific galactose ligands onto the nanofiber surface. We investigated the effect of nanofiber mesh on hepatocyte attachment, migration, spheroid formation and maintenance of the differentiated functions, as compared with smooth 2-D substrates

with or without galactose ligand. It is hypothesized that such functional nanofiber scaffolds can be incorporated into a bioartificial liver assist device design, and together with their textured and porous nature, may promote hepatocyte-scaffold interaction that will improve the stability of the attached cells.

3.3 Experimental Methods

Acrylic acid was purchased from Merck. All other chemicals were purchased from Sigma-Aldrich unless otherwise stated.

3.3.1 Fabrication of PCLEEP Nanofiber Scaffolds

PCLEEP copolymer (Mw: 70,760) was synthesized according to a procedure described by Wen et al. [121]. The PCLEEP copolymer was dissolved in acetone (21.5 wt% concentration) and placed in a plastic syringe fitted with a 27G needle. A syringe pump (KD Scientific) was used to feed the polymer solution into the needle tip. The feed rate of the syringe pump was fixed at 0.3 mL/h. PCLEEP nanofiber meshes were fabricated by electrospinning at 17 kV using a high voltage power supply (Gamma High Voltage Research). The nanofibers were collected onto grounded 15 mm diameter coverslips located at a fixed distance of 80 mm from the needle tip. Fiber diameters and mesh thickness were determined from images obtained using a field emission scanning electron microscope (FESEM) (SL30 FEG, FEI Company). Representative nanofiber images were analyzed using NIH ImageJ software (http://rsb.info.nih.gov/ij/). At least 250 measurements were recorded for each analysis.

As a control, PCLEEP film substrate was prepared by spin-coating 5 wt% PCLEEP solution in acetone at 2000 rpm onto 15 mm diameter coverslips using a spin-coater machine (Brewer Science Inc.).

3.3.1.1 Surface Grafting of Scaffolds with Poly(acrylic acid)

Acrylic acid (AAc) was freshly distilled prior to use. The PCLEEP fibrous scaffolds were cleaned with 70% ethanol in an ultrasonic water bath for 10 min prior to surface grafting. Poly(acrylic acid) (PAAc) was grafted onto the scaffold surface by photo-polymerization, as described by Uchida et al. [32]. Briefly, samples were immersed in aqueous solution containing 2%-7% AAc solution and 0.5 mM $NaIO_4$ in a flat-bottom glass container. The temperature of the solution was maintained at 10^{o}C by cooling the container in an ice-water bath. The solution was then exposed to UV from a 400 W mercury lamp (5000-EC, Dymax) for 15 min. The distance between the samples and the lamp was 25 cm. The PAAc-grafted scaffolds were then thoroughly washed with deionized water at 37^{o}C for more than 36 h to remove any ungrafted PAAc from the surface of the scaffold. Scaffolds modified using 6% AAc solution was used for cell culture.

The amount of PAAc grafting on scaffolds was determined by Toluidine Blue O (TBO) colorimetric staining method [33,34]. Briefly, samples of known areas were immersed in 0.5 mM TBO solution at pH10 and 20^{o}C for 4 h. The samples were then thoroughly washed with water at pH10 and 20^{o}C to remove any non-complexed dye adhering to the surface. The dye was then desorbed from samples in a 50% acetic acid solution, and the concentration determined by spectroscopy at 633 nm (SpectraMax 190, Molecular Devices). The surface carboxyl (COOH) group density (the amount of COOH groups per coverslip area) was calculated from a calibration plot of the OD versus TBO dye concentration and assuming 1:1 stoichiometry of the binding between TBO and surface carboxylic group.

3.3.1.2 Galactosylation of Poly(acrylic acid) Grafted Scaffolds

1-O-(6'-Aminohexyl)-D-galactopyranoside (AHG) was synthesized according to procedures described by Yin et al. (Appendix I) [33]. AHG conjugation onto PAAc-grafted scaffolds was achieved by immersing each scaffold into sodium phosphate buffer (0.1 M, pH 8.0, 1.0 mL) with 1 mg AHG, 1 mg N-hydroxysulfosuccinimide (sulfo-NHS) and 10 mg 1-ethyl-3-(3-dimethylaminopropyl) carbodiimide hydrochloride (EDC). Ten mg of EDC each was added to the reaction mixture at 12 h and 24 h later. After 36 h, the conjugation reaction was stopped. Scaffolds were then thoroughly washed with deionized water and subsequently sterilized and stored in 70% ethanol until use in cell culture.

3.3.2 Hepatocyte Culture and Assays

3.3.2.1 Hepatocytes Isolation

Hepatocytes were harvested from 250 – 300 g male Wister rats by a two-step in situ collagenase perfusion method. Rats were maintained on ad libitum rodent feed and water at room temperature and 40% humidity. All animal procedures were approved by the National University of Singapore's Institutional Animal Care and Use Committee. Hepatocyte viability was determined to be >85% using Trypan Blue.

3.3.2.2 Hepatocyte Attachment Assay

Freshly isolated rat hepatocytes (3.5×10^5) were seeded onto each 15 mm diameter scaffold disks (2×10^5 cells/cm^2), and cultured in William's E medium supplemented with 0.5 mg/mL BSA, 10 ng/mL EGF, 500 ng/mL insulin, 5 nM dexamethasone, 50 ng/mL linoleic acid, 100 mg/mL penicillin, 100 U/mL streptomycin, 50 pM $ZnSO_4$ and 100 nM $CuSO_4$. Cells were maintained in a humidified incubator fed with 5% CO_2. After 3 h of incubation, all unattached cells

were washed off by gentle washing using culture medium, and collected by centrifugation (2,000 rpm). The cell pellet was washed once with PBS and then lysed with cell lysis buffer (Promega).

The protein concentration in the lysate was determined using a BCA protein assay kit (Pierce). The number of unattached cells was determined by comparing the protein concentration in lysate with a standard curve generated with known numbers of cells. Subsequently, the attachment efficiency of hepatocytes on different scaffolds can be calculated based on the cell number of the unattached cells for each scaffold.

3.3.2.3 Hepatocyte Culture Maintenance

The attached hepatocytes on different scaffolds were cultured in supplemented William's E medium as described above. Triplicate samples were maintained for each hepatocyte function assay for each scaffold condition. Fresh medium was replenished daily, and old medium was collected for albumin determination. The collected medium was centrifuged at 4,000 rpm for 10 min and the supernatant was stored at –20^{o}C. At various time points of the culture, morphology of hepatocytes on these scaffolds was viewed under an inverted phase contrast microscope (Carl Zeiss) and imaged on a digital camera (Nikon).

3.3.2.4 Albumin Secretion Assay

The albumin concentration in the culture medium collected at various time points was determined by competitive ELISA method [124]. Briefly, samples were serially diluted, and rabbit peroxidase-conjugated rat albumin antibody (ICN) was added to a final concentration of 0.6 μg/mL. After incubation at 37^{o}C for 2 h, 100 μL aliquots of each sample were transferred to 96-well Maxisorp plates (Nunc), which were pre-coated with 100 μL/well of rat albumin at 0.2 μg/mL in PBS overnight at 4^{o}C, and

washed three times with 0.05% Tween-20 in PBS before use. The samples were incubated at 20^{o}C for 2 h in a humidified chamber. After incubation, the plates were washed three times with 0.05% Tween-20 in PBS and subsequently filled with 100 μL/well 1-Step Turbo TMB-substrate (Pierce). Plates were incubated at 20^{o}C in a humidified chamber for another 30 min and reaction was immediately stopped by adding 100 μL of 1.3 N H_2SO_4. Optical density of the solution in each well was measured at 450 nm using a spectrophotometer (SpectraMax 190, Molecular Devices).

3.3.2.5 Urea Synthesis Assay

On Days 1, 3 and 5, hepatocyte cultures were refreshed with culture medium containing 1 mM NH_4Cl, and incubated for 90 min. The NH_4Cl-containing medium was then collected and the cultures were refreshed with normal culture medium. The medium samples collected were stored at –20^{o}C and subsequently quantified for urea contents using a urea nitrogen assay kit (Sigma).

3.3.2.6 Cytochrome P450 Activity Assay

Cultures were tested for the P450 enzymatic activity (P450-dependent 7-ethoxycoumarin O-deethylase activity) using protocols adapted from Jauregui et al. and others [97,125-127]. Briefly, on Days 1, 4 and 7, hepatocytes were pre-incubated in culture medium containing 50 μM 3-methylcholanthrene (3-Mc) for 24 h to induce cytochrome P450 production. The medium was then replaced with culture medium containing 0.26 mM 7-ethoxycoumarin substrate. After 5 h incubation, the 7-ethoxycoumarin-containing medium was collected and the cultures were refreshed with normal culture medium. The medium samples collected were stored at –20^{o}C and subsequently assayed for 7-hydroxycoumarin (HCOD) using HPLC.

For HPLC analysis, 200 μL aliquots of each sample were pre-incubated in 1.0 M acetate buffer (pH 5.0) with 4.744 units/mL β-glucuronidase, 0.524 units/mL sulfatase, and 4-methylumbelliferone internal standard at 37^{o}C. After 48 h, samples were transferred to glass tubes (13×100mm, Iwaki). Half milliliter of saturated sodium borate buffer (pH 9.0) and 4 mL chloroform was then added. After shaking for 3 min, the aqueous layer in the tubes was aspirated off and discarded. The remaining chloroform layer was dried using a vacuum concentrator (Savant). The dried residue was reconstituted with 200 μL of HPLC mobile phase (1:1 methanol/water). The metabolites, HCOD, were analyzed by reverse-phase HPLC using a Symmetry C18 stainless steel column (Waters) at 1.0 mL/min mobile phase flow rate and a PDA 996 detector (Waters) at 326 nm.

3.3.2.7 Preparation for Scanning Electron Microscopy

Hepatocyte cultures were gently rinsed with PBS and fixed with 3% glutaraldehyde for 30 min at 20^{o}C and postfixed with 1% osmium tetraoxide for 15 min at 20^{o}C. The hepatocytes were then dehydrated using a graded series of ethanol (25%, 50%, 70%, 80%, 90%, 95%, and 100%) followed by CO_2 critical point drying (Samdri 780A). The samples were mounted onto aluminum stubs and gold sputter-coated before viewing under FESEM.

To prepare samples for freeze fracture, hepatocyte cultures were gently rinsed with water after 3% glutaraldehyde fixation. Excess water was removed and samples were cooled in liquid nitrogen for 10 min. Samples were then shattered using a razor blade and immediately placed into a freeze dryer (Labconco) for 24 h. The samples were mounted onto aluminum stubs and gold sputter-coated before viewing under FESEM.

3.3.3 Statistical Analysis

All values were expressed as mean ± standard deviation (SD). Statistical differences were determined by two-tailed student's t-test.

3.4 Experimental Results

3.4.1 Optimization of PCLEEP Electrospinning

PCLEEP fibers were generated by the electrospinning process. The PCLEEP electrospinning process is optimized by gradually increasing the polymer solution concentration until a suitable concentration is found that will produce unbeaded, uniform fibers. We have found the optimal concentration to be 21.5 wt% PCLEEP in acetone. The other parameters for operating the electrospinning process were described in Chapter 3.3.1.

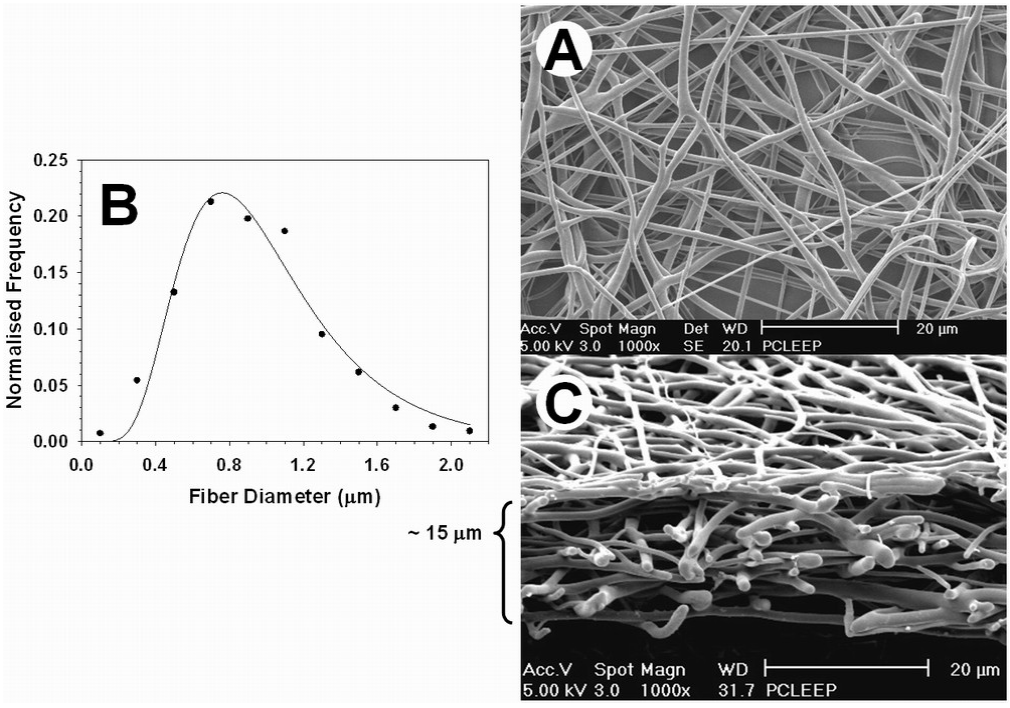

Figure 3.2: SEM characterization of PCLEEP nanofiber mesh. (A) SEM image shows that the mesh is highly porous and the fibers are randomly orientated. (B) Fibers have a diameter distribution between 0.13 μm and 2.3 μm, and an average diameter of 0.76 μm. (C) Mesh thickness is approximately 15 μm.

SEM images showed that nanofibers arranged randomly in the mesh (Fig. 3.2) and their diameters ranged from 300 nm to 1.5 μm (with frequency higher than 5%, Fig. 3.2B). The average diameter was 760 nm. This highly porous mesh contained pores of mainly sub-cellular sizes (<10 μm, Fig. 3.2A). The thickness of the mesh varied with the deposition time. The meshes used for this study had a thickness of approximately 15 μm (Fig. 3.2C).

3.4.2 Optimization of Scaffold Galactosylation Process

Surface conjugation of galactose ligand onto PAAc grafted scaffolds was achieved using the same protocol as Yin et al. and the effectiveness of the conjugation scheme was successfully demonstrated through XPS analysis [33,34]. Since the galactose conjugation efficiency using this scheme was shown to be above 90%, the surface galactose density can therefore be controlled by varying the PAAc grafting density on the scaffold surface [33,34].

The PAAc grafting density of PCLEEP nanofiber mesh was lower than that of PCLEEP spin-coated film when 2-7% of AAc solution was used in the grafting reaction (Fig. 3.3). This result was expected because UV-initiated polymerization required direct exposure of the surface to UV light for surface grafting to occur. Due to its porous nature, the PCLEEP nanofiber mesh had a lower projected flat-area as compared to PCLEEP film. During UV-irradiation, the nanofiber mesh area exposed to UV was less than that of the film on the same 15 mm coverslip, which resulted in the lower grafting density.

Scaffolds modified using 6% AAc were used for cell culture experiments. Under these conditions, nanofiber meshes had an average surface COOH density of 66 nmol/cm^2, whereas PCLEEP films yielded an average surface COOH density of 127

nmol/cm^2. Previous studies had shown that both the attachment and spheroid forming ability of the primary rat hepatocytes cultured on galactosylated PET surfaces were almost independent of the surface graft density of COOH group within the range of 20 to 560 nmol/cm^2 [33,34]. Thus, the difference in COOH densities between 66 and 127 nmol/cm^2 was not expected to lead to significant differences in cell morphology and function, if comparison is made on the same type of substrate.

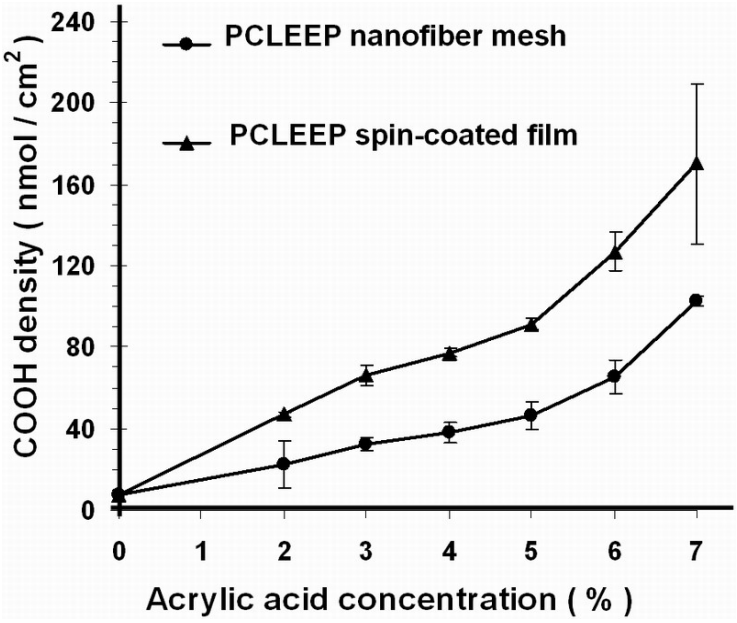

Figure 3.3: Effect of acrylic acid monomer concentration used for UV-initiated graft polymerization on the surface concentration of the grafted carboxyl groups on the PCLEEP nanofiber mesh and spin-coated film surface. Data are means ± SD of 2 independent experiments, each conducted in duplicates.

3.4.3 Hepatocyte Functional Maintenance

For convenience, galactosylated nanofiber mesh and film will be referred to as Gal-nanomesh and Gal-film respectively, while unmodified nanofiber mesh and film will be referred to as Un-nanomesh and Un-film respectively. Hepatocyte attachment efficiency measured at 3 h after cell seeding was shown in Fig. 3.4. Hepatocyte function normalized against the total number of attached cells was evaluated by albumin secretion level (Fig. 3.5), urea synthesis activity (Fig. 3.6) and 3-MC induced

P450 activity (Fig. 3.7) as a function of time. The results were determined from albumin, urea, or HCOD concentrations in the medium respectively.

Hepatocyte attachment was enhanced when seeded on Gal-nanomesh and Gal-film (83% and 90%, respectively) attachment after 3 h (Fig. 3.4), compared with 50-54% attachment for the unmodified surfaces ($p < 0.05$). The cell attachments on Gal-nanomesh and Gal-film conditions were similar, suggesting that the geometry of the substrata does not influence cell adhesion in this system. The improved attachment efficiency on the galactosylated substrates was attributed to cell-scaffold interactions between immobilized galactose ligand on substrates and ASGPR on the surface of hepatocytes.

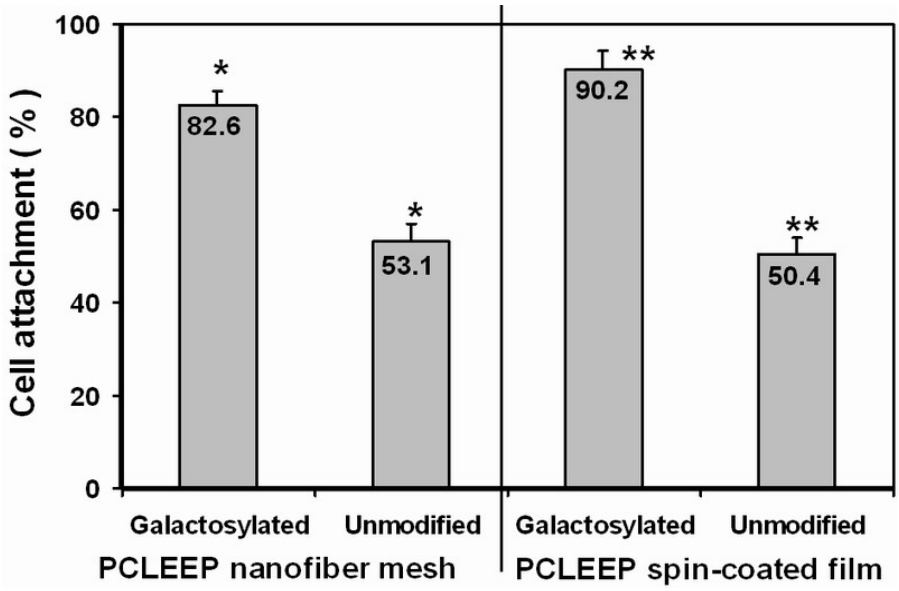

Figure 3.4: Hepatocyte attachment on galactosylated and unmodified nanofiber meshes and spin-coated films 3 h after seeding. *$p < 0.05$; **$p < 0.05$. Data are means ± SD of 2 independent experiments, each conducted where n = 6.

Hepatocytes cultured on galactosylated scaffolds showed higher albumin synthesis function than unmodified substrates, respectively (Fig. 3.5), leading to a bigger difference (> 2 fold) on days 3 – 5. Albumin synthesis function declined gradually for the two galactosylated-substrates during the first 2 – 3 days, and

maintained the same level thereafter. Comparing the two galactosylated-substrates, albumin secretion level of Gal-nanomesh group was about 22% higher than that of Gal-film group for the first two days, but was slightly lower (5% - 9%) than that of Gal-film group from day 3 onwards.

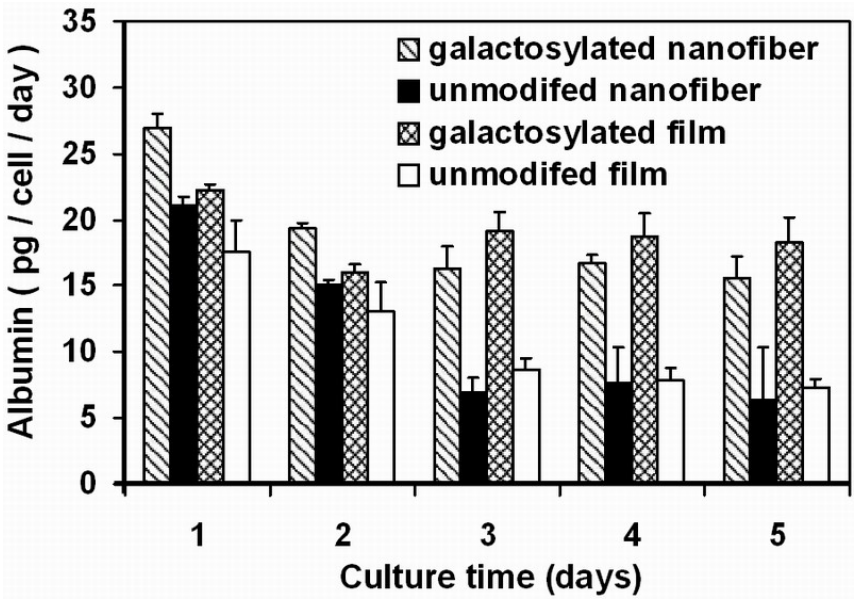

Figure 3.5: Albumin secretion level of hepatocytes at various time points normalized against the total number of attached cells. Data are means ± SD of 2 independent experiments, each conducted in duplicates.

However, the maintenance of urea synthesis function was less pronounced than that of albumin secretion function (Fig. 3.6). Urea synthesis (or ammonium removal) levels for the two galactosylated-substrates were similar throughout the assay period – they declined gradually over time. Interestingly, hepatocytes cultured on unmodified nanofiber substrate maintained urea synthesis function at the similar level as that cultured on galactosylated substrates. They showed about 1.6 and 2.5 fold higher urea synthesis activity than those on Un-film on days 3 and 5, respectively.

Hepatocytes cultured on the two galactosylated substrates responded well to 3-Mc induction and expressed higher levels of induced cytochrome P450 function than those cultured on unmodified substrates (Fig. 3.7), peaking on day 5 (> 4.4 fold). The

nanofiber mesh substrates resulted in higher HCOD synthesis activity than film substrates on day 1, but the difference became less apparent on days 3 and 5.

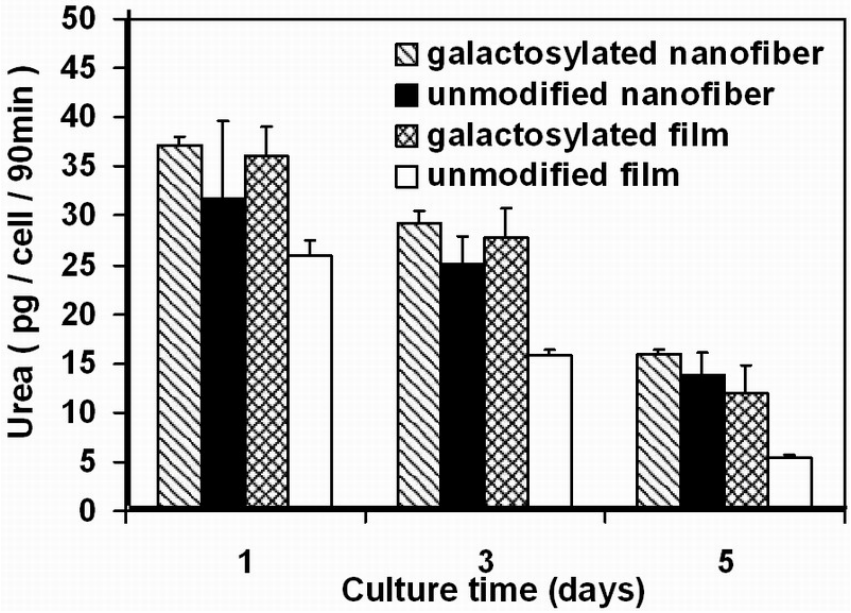

Figure 3.6: Urea synthesis function of hepatocytes at various time points normalized against the total number of attached cells. Data are means ± SD of 2 independent experiments, each conducted in duplicates.

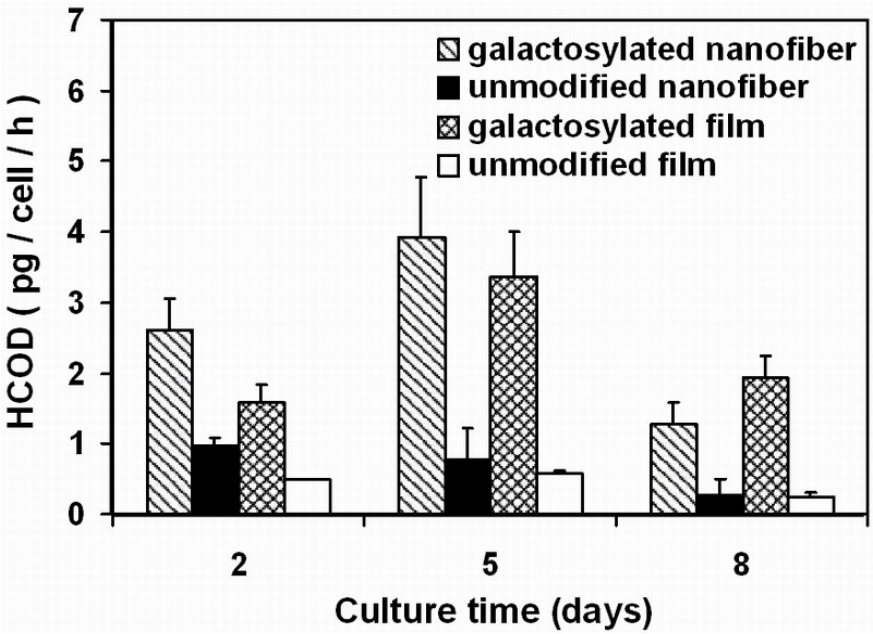

Figure 3.7: 3-Mc induced P450 function of hepatocytes at various time points normalized against the total number of attached cells. Data are means ± SD of 2 independent experiments, each conducted in duplicates.

In addition, a significant difference between the Gal-nanomesh and Gal-film groups was the long-term adherence of attached hepatocytes, as illustrated in Fig. 3.8. No significant cell detachment was observed for Gal-nanomesh throughout the assay period, whereas mature spheroids gradually detached from the Gal-film surface from day 3 onwards. Despite the special care taken during medium change for the Gal-film group, spheroid detachment is inevitable, though these detached spheroids remained viable and functional in the culture well. Only a small number of spheroids remained attached to the Gal-film surface by day 8. The Un-nanomesh and Un-film substrates did not show noticeable amount of cell detachment throughout the culture period.

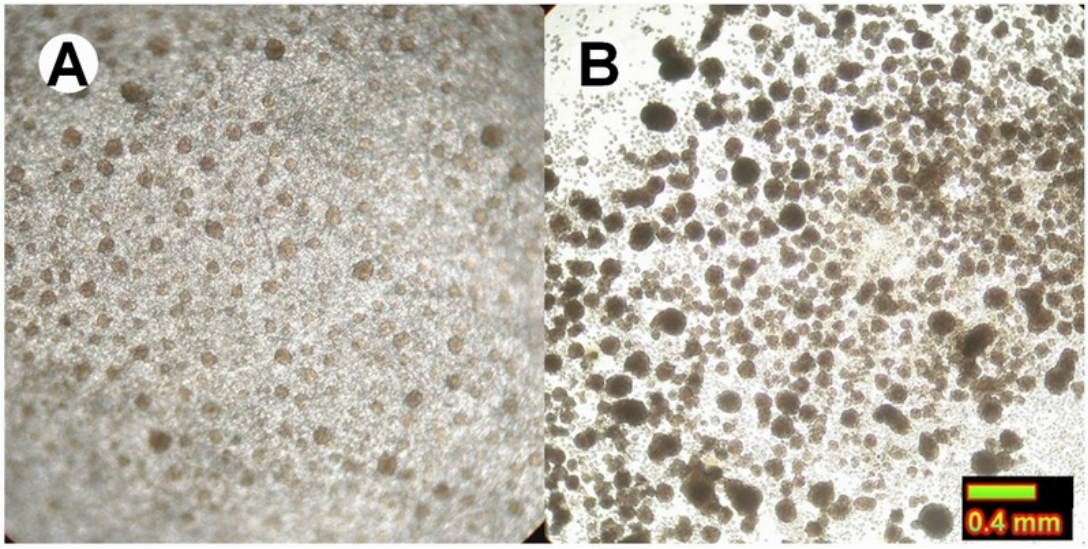

Figure 3.8: Hepatocyte spheroid adhesion on galactosylated scaffolds after 5 days of culture. (A) Hepatocytes cultured on Gal-nanomesh formed undetachable aggregates throughout the scaffold, whereas; (B) Hepatocytes cultured on Gal-film formed spheroids that can be easily detached from the surface, forming a spheroid suspension. Scale bar is applicable to both images as they are taken at the same magnification.

3.4.4 Hepatocyte Morphological Changes

Hepatocytes exhibited very different morphologies when cultured on different substrates. Optical microscope images at 3 h, 1 day and 3 days after cell seeding are presented in Fig. 3.9. Three hours after cell seeding, attached hepatocytes remained

rounded and singular, similar to the morphologies exhibited before cell seeding. Both Gal-nanomesh and Gal-film groups showed a closer packing of cells on the substrates as compared to Un-nanomesh and Un-film groups. This is indicative of the higher cell attachment efficiency on the galactosylated substrates over unmodified substrates.

Hepatocytes cultured on both Gal-nanomesh and Gal-film began to cluster and form aggregates after day 1. Cell movement and aggregation appear to be slightly restricted by the uneven nanofiber surface topography as compared to film surface. By day 3, aggregate formation on Gal-nanomesh was complete, resulting in smaller, more uniform spheroid-like structures of sizes between 20 and 100 μm in diameter, in comparison with the larger spheroids with wider distribution of the spheroid diameter (50–300 μm) on Gal-film. Single cell was rarely seen on Gal-nanomesh, but present on Gal-film substrate (Fig. 3.8 – 3.10). Most single cells lost viability on day 3.

For hepatocytes cultured on unmodified scaffolds, the morphologies displayed were irregular and not as uniform as those on galactosylated substrates. The absence of ligands on substrates to direct or initiate cell migration may be the primary cause of the morphological irregularities. For example, RGD groups on collagen-treated surfaces are known to induce hepatocyte spreading through RGD–integrin interactions [87-92], whereas galactose-modified surfaces direct hepatocytes to form multi-cellular spheroids through a combination of galactose-ASGPR and cell-cell interactions [33,34,112-120]. For unmodified substrates, non-specific hydrophobic interactions and some ionic interactions between the cell membrane and polymer surface probably allowed hepatocyte adhesion to take place. The morphology adopted by the hepatocytes may be due to the variations of these local non-specific interactions. Hepatocytes cultured on Un-nanomesh formed irregular spreading cell

clumps. Similarly, for hepatocytes cultured on Un-film, the cells exhibited both spreading and aggregating morphologies.

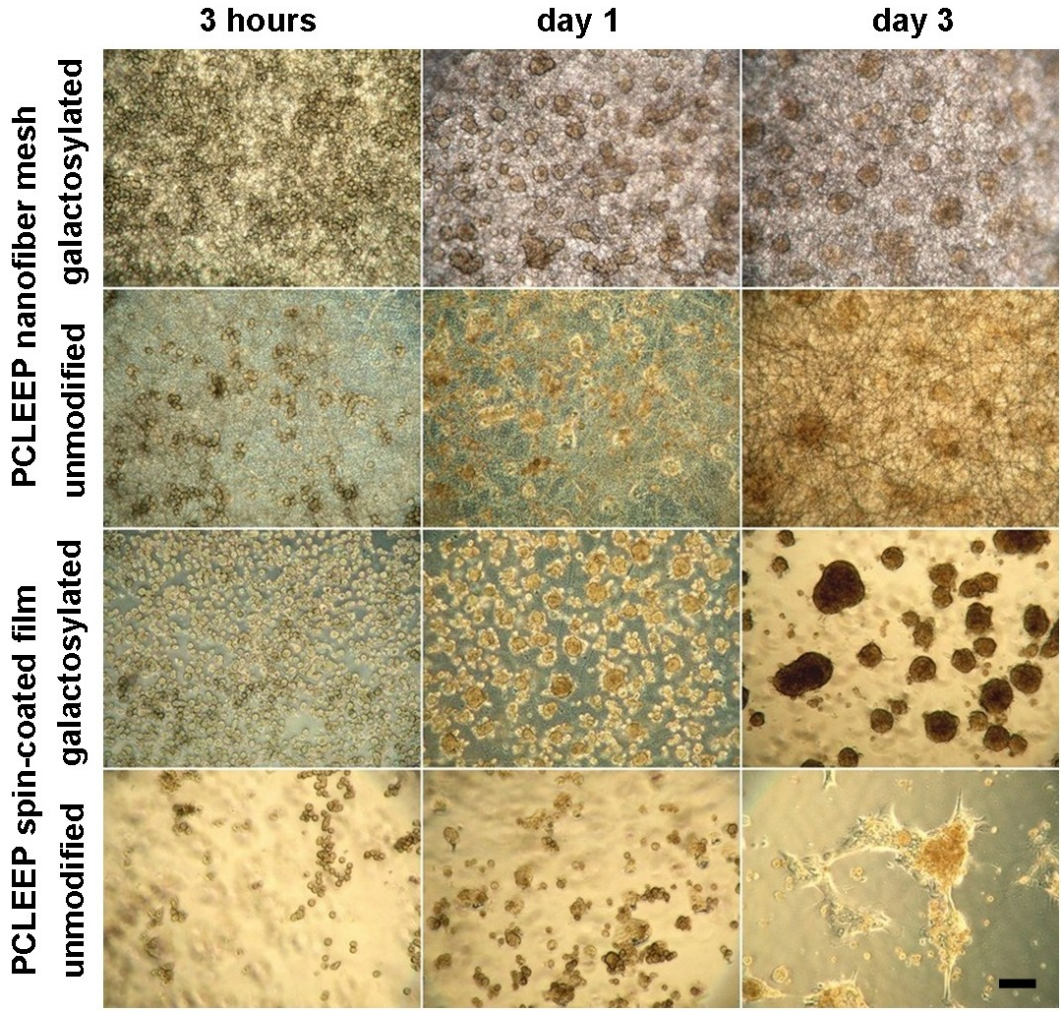

Figure 3.9: Morphology of hepatocytes at 3-h, 1-day and 3-days after seeding when cultured on different substrates. Scale bar represents 100 μm, applicable to all images as they are taken at the same magnification.

SEM images of remaining adherent spheroids on Gal-film showed typical spheroid morphology with a relatively smooth surface (Fig. 3.10A–C). Numerous microvilli also dotted around spheroid surface. These spheroids closely resembled the functional spheroids reported in literature, which exhibited tight cell–cell contact [90,98-101], in contrast with those rough and bumpy spheroids that are damaged by toxicants [128]. SEM images of the spheroid-like aggregates cultured on Gal-

nanomesh also showed similar surface features as compared with the spheroids on Gal-film (Fig. 3.10D–F). However, these aggregates were distinctively flattened onto the nanofiber mesh. The aggregates appeared to engulf the nanofibers, forming an integrated spheroid–nanofiber construct with the nanofiber mesh. This explains the good cell immobilization efficiency of the Gal-mesh substrate observed throughout the culture period, as depicted in Fig. 3.8.

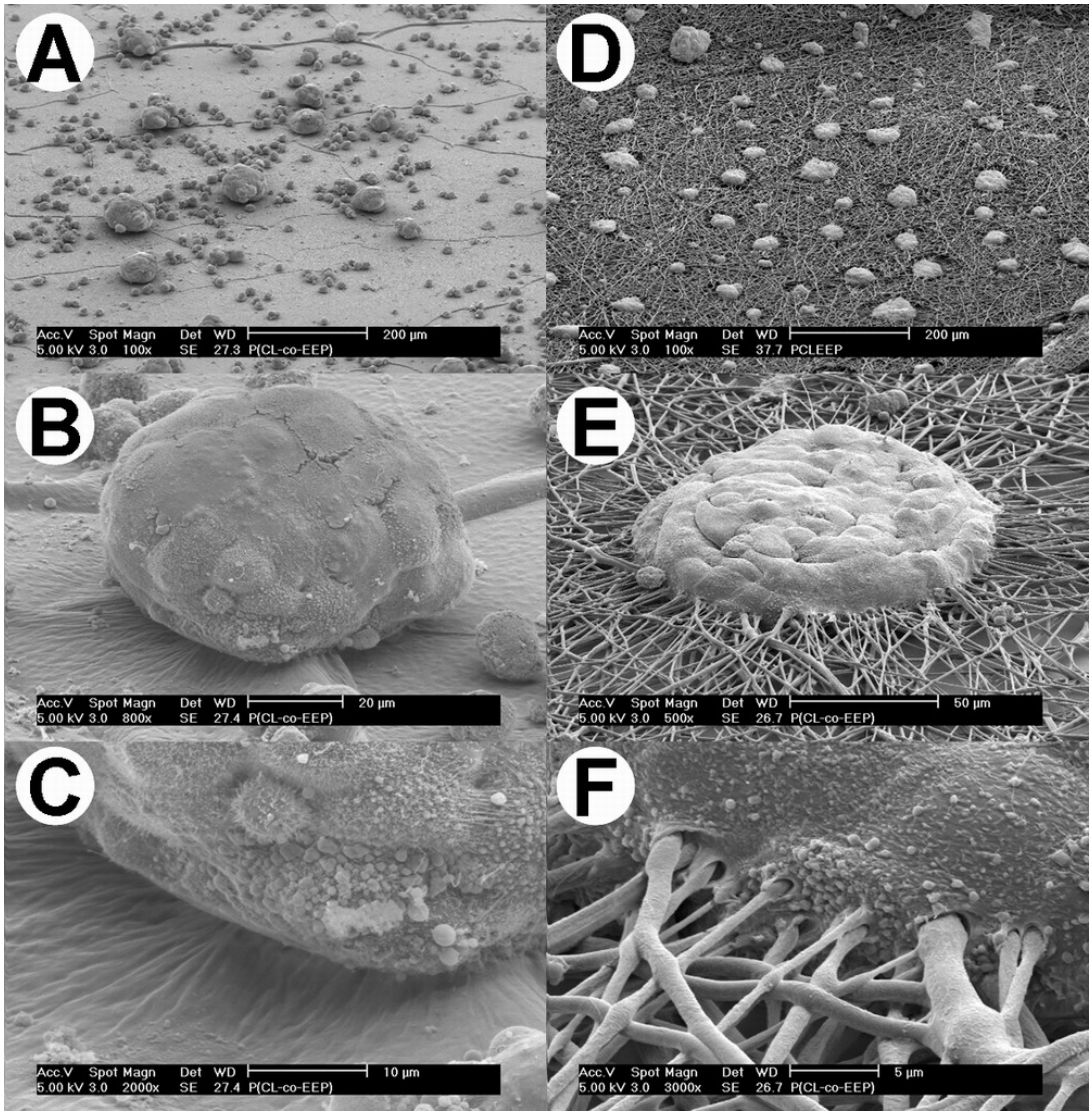

Figure 3.10: SEM images of hepatocytes after 8 days of culture: (A–C) Hepatocytes cultured on Gal-film formed rounded spheroids that did not integrate with the scaffold. In contrast; (D–F) Hepatocytes cultured on Gal-nanomesh showed that the aggregates engulfed the functional nanofibers.

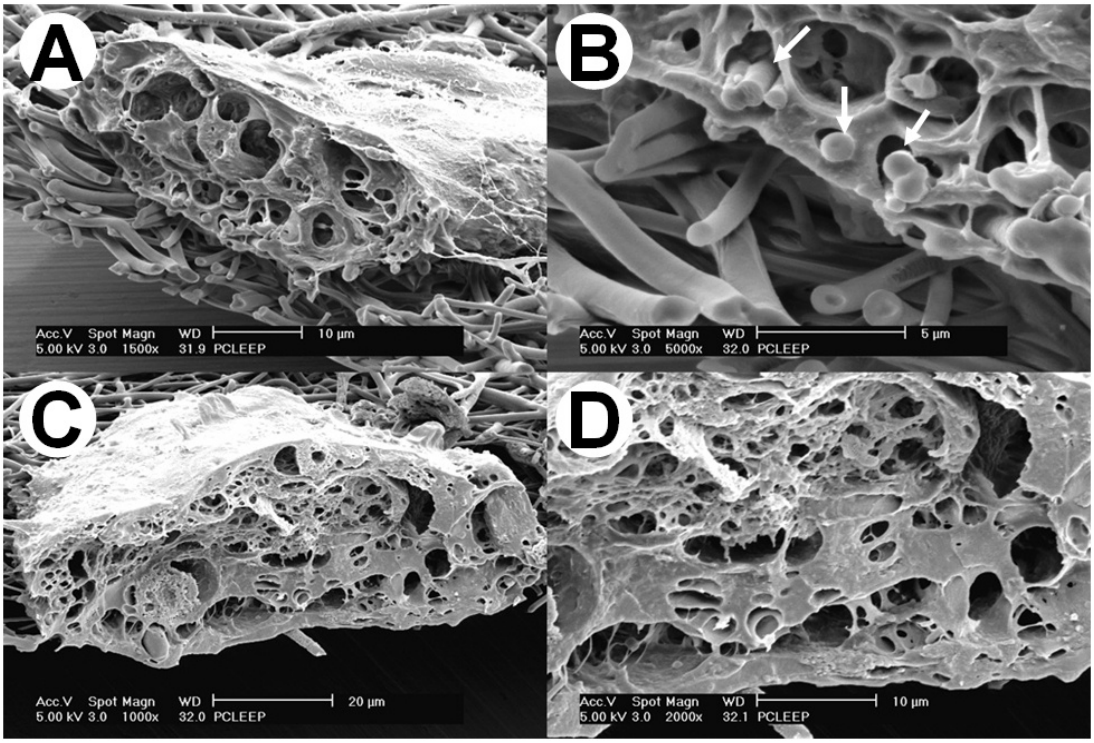

Figure 3.11: SEM images of freeze-fractured hepatocytes on Gal-nanomesh after 8 days of culture: (A & B) PCLEEP nanofibers (arrow) can be found within the hepatocyte aggregate; (C & D) Aggregates exhibit no fibers within, which maybe attributed to degradation of the biodegradable PCLEEP nanofibers.

The freeze-fractured spheroid-like aggregates allow the direct observation of the interior structure of the spheroids (Fig. 3.11). SEM images of the freeze-fractured aggregates showed many voids reminiscent of bile canaliculi channels previously described in literature [90,98-101]. In addition, SEM images also clearly showed that nanofibers could be found within the aggregate (Fig. 3.11A & B). However, in many instances, there were fewer or no nanofibers present inside the aggregates while fibers were found along the immediate exterior of the spheroids (Fig. 3.11C & D). We speculate that the biodegradable PCLEEP nanofiber within the aggregates, in this instance, might have been degraded and absorbed by the hepatocytes.

3.5 Discussion

Previous studies on polyurethane foam scaffolds or collagen-treated silicon scaffolds with micro-channels of super-cellular pore sizes and partition barriers have shown that hepatocyte aggregates would conform to the shape of the pore space [93,94,89-91,105-107]. The partition barriers and pores of the scaffold do influence the way hepatocytes move and organize themselves into multi-cellular aggregates. However, little information is available to suggest how hepatocytes would respond when they are cultured on a micro- or nanofiber substrate with sub-cellular-sized pores, where such a substrate would present itself as a ‘‘rough’’ or ‘‘textured’’ surface to a rounded hepatocyte.

Scaffold micro-architecture and topography have been shown in literature to influence cell migration, adhesion, proliferation and various other cell behaviors, especially for smooth muscle cell, fibroblast or endothelial cell types [14-27,55-59]. However, scaffold topography alone does not promote favorable cell morphology and functional maintenance of primary rat hepatocytes, as shown in the results presented. This is echoed by a number of studies aiming to immobilize hepatocytes in porous scaffolds or on substrates through surface conjugation of functional ligands (e.g. galactosylation [33,34,112-120], collagen treatment [87-92]) or high-density cell entrapment [93,94,105-107].

In this study, our goal was to examine whether the introduction of a sub-cellular sized, highly textured topography, together with the surface-conjugated galactose ligand, would further influence spheroid formation and functional maintenance of hepatocytes. Electrospinning was used because it could lead to polymeric nanofiber mesh with sub-micron diameter fibers (average of ~760 nm), which randomly overlaid one another to form a highly textured, sub-cellular-sized micro-porous

scaffold. This study represents the first one where cell-adhesive molecules are covalently attached to an electrospun scaffold for cell-substrate interaction studies. Galactose ligands (AHG) were covalently conjugated onto the PAAc-grafted nanofiber mesh, because several studies have shown that biomaterial surfaces conjugated with galactose ligands can improve hepatocyte attachment and retain most of the cellular functions [33,34,112-120]. The characteristic attributes of these galactosylated substrates are that:

(1) Hepatocytes specifically adhere to these surfaces through galactose-ASGPR interactions; and

(2) The propensity of hepatocytes to form aggregates or spheroids on them, in concomitance with maintaining higher hepatocyte synthetic functions.

Hepatocytes cultured on galactosylated scaffolds (Gal-nanomesh and Gal-film groups) clearly showed superior functions in terms of cell attachment, albumin synthesis and 3-Mc-induced cytochrome P450 function, and to a less extent, the urea synthesis activity, as compared to hepatocytes cultured on unmodified scaffolds (Un-nanomesh and Un-film control groups). Consistent with previous reports on galactosylated membrane hepatocyte cultures [33,34], the albumin synthesis function and urea synthesis function decreased over time, whereas cytochrome P450 function peaked at day 5 followed by a decrease. This again suggested the complexity of hepatocyte functional maintenance: different set of synthetic functions could be influenced by biochemical cues or topological cues to a different extent.

The initial albumin secretion level and cytochrome P450 activity of hepatocytes on Gal-nanomesh were higher than Gal-film on day 1–2, but the functional profiles at later time points for Gal-nanomesh group and Gal-film group were surprisingly

similar, even though the spheroid morphologies displayed by hepatocytes in these two groups were different: spheroids on the Gal-film appeared mostly spherical, with a small and flattened interface with PCLEEP film; on the other hand, spheroids on Gal-nanomesh were flattened and integrated into the nanofiber mesh scaffold. It appears that so long as individual hepatocytes were able to aggregate and resume appropriate homotypic cell–cell contacts, hepatocyte viability and functions could be maintained at a higher level compared to unmodified substrates, regardless of the resulting shape of the spheroids. It suggests that the biochemical cue (galactose group on the substrate) in this case has a higher impact on cell functional maintenance compared with topological cue (nanofiber substrate *vs.* 2-D film).

Hepatocytes cultured on galactosylated nanofiber mesh presented an interesting morphology: hepatocytes formed spheroids that engulfed the galactosylated nanofibers. As a consequence of this, spheroids were immobilized on the scaffold and would not detach from the substrate upon agitation, unlike those attached on galactosylated film. It appears that galactose-ASGPR ligand-receptor interaction allowed hepatocytes to aggregate around and within the galactosylated nanofiber mesh. This observation indicates that the nanofiber topography enhances the overall cell-substrate interaction, comparing with the galactosylated 2-D film. The increased cell-substrate interaction is significant enough to alter the spheroid morphology (somewhat flattened *vs.* spheroidal).

This hepatocyte spheroid immobilization and stabilization strategy through the use of galactosylated nanofiber scaffolds would be advantageous in the design of a bioartificial liver device, where the hepatocytes could attach to a substrate/scaffold with high surface area immobilized with a cell-specific ligand, maintain their

differentiated functions, and remain stable against the perfusion and shear forces in the bioreactor.

3.6 Concluding Remarks

We have shown in this chapter that hepatocyte functions are maintained on galactosylated nanofiber scaffolds, similar to a galactosylated-film substrate configuration. Interestingly, galactosylated nanofiber scaffolds exhibit the unique property of promoting hepatocyte aggregates and cell infiltration within the mesh and around the fibers, forming an integrated spheroid-nanofiber construct.

This mechanically stable hepatocyte–nanofiber construct suggests the potential application of galactosylated nanofiber scaffold in liver cell culture. For example, this system will have advantages in a bioartificial liver (BAL) setting, where high densities of stable, immobilized spheroids can be maintained on galactosylated nanofiber scaffolds within the BAL bioreactor.

These results also demonstrated that the nanofiber topography together with surface-immobilized galactose ligand synergistically enhance cell-substrate interaction as indicated by hepatocyte adhesion and infiltration, even though this enhanced cell-substrate interaction did not translate into significantly higher functional enhancement as compared to galactosylated film condition.

Therefore, we shall demonstrate in the following chapter how higher hepatocyte functional enhancement (cytochrome P450 activity) can be brought about through further bio-functionalization of the galactosylated nanofiber scaffold.

CHAPTER FOUR

Hepatocyte Cytochrome P450 Inducing Dual-Functional Nanofiber Scaffolds for Hepatocyte Culture

4.1 Summary

In nature, cell survival, proliferation, differentiation and functions are regulated by a set of complex, spatially and temporally controlled milieu of biochemical and topographical cues emanated from the extracellular microenvironment. In order to create a cell culture scaffold that can deliver multiple microenvironmental cues that can influence cell fate and functions, we had designed a novel dual-functional electrospun nanofiber scaffold comprised of two nanofiber mesh layers that were modified differently to induce two separate biological responses from hepatocytes. The first nanofiber layer was galactosylated to mediate hepatocyte attachment and induce aggregation formation, while the second layer was loaded with 3-methylcholanthrene (3-Mc) to enhance cytochrome P450 activity of hepatocytes.

Primary rat hepatocytes cultured on the galactosylated nanofiber scaffolds loaded with different concentrations of 3-Mc were compared for their cell attachment efficiency, albumin secretion activity and their cytochrome P450-dependent 7-ethoxycoumarin O-deethylase activity. This dual functional nanofiber scaffold mediated hepatocyte attachment with slightly lower efficiency as compared to single layer galactosylated nanofiber scaffold. More importantly, cytochrome P450 activity of the hepatocytes cultured on the multi-functional scaffold correlated well with 3-Mc loading level. Transwell experiments showed that transfer of 3-Mc to hepatocytes through cell-fiber direct contact was the dominant transport route. This study

demonstrated the feasibility of creating multi-functional nanofiber scaffolds that serves both as an adhesive substrate and as a delivery vehicle for bioactive molecules.

4.2 Introduction

Electrospun polymeric nanofibers have demonstrated its potential in many biomedical applications, including the production of scaffolds for tissue engineering [14-27] and bioactive molecules delivery [43,67-69]. In the tissue engineering context, the high porosity and surface area to volume ratio achievable in a typical electrospun nanofiber scaffold provided large areas and spaces for cell attachment and the topographical features provided by electrospun fibers play a significant role in regulating cell responses [14-27]. The versatility of the electrospinning process also produced many different fibrous scaffolds with distinct geometry. For example, on axially aligned nanofiber scaffolds, neuronal cells and cardiomyocytes have been shown to grow axially along the fiber's orientation [20,25]. Neuronal cells have also been shown to elongate at different rates on aligned nanofiber scaffolds with different fiber diameters [25].

Recently, nanofiber modification techniques were also explored in order to control specific cell responses through the use of ligands or drugs incorporated into the scaffold. Nanofiber modification techniques can be broadly categorized under 2 methods: The first method involves the doping of bioactive molecules or protein factors into the polymer solution prior to electrospinning (Chapter 2.5.1). This method results in a nanofiber scaffold that can steadily release these molecules or proteins to the cells in culture [43,67-69]. The second method involves chemical modification of the polymer itself that results in covalently attached ligands on the surface of the nanofiber (Chapter 2.5.2) [70-73]. This method resulted in a bioactive nanofiber

surface that can interact with specific ligand receptors on cell membranes and thus inducing specific responses from the cells.

In the previous chapter, we had developed a surface bio-functionalized nanofiber scaffold for primary hepatocyte culture. Poly(acrylic acid) was first grafted onto the fiber surface by photo-polymerization to introduce surface carboxylic acid groups. Subsequently, amine-functionalized galactose ligands were conjugated onto the nanofiber surface using carbodiimide cross-linking chemistry. The galactosylated nanofiber scaffold was able to mediate primary hepatocyte adhesion through the galactose – asialoglycoprotein receptor (ASGPR) interaction. The galactosylated nanofiber scaffold induced the formation of spheroids that enveloped the functional nanofibers, resulting in an integrated spheroid-nanofiber construct.

This unique cell-fiber interaction could maintain hepatocyte viability and certain functions like albumin production and urea synthesis. However, one of the crucial functions, cytochrome P450 enzymatic activity was low, even though it can be induced through stimulation by 3-methylcholanthrene (3-Mc) in the culture media. 3-Mc, a polycyclic aromatic hydrocarbon, is a potent inducer for the induction of CYP1-dependent xenobiotic oxidation, and is used extensively in various hepatocyte studies [97,125-127,129]. However, hepatocyte cytochrome P450 induction required repeated 3-Mc doping in culture medium, as 3-Mc solubility in aqueous solution is low [130,131]. Therefore, we had fabricated a 3-Mc loaded nanofiber scaffold with the assumption that hepatocyte cultured on this scaffold will have enhanced cytochrome P450 activity through the absorption of 3-Mc released by the scaffold.

In this present study, we have designed a dual biofunctional electrospun nanofiber scaffold through the layering of two nanofiber meshes that are modified

differently to induce two separate biological responses from hepatocytes (Fig. 4.1). The first nanofiber layer is galactosylated to mediate hepatocyte attachment and aggregation formation, while the second layer is 3-Mc loaded to enhance cytochrome P450 activity in hepatocytes. Primary hepatocytes cultured on galactosylated nanofiber scaffolds loaded with different concentrations of 3-Mc will be compared for their P450-dependent 7-ethoxycoumarin O-deethylase activity. In addition, the mode of release of 3-Mc to the hepatocytes will also be investigated using transwell cultures.

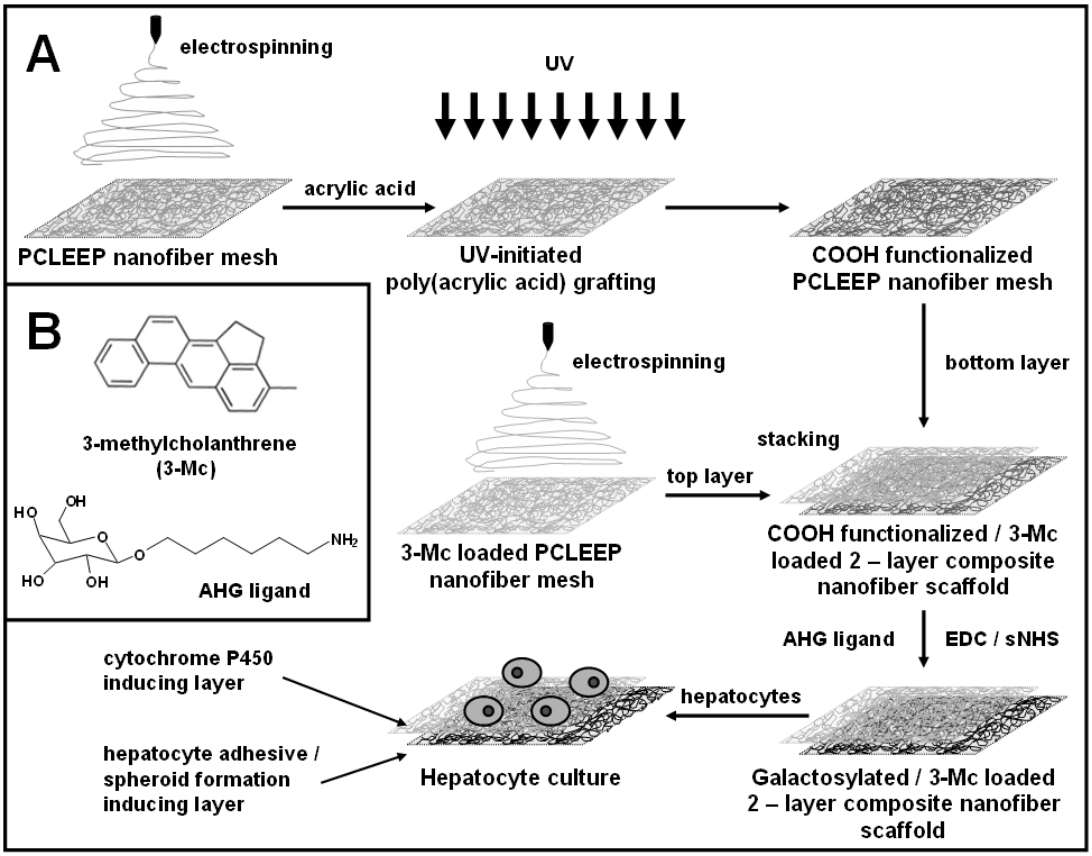

Figure 4.1: (A) Electrospun galactosylated, 3-Mc loaded PCLEEP nanofiber scaffold fabrication scheme. (B) Chemical structures of 3-methylcholanthrene (3-Mc) and 1-O-(6'-aminohexyl)-D-galactopyranoside (AHG), used in the functionalization of the PCLEEP nanofiber scaffold.

4.3 Experimental Methods

All chemicals were purchased from Sigma-Aldrich unless otherwise stated.

4.3.1 Fabrication of Dual-Functional Nanofiber Scaffolds

As illustrated in Fig. 4.1, the dual biofunctional electrospun nanofiber scaffold was systematically assembled through the layering of two nanofiber meshes that are modified differently with different bioactive molecules. The following subsections describe in detail the nanofiber scaffold modification and assembly process.

4.3.1.1 Electrospinning of Undoped Nanofiber Mesh

Detailed protocols for undoped PCLEEP nanofiber layer fabrication can be found in Chapter 3.3.1. The collection time for each mesh was 3 min.

4.3.1.2 Poly(acrylic acid) Grafting of Undoped Nanofiber Mesh

The undoped PCLEEP nanofiber layer was subsequently grafted with Poly(acrylic acid) (PAAc). Detailed protocols for PCLEEP nanofiber PAAc grafting can be found in Chapter 3.3.1.1. 5% AAc solution was used for the grafting reaction. The carboxylic acid group density on the meshes was tested to be between 50-65 nmol/cm^2, using Toluidine Blue O staining method [33].

4.3.1.3 Electrospinning of 3-Mc Loaded Nanofiber Mesh

PCLEEP copolymer was dissolved in 7:3 dichloromethane / methanol solvent mixture at 8.0 wt% concentrations in 2-mL centrifuge tubes. 3-Mc was then added to the polymer solution at 0, 0.1, 1.0, 5.0 and 8.0 wt% of the amount of PCLEEP copolymer in each tube. After 3-Mc had dissolved and thoroughly mixed, the 3-Mc loaded polymer solutions were then electrospun into nanofiber meshes using the same electrospinning parameters as the fabrication of undoped PCLEEP nanofibers (Fig. 4.1). However, the collection time was reduced to 1.5 min to produce a thinner mesh

compared to the undoped PCLEEP nanofiber mesh. The 3-Mc loaded nanofiber mesh were subsequently cut and immobilized over each PAAc-grafted undoped PCLEEP nanofiber mesh. Thus, a carboxylic acid functionalized, 3-Mc loaded 2-layer composite nanofiber scaffold was formed.

4.3.1.4 Galactosylation of Composite Nanofiber Scaffold

To make the composite nanofiber scaffold specific for hepatocyte attachment and aggregation, we further galactosylate the scaffold by conjugating 1-O-(6'-Aminohexyl)-D-galactopyranoside (AHG) onto the carboxylic acid functionalized layer using carbodiimide cross-linking chemistry. Detailed protocols for AHG bio-conjugation onto PAAc-grafted PCLEEP nanofiber mesh can be found in Chapter 3.3.1.2. The morphologies of 3-Mc loaded fibers and galactosylated fibers were imaged using a field emission scanning electron microscope (FESEM, FEI Company) after gold sputter-coating. Representative images were analyzed using ImageJ image processing software (http://rsb.info.nih.gov/ij/) to extract fiber diameter, pore size (area), mesh thickness and Feret's diameter[5] information. At least 250 measurements were recorded for each analysis.

4.3.2 Hepatocyte Culture and Assays

4.3.2.1 Hepatocytes Isolation

Detailed hepatocyte isolation protocol can be found in Chapter 3.3.2.1.

4.3.2.2 Hepatocyte Attachment Assay

Freshly isolated rat hepatocytes (3.5×10^5) were seeded onto each 15 mm diameter composite scaffold disks (2×10^5 cells/cm^2), and cultured in William's E

[5] Feret's Diameter is defined as the longest distance between any two points along the selection boundary, also known as the caliper length.

medium supplemented with 0.5 mg/mL BSA, 10 ng/mL EGF, 500 ng/mL insulin, 15 nM dexamethasone, 50 ng/mL linoleic acid, 2 mM L-glutamine, 100 units/mL penicillin, 0.1 mg/mL streptomycin, 50 pM $ZnSO_4$ and 100 nM $CuSO_4$. For controls, hepatocytes were also cultured on single layer galactosylated nanofiber scaffolds without 3-Mc loaded, as well as on tissue culture polystyrene surface (TCPS). Cells were cultured in a 37^{o}C incubator fed with 5% CO_2. After 3 h of incubation, all unattached cells were washed off by gentle washing using culture medium, and collected by centrifugation (2,000 rpm). The cell pellet was washed once with PBS and then lysed with cell lysis buffer (Promega).

The protein concentration in the lysate was determined using a BCA protein assay kit (Pierce). The number of unattached cells was determined by comparing the protein concentration in lysate with a standard curve generated with known numbers of cells. Subsequently, the attachment efficiency of hepatocytes on different scaffolds was calculated based on the cell number of the unattached cells for each scaffold.

4.3.2.3 Hepatocyte Culture Maintenance

The attached hepatocytes on different scaffolds were cultured in supplemented William's E medium as described above. Fresh medium was replenished daily, and old medium was collected for albumin determination. Collected medium was centrifuged at 4,000 rpm for 10 min and the supernatant was stored at –20^{o}C.

4.3.2.4 Cytochrome P450 Activity Assay

Cultures were tested for the P450 enzymatic activity (P450-dependent 7-ethoxycoumarin O-deethylase activity) as described previously [97,125-127], with modifications. 3-Mc and 7-ethoxycoumarin first were dissolved in dimethylsulfoxide (DMSO) and then diluted to their working concentrations with culture medium. The

final concentration of DMSO was below 0.3%. On Days 1, 3, and 5, the control conditions (hepatocytes cultured on single layer galactosylated nanofiber scaffolds without 3-Mc loaded, and on TCPS control) were pre-incubated in culture medium containing 0.05 mM 3-Mc for 24 h to induce cytochrome P450 production. Then on Days 2, 4, and 6, all culture conditions were refreshed with culture medium containing 0.26 mM 7-ethoxycoumarin substrate. After 5 h incubation, the 7-ethoxycoumarin-containing medium was collected and the cultures were refreshed with normal culture medium. The medium samples collected were stored at –20^{o}C and subsequently assayed for 7-hydroxycoumarin (HCOD) using HPLC. Subsequently, the samples are processed for HPLC analysis as described in Chapter 3.3.2.6.

4.3.2.5 Albumin Secretion Assay

Detailed protocols for the albumin secretion assay can be found in Chapter 3.3.2.4.

4.3.2.6 Transwell Cultures

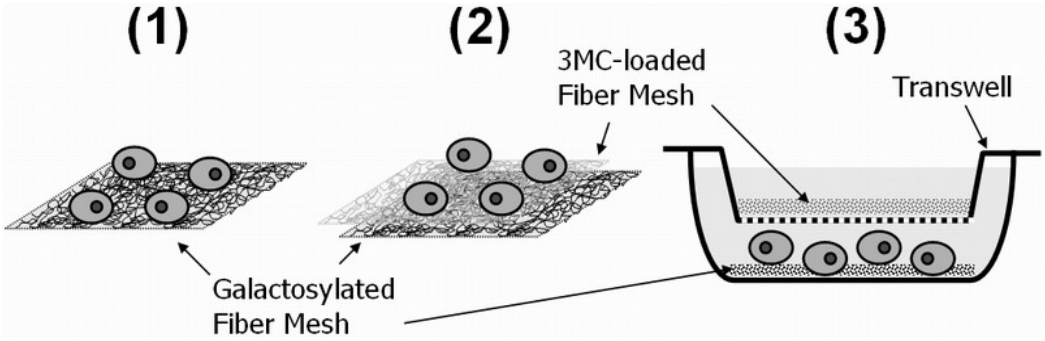

Figure 4.2: Scaffold condition illustration for transwell experiment. (1) Galactosylated nanofiber scaffold, (2) 8.0wt% 3-Mc loaded galactosylated nanofiber scaffold, and (3) Transwell scaffold configuration.

Three different scaffold conditions were tested as illustrated in Fig. 4.2: (1) Undoped galactosylated nanofiber scaffold, (2) 8.0 wt% 3-Mc loaded galactosylated

nanofiber scaffold, and (3) a transwell configuration where the bottom partition (containing an undoped galactosylated nanofiber scaffold) is separated from the top partition (containing a 8.0 wt% 3-Mc loaded nanofiber mesh) through a 400 nm pore size polyester membrane transwell insert (Corning). For the third condition, hepatocytes were seeded onto the bottom partition only, so the cells have no physical contact with the 3-Mc loaded nanofiber mesh in the upper partition. The hepatocytes were cultured in supplemented William's E medium and cultures on days 2, 4, and 6 were tested for the P450 enzymatic activity as described above.

4.3.3 Statistical Analysis

All values were expressed as mean ± standard deviation (SD). Statistical differences were determined by two-tailed student's t-test.

4.4 Experimental Results and Discussion

4.4.1 Dual-Functional Nanofiber Scaffold Characterization

A schematic of scaffold fabrication process was illustrated in Fig. 4.1. Briefly, a thicker undoped PCLEEP nanofiber mesh and a thinner 3-Mc loaded PCLEEP nanofiber mesh were separately fabricated through electrospinning. After the undoped mesh was grafted with poly(acrylic acid), the 2 meshes were then stacked together, with the 3-Mc loaded mesh forming the top layer. Subsequently, a galactose ligand was conjugated onto the poly(acrylic acid) grafted layer, thus creating a galactosylated, 3-Mc loaded composite nanofiber scaffold.

Image analysis of the thicker undoped mesh showed a fiber diameter distribution of 730 ± 270 nm (Fig. 4.3A), while similar analysis of the thinner 3-Mc loaded mesh showed comparable fiber diameter distribution of 760 ± 280 nm (Fig. 4.3B). 3-Mc

loading at all concentrations did not affect the resultant fiber diameter ($p > 0.05$ compared with undoped fibers). This result was expected as 3-Mc is an uncharged molecule, and it was established extensively in literature that only charged molecules can significantly affect the electrospun fiber diameters [12,41-44]. Image analysis of the thinner 3-Mc loaded mesh also showed a mesh thickness of 1–3 fiber diameters thick, with a wide through-pore size distribution of 7.4 ± 7.2 μm^2 and through-pore Feret's diameter of 2.7 ± 1.3 μm (Fig. 4.3B).

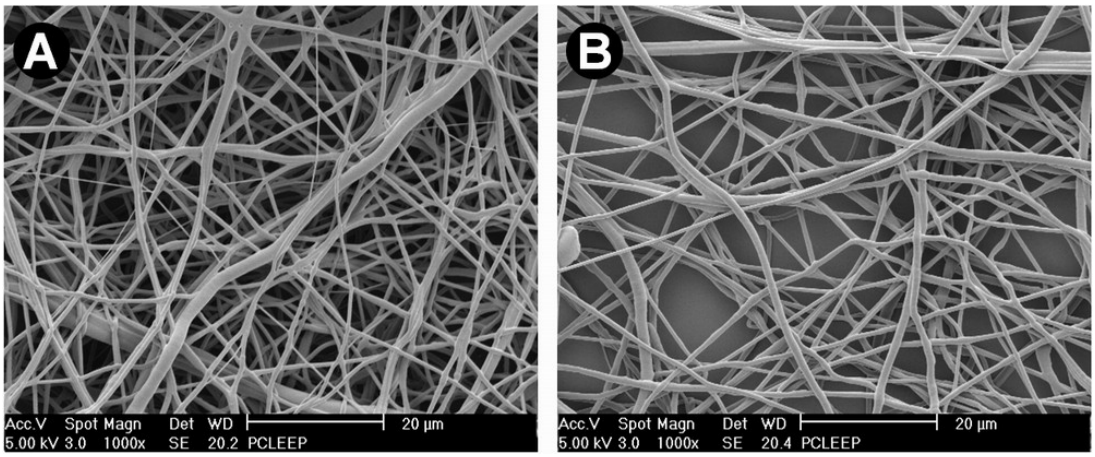

Figure 4.3: SEM images of electrospun PCLEEP nanofiber mesh layers: (A) Denser bottom layer that was functionalized with AHG ligand; (B) 3-Mc loaded (5 wt% of PCLEEP) nanofiber top layer that will be stacked over the denser bottom layer. Fibers in the top layer were less dense and numerous through-pores were present to facilitate hepatocyte interaction with the galactosylated bottom layer.

It is worth noting that our initial attempt was to create a single galactosylated 3-Mc loaded electrospun nanofiber mesh layer instead of a dual layer. However, we were unable to achieve this because the UV-initiated poly(acrylic acid) grafting post-electrospinning step will also modify the 3-Mc loaded in the fiber, rendering it non-bioactive. Thus a two layer stacking fabrication approach was necessary in this case. An obvious advantage of the two-layered nanofiber scaffold was that it allowed the titration of two different types of cues independently.

4.4.2 Hepatocyte Attachment Efficiency

Hepatocytes cultured on various galactosylated 3-Mc loaded composite nanofiber scaffolds (gnPCLEEP with 0 to 8% 3-Mc) exhibited similarly high hepatocyte attachment efficiency (76% ± 2.3%) 3 h after cell seeding (Fig. 4.4). The 3-Mc concentration in nanofiber scaffold did not significantly influence cell attachment efficiency ($p > 0.05$ comparing the cell attachment efficiencies of all composite scaffolds conditions). Without surface galactosylation (TCPS control), the attachment efficiency was poor (30%). Cell attachment was highest (84%) for single layer galactosylated scaffolds (gnPCLEEP control), suggesting that for the composite scaffolds, the upper non-galactosylated layer could slightly hinder cell attachment ($p < 0.05$ compared to cell attachment efficiencies of composite scaffold conditions). Obviously, this effect will depend on the thickness and pore size of the upper layer. In this study, the upper layer was thin and highly porous (Fig. 4.3B) and the hepatocytes could still interact with the lower galactosylated nanofiber layer.

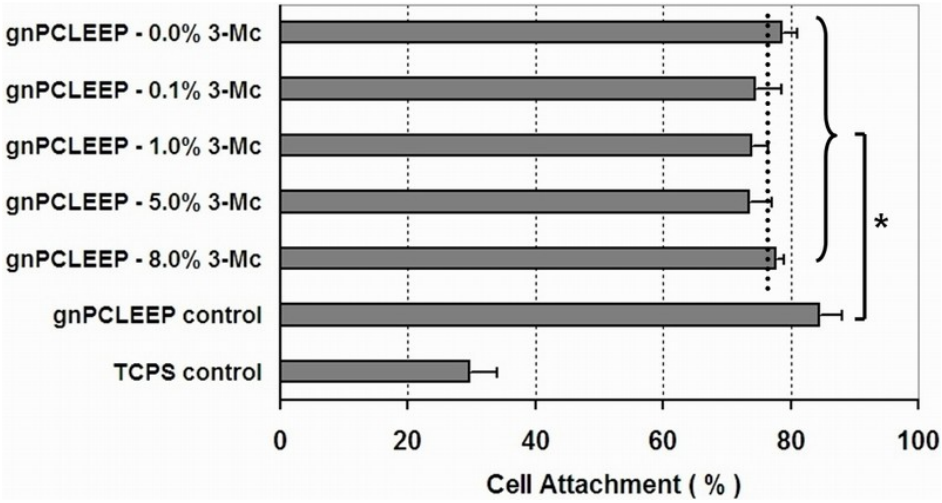

Figure 4.4: Hepatocyte attachment on various galactosylated 3-Mc loaded composite nanofiber scaffolds (gnPCLEEP (0.0-8.0)% 3-Mc), single layer galactosylated scaffolds (gnPCLEEP control) and TCPS control 3 h after cell seeding. Dotted line represents combined mean of gnPCLEEP (0.0-8.0)% 3-Mc conditions. Data are means ± SD, n = 6. * indicates $p < 0.05$.

4.4.3 Cytochrome P450 Function

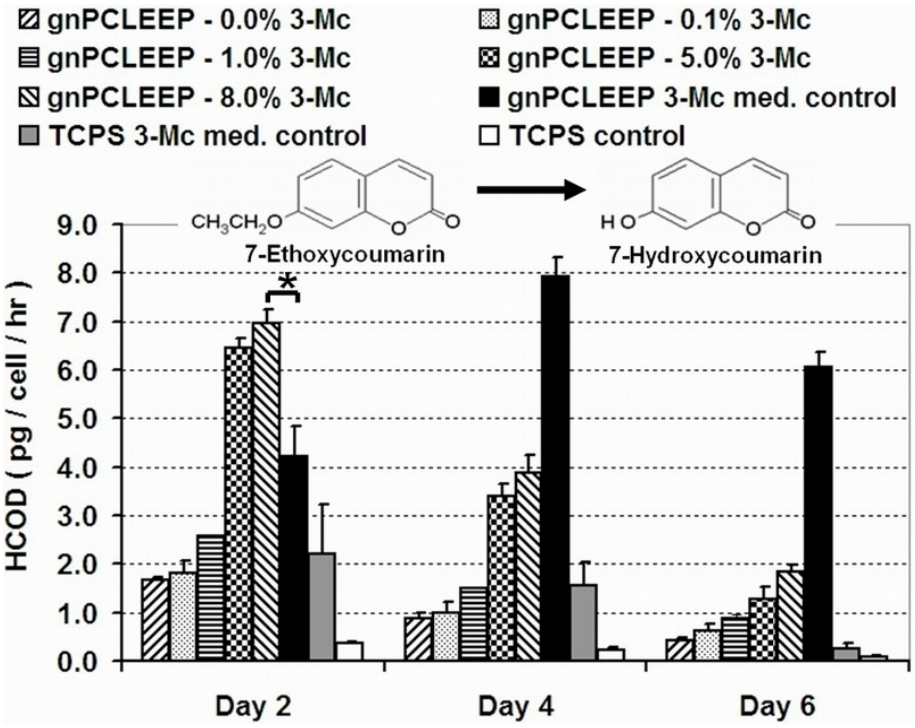

Figure 4.5: Cytochrome P450 function of hepatocytes at various time points normalized against the total number of attached cells. Hepatocytes were cultured on galactosylated 3-Mc loaded composite nanofiber scaffolds, on single layer galactosylated scaffolds in 3-Mc containing medium (gnPCLEEP 3-Mc med. control) and on TCPS controls. Data are means ± SD, n = 3. * indicates $p < 0.05$.

On galactosylated 3-Mc loaded composite scaffolds, the hepatocyte cytochrome P450-dependent 7-ethoxycoumarin O-deethylase activity was strongly correlated with the 3-Mc concentration loaded into the scaffolds (Fig. 4.5). The hepatocyte cytochrome P450 activity increased with 3-Mc concentration, with the highest HCOD production rate recorded at 7.0 pg/cell/h for gnPCLEEP 8.0% 3-Mc scaffold condition on day 2. This rate is significantly higher ($p < 0.05$) than the gnPCLEEP 3-Mc medium control condition on day 2 (4.2 pg/cell/h), where the 3-Mc concentration used (0.05 mM) was the highest concentration reported in literature that will not interfere with other hepatocyte functions [97,126,127]. This result showed that drug-loaded

nanofiber was a more efficient lipophilic drug delivery vehicle as compared to supplementation into the medium, especially at early culture time points.

Hepatocytes cultured on the galactosylated 3-Mc loaded composite scaffolds showed decreased cytochrome P450 activity with time. This can be attributed to the gradual loss of 3-Mc from the nanofiber, which was depleted through gradual diffusion and metabolization [129] by the attached hepatocytes. In contrast, P450 function of hepatocytes cultured on single layer galactosylated scaffold controls with daily supplementation of 3-Mc in the medium peaked at day 4 (7.9 pg/cell/h). We have attributed this observation to hepatocyte reorganization on the galactosylated scaffold, which may have changed the cytochrome P450 inducing susceptibility (Chapter 3.4 & 3.5).

4.4.4 Albumin Synthesis Function

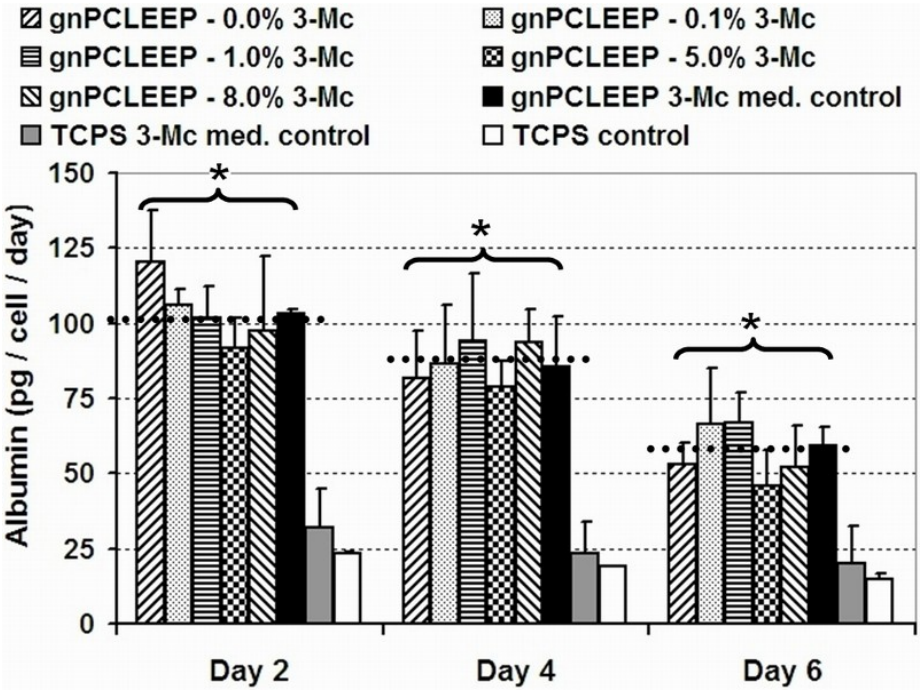

Figure 4.6: Albumin synthesis function of hepatocytes at various time points normalized against the total number of attached cells. Dotted line represents combined mean of gnPCLEEP (0.0-8.0)% 3-Mc and gnPCLEEP 3-Mc med. control conditions. Data are means ± SD, n = 3. * indicates $p > 0.05$.

Hepatocytes cultured on non-galactosylated (TCPS) surfaces showed poorer albumin synthesis function as compared to hepatocytes cultured on galactosylated scaffolds (Fig. 4.6). In addition, hepatocytes cultured on galactosylated composite scaffolds with no 3-Mc loaded (gnPCLEEP 0% 3-Mc), galactosylated 3-Mc loaded composite scaffolds (gnPCLEEP (0.1-8.0%) 3-Mc), and gnPCLEEP 3-Mc medium control all showed comparable albumin secretion profiles ($p > 0.05$) throughout the culture (Fig. 4.6). This highlights that the hepatocyte albumin synthesis function was not affected by the various 3-Mc concentrations loaded in composite scaffolds.

4.4.5 Mechanism of 3-Mc Transport from Nanofiber to Cell

Two 3-Mc transport mechanisms were possible: (1) 3-Mc could be transported by first through diffusion from fiber into the medium, and then transported from the medium into the hepatocytes; and/or (2) 3-Mc could be directly transported through diffusion from the 3-Mc fibers to the hepatocyte through fiber – hepatocyte membrane contact. A transwell culture was then set up to investigate the mode of 3-Mc transfer to hepatocytes (Fig. 4.7).

Results show that for hepatocytes cultured in the transwell condition (gnPCLEEP 8.0% 3-Mc transwell), the cytochrome P450 function remained low (1.3-1.6 pg/cell/h) but consistently higher than the non 3-Mc scaffold culture (gnPCLEEP control, 0.4-0.8 pg/cell/h) throughout the entire culture period, indicating that the former 3-Mc transport mechanism may only play a minor role in 3-Mc delivery. This observation maybe due to 3-Mc low solubility (1.07×10^{-8} M) under aqueous condition [130,131], which made dissolution into the medium limited. On the other hand, hepatocytes cultured on the dual functional gnPCLEEP 8.0% 3-Mc scaffold expressed cytochrome P450 function (3.2-6.3 pg/cell/h) that was significantly higher ($p < 0.05$)

than that of gnPCLEEP 8.0% 3-Mc transwell condition throughout the entire culture period, indicating that the latter 3-Mc transport mechanism as the more dominant 3-Mc delivery route. This result suggests that due to the adhesion of hepatocytes on the galactosylated nanofibers, the hepatocytes had direct contact with the 3-Mc loaded fibers; this cell – 3-Mc fiber contact might have played an important role in facilitating the diffusion of 3-Mc from the fibers to the hepatocytes.

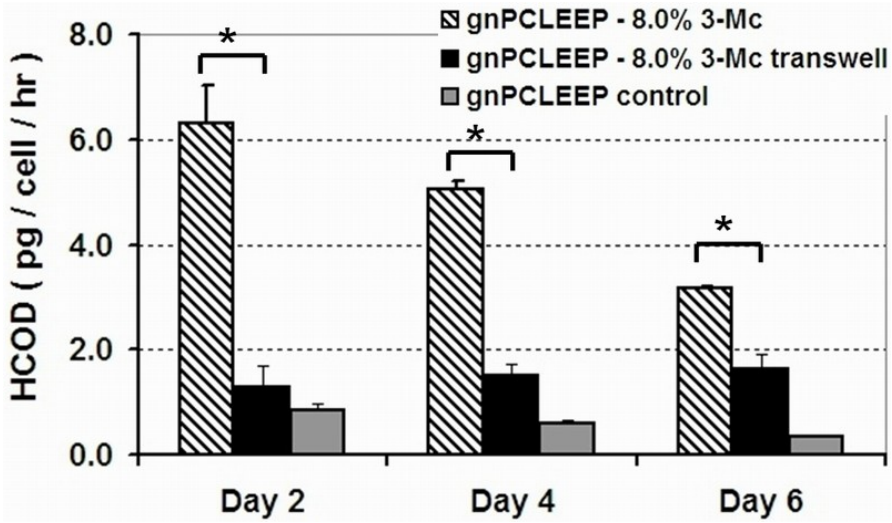

Figure 4.7: Cytochrome P450 function of hepatocytes at various time points normalized against the total number of attached cells. For gnPCLEEP 8% 3-Mc transwell condition, hepatocytes were cultured without physical contact with the 8.0% 3-Mc mesh. Data are means ± SD, n = 3. * indicates $p < 0.05$.

4.5 Concluding Remarks

By taking advantage of the porous and layer-forming properties of electrospun nanofibers, we had designed a dual functional scaffold that induces two different biological responses from hepatocytes. Galactose bio-functionalization on nanofibers resulted in a scaffold that can induce hepatocyte adhesion and re-organization, while 3-Mc loading into the fiber, working together with fiber galactosylation, resulted in a hepatocyte bioactive scaffold that can also regulate the hepatocyte cytochrome P450 function. In essence, this hepatocyte-drug delivery model can be modified to deliver

many other lipophilic bioactive molecules [130,131] that may have therapeutic effects for liver cell cultures. By careful understanding of cell-substrate interactions and bioactive molecules effects of other cell models, we could extend this multi-functional scaffold strategy to induce synergistic cellular responses for other cell culture applications.

In the following chapter, we will further investigate the efficacy of this nanofiber bio-functionalization strategy with another cell culture system: hematopoietic stem / progenitor cell expansion. This time, using amine molecule bio-functionalization, we will explore the synergistic effects that nanofiber topography and surface immobilized biochemical cues play in enhancing cell-scaffold interactions and regulating cellular functions like cell proliferation and multipotency phenotype maintenance.

CHAPTER FIVE

Aminated Nanofiber Scaffolds Enhance Adhesion and Expansion of Human Umbilical Cord Blood Hematopoietic Stem/Progenitor Cells

5.1 Summary

Interaction between hematopoietic stem/progenitor cells (HSPCs) and their extra cellular matrix components is an integral part of the signaling control for HSPC survival, proliferation and differentiation. We hypothesized that both substrate topographical cues and biochemical cues could act synergistically with cytokine supplementation to improve *ex vivo* expansion of HSPCs.

In this study, we compared the *ex vivo* expansion of human umbilical cord blood $CD34^+$ cells on unmodified, hydroxylated, carboxylated and aminated nanofibers and films. Results from 10-day expansion cultures showed that aminated nanofiber mesh and film were most efficient in supporting the expansion of the $CD34^+CD45^+$ cells (195-fold and 178-fold respectively), as compared to tissue culture polystyrene (50-fold, $p < 0.05$). In particular, aminated nanofiber meshes supported a higher degree of cell adhesion and percentage of HSPCs, as compared to aminated films. SEM imaging revealed the discrete colonies of cells proliferating and interacting with the aminated nanofibers.

This study highlights the potential of a biomaterials approach to influence the proliferation and differentiation of HSPCs *ex vivo*.

5.2 Introduction

Umbilical cord blood is a promising alternative source of hematopoietic stem/progenitor cells (HSPCs) for allogeneic and autologous hematopoietic stem cell transplantation for the treatment of a variety of hematological disorders and as a supportive therapy for malignant diseases [132-140]. However, the low number of HSPCs obtainable from a single donor restricts its widespread application as a viable source of transplantable hematopoietic cells in adults [141-145]. As the success of HSPC transplantation is dependent on both the cell dose and the pluripotency of the cells that are transplanted, an efficient and practical *ex vivo* expansion strategy is necessary to produce sufficient quantity of HSPCs that can engraft and sustain long-term hematopoiesis for adult patients.

In conventional expansion culture, HSPCs are generally regarded as suspension cells and numerous protocols implement HSPC suspension culture in the presence of various combinations of early acting cytokines [132-139,173-177]. They are often performed in flasks or bags that provide no micro-architecture for cellular interaction with the substrate. However, it is generally accepted that the native bone marrow microenvironment provides a complex 3-D meshwork of extracellular matrix (ECM) that serves as a stem cell niche to regulate HSPC functions [137-140]. A growing body of evidence suggests the importance of surface chemistry as well as topographical features on the rate of HSPC proliferation and $CD34^+$ cell expansion [178-185]. These results suggest that biochemical as well as topographical cues could be actively involved in dictating the proliferation and differentiation of cultured HSPCs.

Electrospinning has recently been employed as a versatile technique to produce polymeric fibrous substrates for cell culture and tissue engineering applications [14-

27,63-66]. Several studies have shown that these fibrous scaffolds can enhance cellular responses like cell adhesion and cell phenotype maintenance [14-27,63-66]. In the previous chapters, we have demonstrated that polymeric nanofiber mesh with surface-conjugated galactose ligands stimulate the formation of hepatocyte spheroids that engulf the modified nanofibers, resulting in an integrated spheroid-nanofiber construct. This suggests that the functionalized nanofiber mesh enhanced hepatocyte-substrate interaction.

This observation prompted us to investigate whether the nano-topographical cues and various chemical cues on the nanofiber surface can synergistically influence HSPC adhesion, proliferation and multipotency phenotype maintenance. As the first of a series of studies, we examined HSPC expansion on surface-functionalized polyethersulfone (PES) nanofiber meshes and PES films. PES has been widely used as a non-degradable hollow fiber material in bioreactors for culturing mammalian cells [186,187]. It has been chosen as the substrate material because of its ease of processibility: (1) it can be dissolved and electrospun into nanofibers using mild solvents such as DMSO (Fig. 2.3); (2) PES membranes are commonly surface-modified through UV or plasma treatments [188]; and (3) the polymer is stable in solvents like acetonitrile, in which amination reactions can be carried out efficiently.

In this study, PES nanofibers and films were surface-conjugated with the simplest set of functional groups: carboxylic, hydroxyl and amino groups (Fig. 5.1). These set of surface functional groups have been shown to mediate different patterns of focal adhesion by immature osteoblast-like cells and different degrees of differentiation [189]. In this chapter, we have demonstrated that these surface-bound functional groups effected different levels of HSPC adhesion, proliferation, and

multipotency phenotype maintenance. In addition, the aminated nanofiber mesh induced the formation of unique cell colonies.

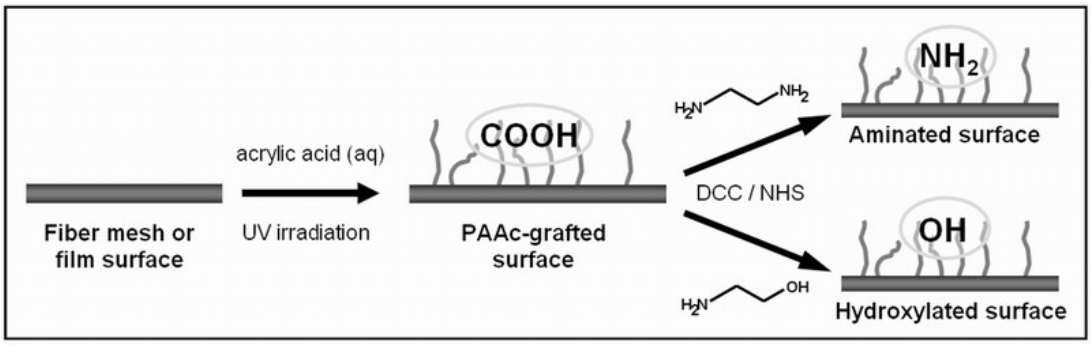

Figure 5.1: PES scaffold surface modification scheme.

5.3 Experimental Methods

All chemicals were purchased from Sigma-Aldrich unless otherwise stated.

5.3.1 Fabrication of PES Nanofiber Scaffolds

Polyethersulfone (PES) granules (Mw: 55,000) was purchased from Goodfellow Cambridge Limited. PES pellets were dissolved in dimethylsulfoxide (DMSO) at 20 wt% concentration and placed in a plastic syringe fitted with a 27G needle. A syringe pump (KD Scientific) was used to feed the polymer solution into the needle tip. The feed rate of the syringe pump was fixed at 0.3 mL/h. The PES nanofiber meshes were fabricated by electrospinning at 13 kV using a high voltage power supply (Gamma High Voltage Research). Nanofibers were collected directly onto grounded 15 mm diameter glass coverslips (Paul Marienfeld) located at a fixed distance of 160 mm from the needle tip, over a collection time of 25 min. PES films were fabricated by dip-coating glass in 10 wt% PES in DMSO. The deposited nanofiber and film samples were washed thoroughly in distilled water and then in ethanol to remove any residual DMSO, and subsequently dried and stored in a desiccator.

5.3.1.1 Surface Grafting of Scaffolds with Poly(acrylic acid)

Acrylic acid (AAc) (Merck) was distilled and stored at -20°C prior to use. Poly(acrylic acid) (PAAc) was grafted onto the PES nanofiber mesh surface by photo-polymerization, as described previously in Chapter 3.3 with slight modification on the grafting conditions. Briefly, samples were immersed in aqueous solution containing 3% AAc solution and 0.5 mM $NaIO_4$ in a flat-bottom glass container. The temperature of the solution was maintained at 8°C by cooling the container in a cold-water bath. The samples were then exposed to UV from a 400 W mercury lamp (5000-EC, Dymax) for 2 min at a distance of 25 cm. The PAAc-grafted meshes were then thoroughly washed with deionized water at 37°C for over 36 h to remove any ungrafted PAAc from the surface of the scaffold and dried in a storage desiccator.

5.3.1.2 Amination of Poly(acrylic acid) Grafted Scaffolds

The PAAc-grafted PES nanofiber mesh and films were further conjugated with ethylenediamine (EtDA) using a 2-step carbodiimide cross-linking method (Fig 5.4). Briefly, each scaffold was first gently shaken in 2 mL acetonitrile containing 50 mM N-hydroxysuccinimide (NHS) and 50 mM dicyclohexylcarbodiimide (DCC). After 6 h, the reaction solution was carefully aspirated and each scaffold was immediately immersed into 2 mL acetonitrile containing 0.03 mmol EtDA. After 12 h, the reaction solution was carefully aspirated and each scaffold was thoroughly washed in absolute ethanol to remove any dicyclohexyl urea (DCU), which is a by-product of the conjugation reaction.

As for control, several PAAc-grafted PES nanofiber meshes were hydroxylated instead, by conjugation with ethanolamine using the same modification protocol as described above. All substrates were subsequently sterilized in 70% ethanol, then loaded into 24-well tissue culture plates (Nunc) and stored in sterile PBS until use.

5.3.1.3 Surface Analysis of PES Scaffolds

Surface amine density was quantified according to the method described by Kakabakos et al. [190]. Briefly, primary amino groups on the substrates were first converted to sulfhydryl groups through reaction with excess 2-iminothiolane (Pierce). The surface sulfhydryl groups were then determined using a BCA assay kit (Pierce) using L-cysteine to generate a standard curve.

Surface wettability of the various substrates was characterized by measuring the water contact angle at room temperature using a video contact angle goniometer (Advanced Surface Technology).

Samples of unmodified and aminated PES nanofiber meshes were also imaged using a field emission scanning electron microscope (FESEM, FEI Company) for detection of any morphology changes caused by the entire amination process. Fiber diameters were measured by analyzing representative SEM mages of nanofibers using NIH ImageJ software (http://rsb.info.nih.gov/ij/). At least 250 measurements were recorded for each analysis.

5.3.2 Hematopoietic Stem Cell Culture and Assays

Frozen human umbilical cord blood $CD34^+$ HSPCs were purchased from AllCells, which were obtained from normal volunteers participating in an Institute Reviewing Board (IRB) approved donor program (AllCells). The $CD34^+$ purity in the HSPC was determined to be 98% by flow cytometry and the viability was determined to be more than 97% by Trypan blue. Purified recombinant human stem cell factor (SCF), Flt-3 ligand (Flt3), thrombopoietin (TPO) and IL-3 was purchased from Peprotech Inc. The StemSpan^{TM} serum-free expansion medium and MethoCult GF+ H4435 medium were all from StemCell Technologies.

5.3.2.1 *Ex Vivo* Hematopoietic Expansion Culture

For *ex vivo* HSPC expansion cultures, different substrates were secured at the bottoms of wells of a 24-well tissue culture plate. Six hundred HSPCs were seeded onto each scaffold in 0.6 mL StemSpan™ serum-free expansion medium, which consists of 1% BSA, 0.01 mg/mL recombinant human insulin, 0.2 mg/mL human transferrin, 0.1 mM 2-mercaptoethanol and 2 mM L-glutamine in Iscove's MDM, supplemented with 0.04 mg/mL low density lipoprotein (Athens Research and Technology Inc.), 100 ng/mL SCF, 100 ng/mL Flt3, 50 ng/mL TPO and 20 ng/mL IL-3. Cells were cultured at 37°C in an atmosphere containing 5% CO_2 for 10 days without medium change. Similar cultures were also performed on tissue culture polystyrene surface (TCPS), which serve as a positive control in this study. In total, 8 surface conditions were tested: TCPS, PES-(unmodified, carboxylated, aminated) films and PES-(unmodified, carboxylated, hydroxylated, aminated) nanofiber meshes.

Cells were harvested after 10 days of expansion. All substrates were washed once with non-trypsin cell dissociation solution and twice with 2% FBS Hanks' buffer at 5-10 min intervals between each wash. The cell suspensions collected were then concentrated through centrifugation at 500×g for 10 min. Aliquots of the concentrated cells were then used for cell counting by a hematocytometer, flow cytometry analysis, as well as for colony-forming cell assays.

5.3.2.2 Flow Cytometry

Fluorescently labeled antibodies for CD34 and other cell surface markers (CD13, CD15, CD19, CD38, CD45 and GlyA) were purchased from BD Biosciences. Fluorescently labeled antibodies for CD41 were purchased from Dako. Cell aliquots were incubated at 4°C for more than 30 min in 2% FBS Hanks' buffer in the presence

of various antibody combinations. After antibody staining, the cells were washed twice using Hanks' buffer and fixed in 1% paraformaldehyde.

Cells were analyzed by triple-color flow cytometry on a FACSCalibur analyzer (BD Biosciences). Relevant isotype controls were also included to confirm specificity and for compensation setting. At least 20,000 events were acquired. The Milan-Mulhouse gating method was used for cell enumeration [151], where a double gating ($CD34^+CD45^+$) strategy was used to identify the primitive hematopoietic progenitor cell population in the *ex vivo* expansion cultures. The CD34 marker is generally expressed by primitive hematopoietic progenitor cells, while CD45 marker is expressed on all cells of hematopoietic origin with the exception of red blood cells and their immediate precursors.

5.3.2.3 Colony-Forming Cell Assay

Aliquots of expanded cells from each scaffold condition in the expansion cultures were suspended into 3.3 mL of MethoCult GF+ H4435 medium (StemCell Technologies) and the cell suspension was plated onto two 35mm culture dish (1.1 mL each) as instructed in the procedure manual by StemCell Technologies. Duplicate assays are performed for each condition. The culture dishes were then incubated at 37°C, 5% CO_2 for 14 days, after which the number of erythropoietic colonies [erythroid burst-forming units (BFU-E)], granulopoietic colonies [granulocyte-macrophage CFU (CFU-GM)], and multilineage colonies (CFU-GEMM) were determined by manual counting under an inverted microscope. Positive colonies are scored on the basis of an accumulation of 20 or more cells. As a control, freshly thawed HSPCs were also evaluated for colony-forming potential.

5.3.2.4 Preparation for Scanning Electron Microscopy

Selected cultures samples were gently rinsed with PBS, fixed with 3% glutaraldehyde for 30 min at 20°C, and post-fixed with 1% osmium tetraoxide for another 15 min at 20°C. Samples were then dehydrated using a graded series of ethanol (25%, 50%, 70%, 90%, 95%, 100%, 100%) followed by hexamethyldisilazane drying. The samples were mounted onto aluminum stubs and gold sputter-coated before viewing under FESEM.

5.3.2.5 Preparation for Laser Scanning Confocal Microscopy

Selected culture samples were gently rinsed with Hanks' buffer and fixed with 1% formaldehyde for 10 min at 20°C and immediately washed with 2% FBS Hanks' buffer. Samples were then incubated with PE-labeled CD34 antibodies in 2% FBS Hanks' buffer for >30 min at 4°C. For nuclear staining, Syto16 (Invitrogen) was used. Fluorescent images were taken using a laser confocal microscope (Leica).

5.3.3 Statistical Analysis

All data were presented as mean ± standard deviation (SD). The statistical significance of the data obtained was analyzed by the Student's t-test. Probability values of $p < 0.05$ were interpreted as denoting statistical significance.

5.4 Experimental Results

5.4.1 Modification of PES Substrates and Surface Characterization

Nonwoven PES nanofiber meshes were prepared by electrospinning. Parameters that significantly influence the diameter, consistency and uniformity of the electrospun PES fibers included PES concentration in DMSO, applied voltage and needle-collector distance. These parameters were adjusted until unbeaded and uniform fibers could be obtained. The optimal conditions for obtaining such PES nanofiber

meshes were described in the Methods section. Under the optimized condition, fibers with an average diameter of 529 ± 114 nm were obtained (Fig. 5.2A & 5.2C). PES films were prepared as a 2-D control by dip-coating glass coverslips with a diameter of 15 mm. The film surface exhibited submicron bumps and the average film thickness was 22.5 ± 3.9 μm as analyzed from SEM images of freeze-fractured PES films.

The PES fiber meshes and films were first carboxylated by UV-initiated poly(acrylic acid) grafting. Amino or hydroxyl groups were subsequently introduced to the fiber or film surfaces by reacting ethylenediamine or ethanolamine with the surface carboxylic acid groups using carbodiimide chemistry. SEM images comparing unmodified and aminated PES nanofiber mesh (Fig. 5.2B) did not show any significant morphological difference, indicating that the modification steps did not cause significant degradation/ablation of PES.

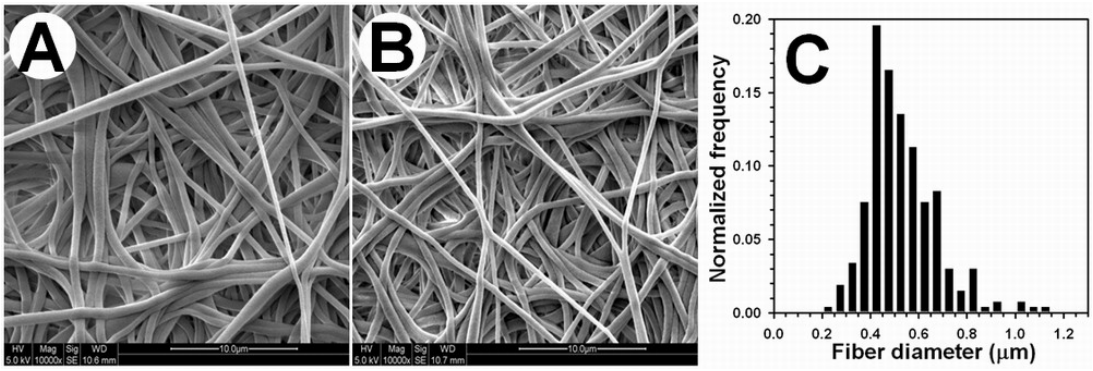

Figure 5.2: SEM images of electrospun PES nanofiber mesh: (A) unmodified; (B) after surface conjugation with ethylenediamine. (C) Fiber diameter distribution profile of PES fibers, electrospun from a 20 wt% PES in DMSO solution (at least 250 measurements taken).

Table 5.2 show that after PAAc grafting, the contact angle of PES film dropped from 76º to 53º, suggesting an increased surface wettability. The wettability further increased after amination (contact angle was 7º for aminated PES film). The contact

angle of the unmodified nanofiber mesh (133º) was higher than PES film (76º). However, the contact angle of PES nanofiber meshes decreased from 133º to 0º after PAAc grafting. Similar observations on the wettability of modified nanofiber surfaces were also reported by Fujihara et al. [191]. After carboxylation, the micropores in the relatively more hydrophilic nanofiber mesh exerted a capillary effect that imbibed the water droplet into the scaffold [192,193]. The aminated and hydroxylated PES fiber meshes also exhibited an un-measurable contact angle (~ 0º). The density of conjugated primary amino groups on aminated PES nanofiber and film was between 40–60 nmol/cm^2, as quantified by the Kakabakos' method [190]. All other surfaces showed a background amine density of < 5 nmol/cm^2.

Table 5.1: Characterization of surfaces modified with various functional groups.

Surface	Water contact angle (deg.)	Primary amine group density (nmol/cm^2)
TCPS	56.0 ± 1.4	0.4 ± 0.3
PES film	76.2 ± 5.1	0.9 ± 0.5
PES carboxylated film	52.9 ± 7.3	3.4 ± 0.8
PES aminated film	7.2 ± 2.7	50.1 ± 12.5
PES fiber	133.1 ± 1.8	1.3 ± 1.2
PES carboxylated fiber	N.D.*	4.0 ± 0.0
PES hydroxylated fiber	N.D.*	1.8 ± 0.8
PES aminated fiber	N.D.*	56.2 ± 12.6

Data shown are means ± SD of triplicate surfaces.

* N.D. The contact angle was too low (~0º) to be measured accurately.

5.4.2 *Ex Vivo* HSPC Expansion on Various PES Substrates

Efficiency of various substrates (unmodified and modified films and nanofiber meshes) in supporting HSPC expansion was evaluated in a 10-day expansion culture.

Fig. 5.3 shows the total nucleated cell fold expansion and $CD34^+CD45^+$ cell fold expansion after a 10-day expansion culture on different substrates.

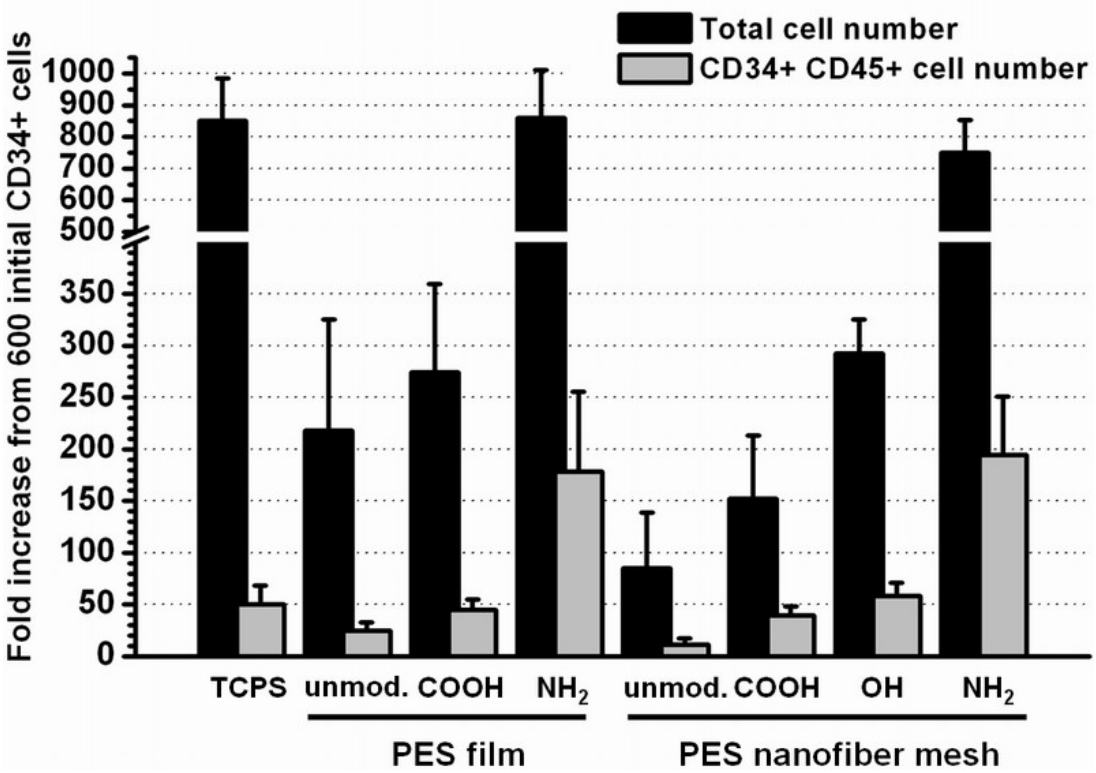

Figure 5.3: Fold expansion of total nucleated cells and $CD34^+CD45^+$ cells following a 10-day culture of 600 human cord blood HSPCs on different substrates. Total cell numbers were determined by hematocytometer cell counting, while $CD34^+CD45^+$ cells were determined by FACS analysis at the end of culture. Data shown are means ± SD of 3–8 independent experiments, each conducted in triplicates. Unmodified, carboxylated, hydroxylated and aminated conditions were designated as "unmod.", "COOH", "OH" and "NH_2" respectively.

Cells harvested from the expansion cultures showed greater than 95% viability in all culture conditions. Noticeable differences were observed in the cell proliferation response of HSPCs to the different substrates. HSPCs cultured on unmodified, carboxylated and hydroxylated PES nanofiber meshes and films yielded low proliferation (85- to 293-fold expansion) of total nucleated cells compared to that cultured on TCPS (850-fold). The $CD34^+CD45^+$ cell fraction was between 11.3% – 26.1% of total cells as analyzed by flow cytometry, which corresponded to a low (11-

to 58-fold) $CD34^+CD45^+$ cell expansion. Although HSPCs cultured on TCPS surface proliferated extensively (850-fold), the fraction of $CD34^+CD45^+$ cells was only 5.8% of total expanded cells, thus resulting in only about 50-fold expansion of $CD34^+CD45^+$ cells.

In contrast, the expansion of $CD34^+CD45^+$ cells on aminated film and nanofiber mesh was significantly better than other test groups ($p < 0.05$): aminated PES nanofiber mesh yielded 751-fold expansion of total cells and 195-fold expansion of $CD34^+CD45^+$ cells (25.9% of total cells), whereas aminated PES film yielded 859-fold expansion of total cells and 178-fold expansion of $CD34^+CD45^+$ cells (20.8% of total cells). There was no statistically significant difference in fold expansion of $CD34^+CD45^+$ cells cultured on aminated PES nanofiber mesh, compared with that on PES film ($p > 0.05$).

5.4.3 Colony-Forming Cell Assay

CFU assays (Fig. 5.4) were conducted to evaluate the fraction of primitive progenitor cells in the expanded cultures. Consistent with total and $CD34^+CD45^+$ cell expansion results, cells expanded on unmodified, carboxylated and hydroxylated PES nanofiber meshes and films yielded lower total CFU counts (1071 ± 560 to 1996 ± 213) as compared to TCPS (2890 ± 450), aminated PES film (3471 ± 371), and aminated PES nanofiber mesh (3996 ± 358).

Interestingly, for aminated PES substrates, a significant difference was observed in the number of more primitive CFU-GEMM units generated by cells expanded on film versus nanofiber mesh with 20% (704/3471) and 28% (1124/3996) of total colony counts, respectively ($p < 0.05$). TCPS on the other hand, generated only 15%

(433/2890) CFU-GEMM units ($p < 0.05$ compared with aminated film or nanofiber mesh groups).

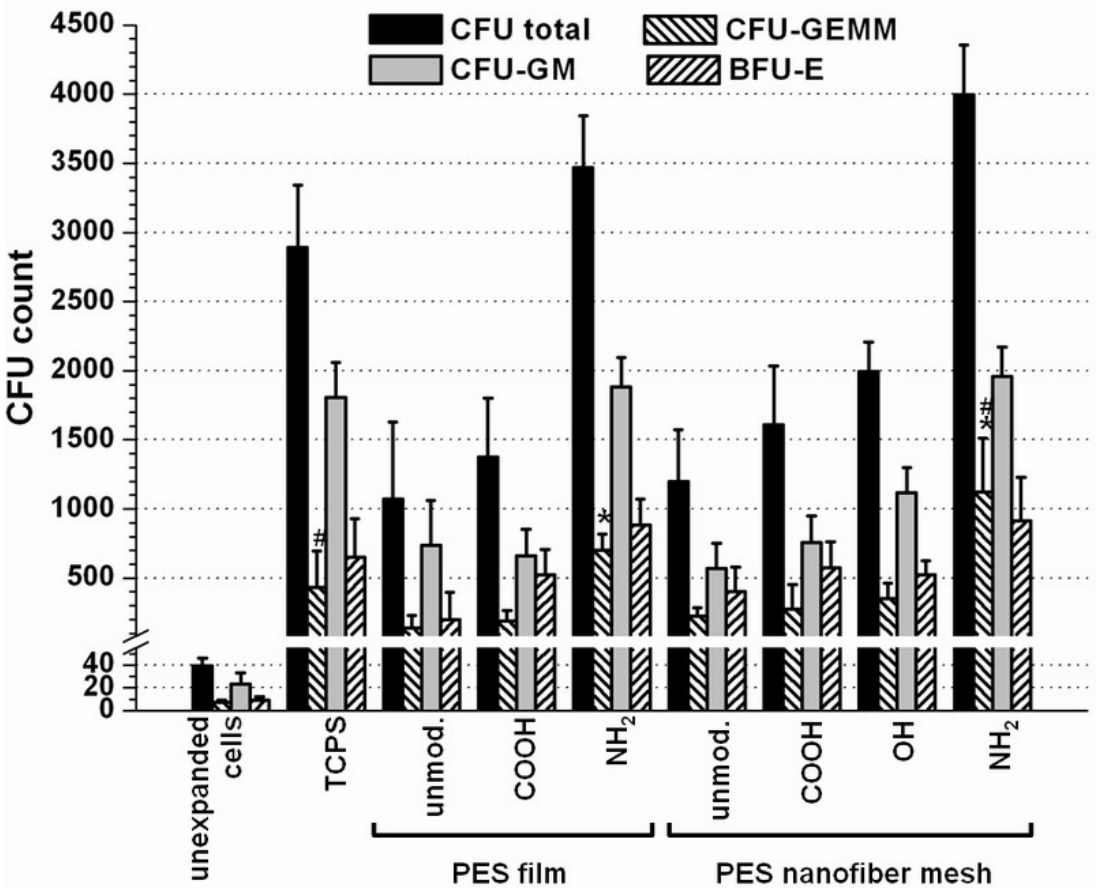

Figure 5.4: CFU counts generated after 14 days of culture, using the cells from the 10-day expansion cultures on various substrates and from the unexpanded HSPCs. Data are normalized to CFU number per 100 initial unexpanded HSPCs. Data shown are the mean ± SD of 3–8 experiments, each conducted in triplicates. * $p < 0.05$; # $p < 0.05$. Unmodified, carboxylated, hydroxylated and aminated conditions were designated as "unmod.", "COOH", "OH" and "NH2" respectively.

In contrast, TCPS generated relatively higher percentages of CFU-GM units (63%), indicating significant differentiation commitment of the TCPS-expanded cells towards the myeloblast / monoblast lineage, as compared to both aminated PES film and nanofiber scaffold (55% and 49%, respectively, $p < 0.05$ for TCPS *vs.* PES film, $p < 0.01$ for TCPS *vs.* PES nanofiber, $p > 0.05$ for PES film *vs.* PES nanofiber).

5.4.4 Expanded HSPC Surface Marker Expression

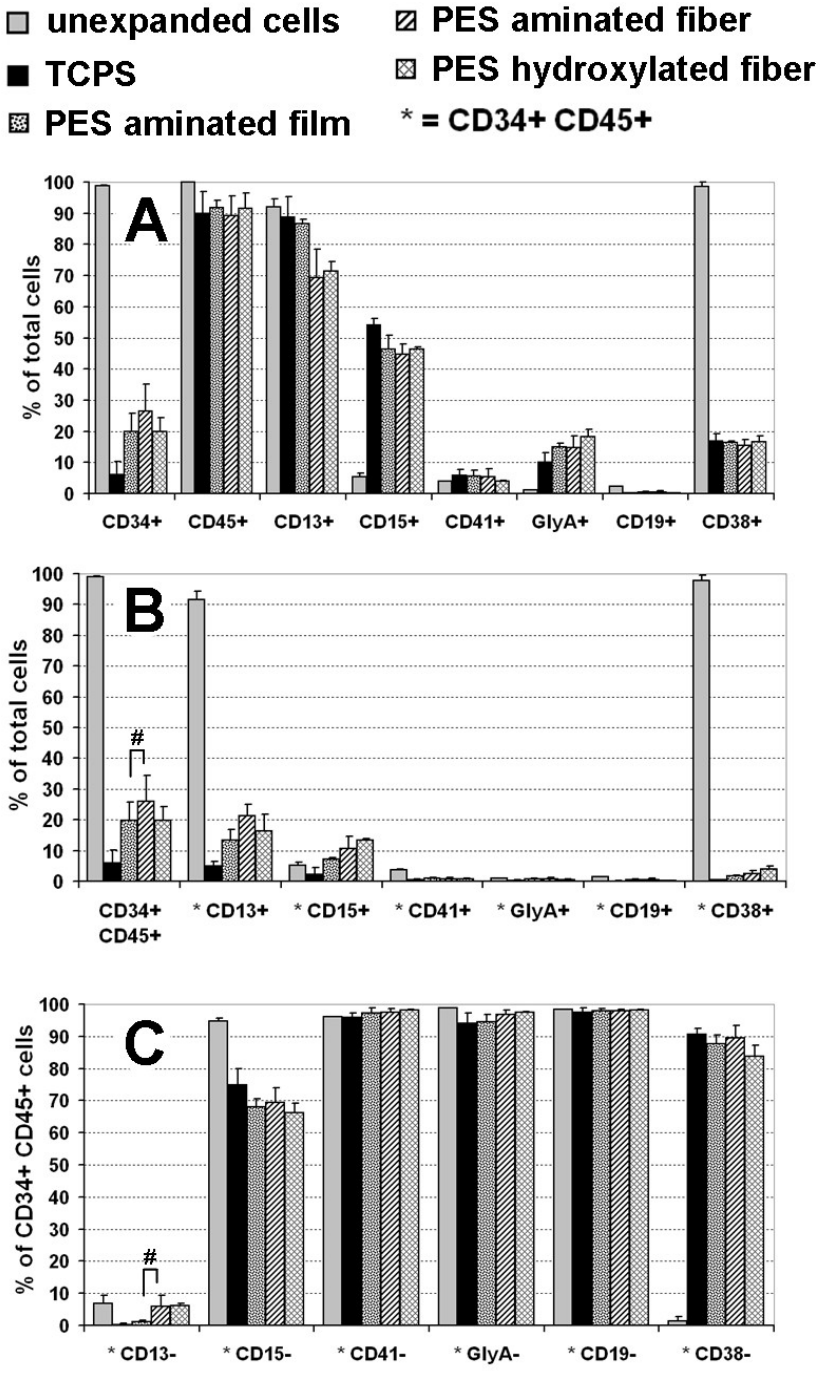

Figure 5.5: Surface antigen expression on cells after 10-day *ex vivo* expansion on different substrates. (A) Percentage of total cells that are CDX+. (B) Percentage of total cells that are $CD34^+CD45^+CDX^+$. (C) Percentage of the $CD34^+CD45^+$ cell population that are $CD34^+CD45^+CDX^-$. "CDX" represents CD34, CD45, CD13, CD15, CD41, GlyA, CD19 or CD38. Data shown are mean ± SD of 3–6 experiments, each conducted in duplicates. # denotes statistical significance of $p < 0.05$.

The lineage marker expression of the expanded cells was analyzed by flow cytometry (Fig. 5.5). Only cells expanded on TCPS, aminated PES film and nanofiber mesh, and hydroxylated nanofiber mesh were analyzed because they generated sufficiently high numbers of cells for complete lineage marker expression analysis. Lineage marker expression of freshly thawed, unexpanded cord blood HSPCs was also analyzed as a control. In addition to the definitive human blood progenitor markers which include CD34, CD45 and CD38, the cells were also evaluated for markers for myeloblast / monoblast (CD13, CD15), megakaryoblast (CD41), erythroid (GlyA) and pro-B cell (CD19) lineages. The following observations can be made:

(1) Unexpanded HSPC stocks showed high expression of CD34 (98%), CD45 (99%), CD13 (92%) and CD38 (98%) (Fig. 5.5A);

(2) Cells expanded on all substrates expressed negligible levels of CD19 (<1%), whereas cell populations expressing CD15, CD41 or GlyA increased (Fig. 5.5A);

(3) Cells expanded on aminated PES nanofiber showed the highest percentage (25.9% ± 8.5%) of $CD34^{+}CD45^{+}$ cells (Fig. 5.5B);

(4) The $CD34^{+}CD45^{+}$ cell population of expanded cells were primarily negative for CD41, GlyA and CD19 but co-expression of CD13 and CD15 was significant (Fig. 5.5C);

(5) The $CD34^{+}CD45^{+}$ fraction of expanded cells displayed lower CD38 co-expression compared to unexpanded cells (Fig. 5.5C), an effect that had been attributed to serum-free culture condition [184,194];

(6) The $CD34^+CD45^+$ cell population expanded on aminated and hydroxylated PES nanofiber meshes showed lower CD13 expression compared to cells expanded on TCPS and aminated PES film (Fig. 5.5C).

5.4.5 Imaging of Adherent Cells on Aminated Substrates

After 10 days of expansion culture, some samples were processed for SEM and confocal laser microscopy to detect the presence of any adherent cells on these substrates. It was noted that expanded cells adhered weakly to TCPS, unmodified, carboxylated film and nanofiber, and hydroxylated PES nanofiber substrates; and most of these cells could easily be detached with very gentle rinsing. As such, only sparsely scattered cells could be seen under SEM. This observation confirmed the weak adhesion of HSPCs on these substrates. In contrast, on aminated PES nanofiber mesh and film, cell adhesion was evident, although the arrangement of adherent cells on these two substrates appeared to differ greatly (Fig. 5.6).

On aminated PES nanofiber mesh, approximately 40% cells were adherent following 3 gentle washes; distinct and circular cell colonies were abundant on the mesh (Fig. 5.6A). Cell colonies ranged from 100 μm to 1.3 mm in diameter, with cells numbering between 50 to a few thousand. In some of the larger colonies, cells could be seen densely packed at the center but thinned out towards the periphery of the colony. At high magnification, the adherent cells could be seen to be anchored via numerous processes in intimate contact with the aminated nanofibers as well as processes from other cells, indicative of cell-fiber and cell-cell interactions (Fig. 5.6B & 5.6C).

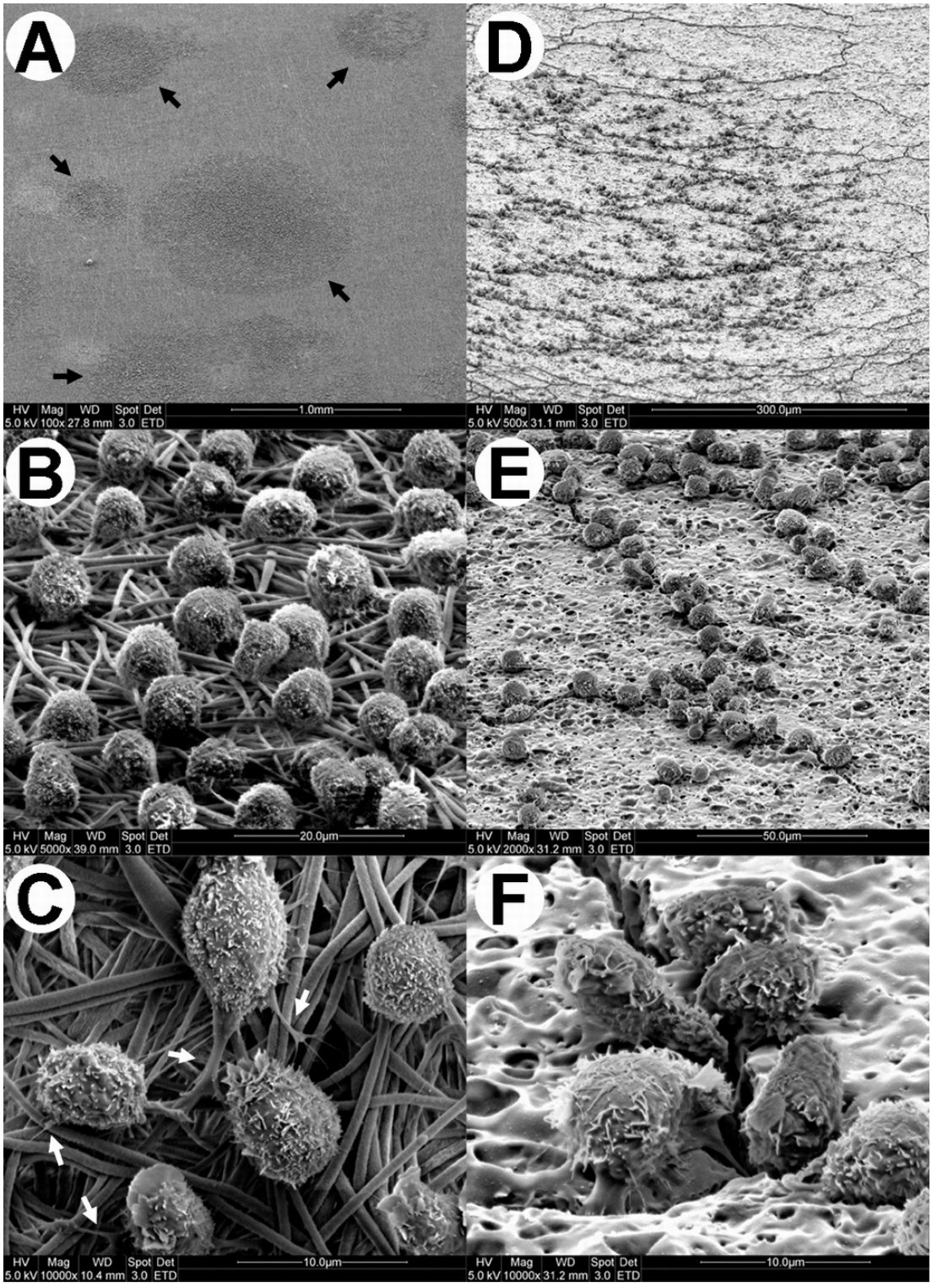

Figure 5.6: SEM images of human cord blood HSPCs after a 10-day expansion culture on aminated PES nanofiber mesh (A-C) and on aminated PES film (D-F) at various magnifications. Abundant distinct, circular cell colonies are evident on the aminated nanofiber scaffold (black arrows). Filopodia extend from the cells and interact with the aminated nanofibers (white arrows). On aminated film, fewer cells are adherent without colony formation; cells appear to attach along cracks.

On aminated film substrates, however, about 25% total cells were adherent, but only sparsely on the surface, compared to adherent cells on aminated nanofiber mesh (Fig. 5.6D). No discrete cell colony was evident but instead, the adherent cells appeared to align along crevasses (defects generated during film processing) on the surface of the film (Fig 5.6E). We also observed that most of the adherent cells along the edges of the crevasses sent filopodia into the fissures (Fig. 5.6F). Cells on the smooth surface were washed off by gentle rinsing with PBS.

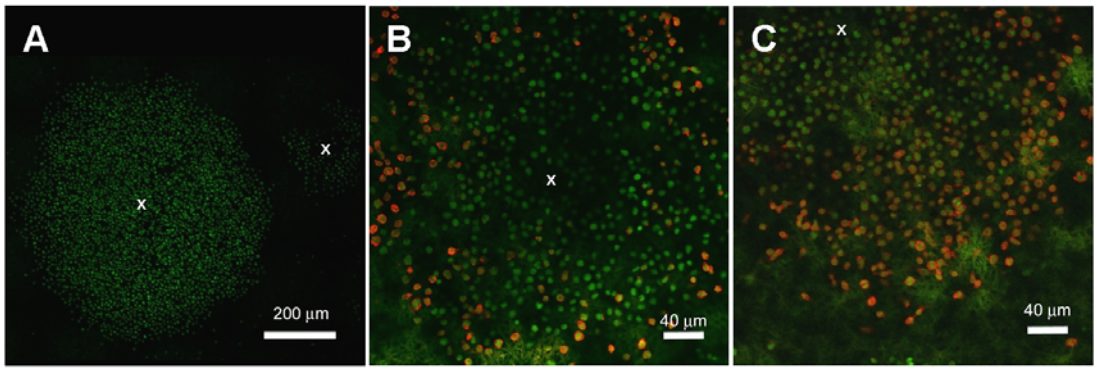

Figure 5.7: Confocal laser microscopy images of human cord blood HSPCs after a 10-day expansion culture on aminated PES nanofiber mesh. Green indicates Syto16 nuclear staining and red indicates CD34-PE staining. (A) Fluorescent image of two representative cell colonies stained with Syto16. (B, C) $CD34^+$ cells can be found on these cell colonies and they appear to concentrate around the periphery of the colonies. "x" denotes the approximate center of the cell colony.

Prompted by the observation of the unique cell colonies on the surface of aminated nanofiber mesh, we proceeded to investigate the CD34 antigen expression among the adherent cell population. Indeed, confocal laser microscope imaging confirmed that a fraction of the cells in the cell colonies showed positive staining with CD34-PE antibody (Fig. 5.7). Interestingly, the $CD34^+$ cells were located mostly around the peripheries of the cell colonies. Cells at the center of the colonies appeared to be predominantly $CD34^-$. This suggests that HSPCs and the expanded cells were

proliferating in an outward, radial manner along the surface of aminated nanofiber mesh, resulting in the formation of circular cell colonies.

5.5 Discussion

This report focuses on examining the effects of surface functional groups, together with surface topography, on the proliferation and differentiation of HSPCs under a typical expansion condition – using commercially available serum-free stem cell media. The results show that under typical culture condition (StemSpan™ serum-free expansion medium and a cytokine cocktail), both substrate chemistry (amino *vs.* hydroxyl *vs.* carboxyl groups) and topographical features affect the expansion outcome.

HSPCs cultured on unmodified, hydroxylated or carboxylated PES substrates exhibited low proliferation. In contrast, HSPCs cultured on aminated PES substrates were able to proliferate as rapidly as those cultured on TCPS, with the advantage that the fold expansion of $CD34^+$ cells on aminated substrates was more than 3.5 times higher than that on commercial TCPS surface (Fig. 5.3); the expanded cells also generated higher numbers of CFU-total and CFU-GEMM counts (Fig. 5.4). These observations indicate that aminated substrate may play a role in facilitating HSPC proliferation and/or maintenance of the HSPC phenotype.

One possible mechanism to account for the observed effects is that the aminated substrate, being positively charged, could selectively enrich certain protein components from the medium, which then contribute to the expansion outcome [189,195]. Keselowsky et al. [189] have shown that the functional presentation of adsorbed fibronectin was different on hydroxylated, methylated, aminated and

carboxylated surfaces, which consequently led to variations in cell adhesion and differentiation. It is possible that aminated PES surface mediated HSPC proliferation by a similar mechanism – by binding critical cytokines and growth factors from the medium, and presenting them in a more effective immobilized form, thereby mimicking a salient feature of the bone marrow hematopoietic stem cell niche [137-140,196,197].

Another possible mechanism by which aminated surface enhanced HSPC expansion and $CD34^+$ phenotype maintenance is by its direct interaction with the HSPCs through their surface CD34 antigen. CD34 antigen is a highly sialylated and negatively charged glycophosphoprotein, and its expression decreases as HSPCs become differentiated [146-156]. We therefore postulate that a positively charged "ligand" – in this case the surface-bound amine groups – could bind and engage the negatively charged CD34 antigen, and the engagement of CD34 antigens on HSPCs might activate downstream signaling pathways that subsequently influence fate choices upon proliferation [150]. Tada J. et al. have shown that stimulation of undifferentiated hematopoietic (myeloblastic leukemia cell line) KG1a cells with anti-CD34 antibody induces homotypic cytoadhesion [150]. Binding of aggregating antibody to CD34 antigens induced tyrosine phosphorylation, cell polarization and adhesion, and perhaps cell motility. Interestingly, being co-localized with F-actin, the crosslinked CD34 "cap" is quite stable and persists on the cell surface for at least 2 days after stimulation, whereas many other cell-surface molecules are rapidly internalized for degradation or recycling, upon stimulation. It is possible that the aminated PES surface serves the same role by engaging cell surface CD34 antigen.

The most interesting finding of this study is that surface topography also plays a role in HSPC adhesion and expansion. Aminated nanofiber mesh mediated the highest

degree of cell adhesion on substrate; and the expanded $CD34^+CD45^+$ cells on aminated PES nanofiber mesh exhibited a lower monoblastic ($CD13^+$) phenotype (Fig. 5.5C) and higher CFU potential (Fig. 5.4) compared to the same population of cells expanded on aminated PES film. Moreover, the adherent hematopoietic cells on the aminated nanofiber displayed numerous filopodia and attachment sites on the fibers (Fig. 5.6A-5.6C), which might mediate cell migration that allows rearrangement of the proliferated cells on the substrate surface. A consequence of this stronger adhesion was that the cells proliferated on the nanofiber mesh surface in a radial and outward planar fashion, resulting in distinct, circular colonies.

We do however observe that HSPCs did not survive on aminated surfaces in the absence of cytokine supplementation, suggesting that aminated nanofiber substrate itself is not sufficient to induce the proliferation of HSPCs. The surface-bound amino groups and topographical cue are therefore likely to play a supporting/synergistic role for cytokines and growth factors (supplemented in the medium) to influence HSPC proliferation and differentiation.

Although the precise mechanisms by which amine group and nanofiber topography mediate more efficient adhesion and expansion of $CD34^+CD45^+$ cells remains to be elucidated, our data suggest a positive correlation between substrate-adhesion of HSPCs with higher expansion efficiency of $CD34^+CD45^+$ cells. A recent study suggests that HSPC-substrate adhesion is required for cell migration and homing [157]; this HSPC-substrate adhesion might be part of the natural process occurring in the hematopoietic stem cell niche that governs the proliferation and differentiation of HSPCs [198].

5.6 Concluding Remarks

The *ex vivo* expansion of hematopoietic stem cells is one of the most challenging fields in cell culture. This is a rapidly growing area of tissue engineering with many potential applications in transfusion medicine, bone marrow transplantation or gene therapy. Over the last decade much progress has been made in understanding hematopoietic differentiation, identification and isolation of HSPC subtypes, discovery of cytokines and in the development of a variety of culture scaffold and bioreactor techniques. All this has led to a number of preliminary clinical trials that highlighted the benefits that can be obtained from the use of expanded hematopoietic cells in therapy. Moreover, as we understand the complexity and the regulation of hematopoiesis, it becomes obvious that cultivation techniques and concepts must constantly evolve and improve in order to expand HSPCs efficiently and effectively.

In this chapter, we demonstrated the effectiveness of surface modified electrospun PES nanofiber mesh as potential scaffolds for *ex vivo* HSPC expansion under serum-free conditions. The expansion profiles of human umbilical cord HSPCs are evidently different following a 10-day culture on modified and unmodified polymeric substrates with different functional groups and nanofiber topographical cue. Among the carboxylated, hydroxylated, and aminated PES substrates and TCPS, aminated PES substrates mediated the highest expansion efficiency of $CD34^+CD45^+$ cells and CFU potential. Aminated nanofiber mesh could further enhance the HSPC-substrate adhesion and expansion of CFU-GEMM forming progenitor cells. Although the underlying mechanisms remain to be elucidated, this study clearly underscores the importance of culture substrate in influencing the proliferation and differentiation of HSPCs.

In the following chapter, we will seek to better understand the mechanism by which aminated nanofibers mediate these cellular responses by investigating the effects of spacer chain lengths of the grafted amine groups. In addition, the multipotency maintenance potential, differentiation characteristics and engraftment potential of the cells expanded from aminated nanofiber scaffolds will be further investigated through short-term and long-term clonogenic assays and NOD/SCID mouse engraftment assays.

CHAPTER SIX

Nanofiber Scaffolds Modified with Different Spacer-Length Amines Modulate Hematopoietic Stem/Progenitor Cell Maintenance and Proliferation Kinetics

6.1 Summary

We have shown in the previous chapter that aminated nanofiber scaffold can effectively enhanced HSPC proliferation, while supporting the multipotency phenotype (CFU-GEMM) of the cells expanded in HSPC *ex vivo* expansion cultures. In this present study, the effects of the nanofiber scaffolds immobilized with amine functional groups of increasing 2-, 4- and 6-carbon spacer chain lengths (EtDA, BuDA and HeDA conditions, respectively) on *ex vivo* expansion and maintenance of HSPCs is investigated.

Results show that EtDA and BuDA nanofiber scaffold showed similar expansion profiles (773- and 805-fold expansion, respectively) and the expanded cells maintained 25.9% and 29.2% of the $CD34^+CD45^+$ phenotype, respectively. Interestingly, HSPC proliferation on HeDA nanofiber scaffold was significantly lower (210-fold), although the $CD34^+CD45^+$ cell fraction was the highest at 41.1% of total cells. This increased $CD34^+CD45^+$ percentage offsets the low cell proliferation and cells expanded from HeDA nanofiber scaffold exhibited similar CFU-GEMM and LTC-IC maintenance as compared to cells expanded from EtDA and BuDA nanofiber scaffolds, although the NOD/SCID mice engraftment potential was not as efficient.

This study further suggests the importance of immobilized amino functional groups in influencing cell-scaffold interactions and modulating HSPC proliferation kinetics and multipotency maintenance in aminated nanofiber scaffolds.

6.2 Introduction

In Chapter 5, we have demonstrated that surface covalent immobilization of functional groups could mediate HSPC-substrate adhesion and proliferation. In particular, we discovered in ethylenediamine-modified nanofiber scaffolds that surface biochemical cues and topographical cues both played synergistic roles in enhancing HSPC-substrate adhesion and maintenance of HSPC proliferation and multipotency. HSPCs proliferated well on aminated nanofiber scaffolds and the expanded cells generated the highest maintenance of primitive CFU-GEMM forming cells. Scanning electron microscopy imaging also revealed that the HSPCs extended numerous uropodia that associated intimately with the aminated nanofibers and anchored the cells to the fibrous scaffold. In addition, the unique HSPC proliferation pattern on these aminated nanofibers resulted in the formation of abundant distinct, densely packed circular cell colonies on the scaffold surface. This observation was in sharp contrast to HSPC interaction with aminated film, where there were only sparse adherent cells on the film surface, and most of the adherent cells were found anchored along crevasses on the film surface.

The finding that surface amino groups and nanofiber topography could synergistically act to promote the adherence of HSPCs and regulate their proliferation is novel and unexpected. In this study, we further investigate the effect of amine-conjugation on HSPC expansion, with a long term goal to better understand the mechanism by which aminated nanofibers mediate these cellular responses (Fig. 6.1).

Several studies had shown that spacer properties can affect the interaction between cells and immobilized biofunctional molecules such as ligands [199,200], providing motivation to investigate the effect of chain length of the grafted amines on the proliferation rate and phenotype of cultured cord blood HSPCs. The differentiation and engraftment potential of the cells was assessed by clonogenic assays and NOD/SCID mouse engraftment assays, respectively.

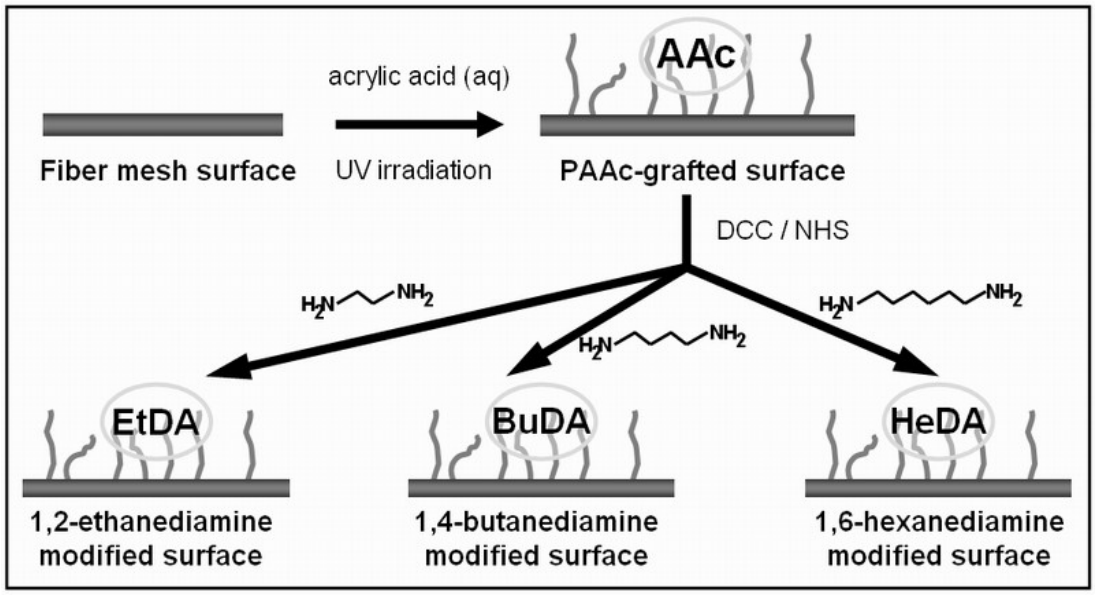

Figure 6.1: PES scaffold amination scheme with different spacer chain length amines.

6.3 Experimental Methods

All chemicals were purchased from Sigma-Aldrich unless otherwise stated.

6.3.1 Fabrication of PES Nanofiber Scaffolds

Detailed protocols for PES nanofiber scaffold fabrication can be found in Chapter 5.3.1.

6.3.1.1 Surface Grafting of Scaffolds with Poly(acrylic acid)

The PES nanofibers were subsequently grafted with Poly(acrylic acid) (PAAc). Detailed protocols for PES nanofiber PAAc grafting can be found in Chapter 5.3.1.1.

6.3.1.2 Amination of Poly(acrylic acid) Grafted Scaffolds

The PAAc-grafted PES nanofiber meshes were further conjugated with 1,2-ethanediamine (EtDA), 1,4-butanediamine (BuDA) or 1,6-hexanediamine (HeDA) using carbodiimide cross-linking method (Fig. 6.1). Briefly, each scaffold was first gently shaken in 2 mL acetonitrile containing 50 mM N-hydroxysuccinimide and 50 mM dicyclohexylcarbodiimide. After 6 h, the reaction solution was carefully aspirated and each scaffold was immediately immersed into 2 mL acetonitrile containing 0.03 mmol EtDA, BuDA or HeDA. After 12 h, the reaction solution was carefully aspirated and each scaffold was thoroughly washed in absolute ethanol to remove any dicyclohexyl urea, which is a by-product of the conjugation reaction. All substrates were subsequently sterilized in 70% ethanol, then loaded into 24-well tissue culture plates (Nunc) and stored in sterile PBS until use.

Surface characterization and atomic compositions of various PES nanofiber surfaces were determined using XPS (PHI-1800, Physical Electronics). Binding energies were referenced to the CC/CH_2 C(1s) peak at 284.6 eV.

6.3.2 Hematopoietic Stem Cell Culture and Assays

Frozen human umbilical cord blood $CD34^+$ HSPCs were purchased from AllCells. The $CD34^+$ purity in the HSPC was determined to be 98% by flow cytometry and the viability was determined to be more than 97% by Trypan blue. Purified recombinant human stem cell factor (SCF), Flt-3 ligand (Flt3), thrombopoietin (TPO) and IL-3 was purchased from Peprotech Inc. Low density lipoprotein (LDL) was purchased from Athens Research & Technology Inc. The StemSpan^{TM} serum-free expansion medium, MethoCult GF+ H4435 and MyeloCult H5100 were all from StemCell Technologies.

6.3.2.1 *Ex Vivo* Hematopoietic Expansion Culture

Six hundred HSPCs were seeded onto each scaffold. HSPCs were cultured in 0.6 mL StemSpan™ serum-free expansion medium supplemented with 0.04 mg/mL LDL, 100 ng/mL SCF, 100 ng/mL Flt3, 50 ng/mL TPO and 20 ng/mL IL-3 at 37^{o}C, 5% CO_2 for 10 days. Similar cultures were also performed on tissue culture polystyrene surface (TCPS), which served as a positive control in this study. In total 6 surface conditions were tested: TCPS, unmodified PES nanofiber mesh (Unmod.), carboxylated nanofiber mesh (AAc), and nanofiber mesh aminated with EtDA, BuDA or HeDA.

On day 10, the expanded cells were harvested and aliquoted. Briefly, all substrates were washed once with non-trypsin cell dissociation solution and twice with 2% FBS Hanks' buffer at 5-10 min intervals between each wash. The cell suspensions collected were then concentrated through centrifugation at 500 ×g for 10 min. Aliquots of the concentrated cells were then used for cell counting by a hematocytometer, flow cytometry analysis, colony-forming cell assays, long-term culture-initiating cell assay and mouse engraftment assay.

6.3.2.2 Flow Cytometry

Fluorescently labeled antibodies for CD13, CD34 and CD45 were purchased from BD Biosciences (USA). The cell samples were incubated with antibodies at 4^{o}C for more than 30 min in 2% FBS Hanks' buffer. After antibody staining, the cells were washed twice with Hanks' buffer and fixed in 1% paraformaldehyde. Cells were analyzed by flow cytometry on a FACSCalibur analyzer (BD Biosciences). Relevant isotype controls were also included to confirm specificity and for compensation setting. At least 20,000 gated events were acquired. The Milan-Mulhouse gating method was used for cell enumeration [151].

6.3.2.3 Preparation for Scanning Electron Microscopy

Selected cultures samples were gently rinsed with PBS, fixed with 3% glutaraldehyde for 30 min at 20°C, and post-fixed with 1% osmium tetraoxide for another 15 min at 20°C. Samples were then dehydrated using a graded series of ethanol (25%, 50%, 70%, 90%, 95%, 100%, 100%) followed by hexamethyldisilazane drying. The samples were mounted onto aluminum stubs and gold sputter-coated before viewing under field emission scanning electron microscope (SEM, FEI Company).

6.3.2.4 Colony-Forming Cell Assay

Detailed protocols for CFC assay can be found in Chapter 5.3.2.3.

6.3.2.5 Long-Term Culture-Initiating Cell Assay

For LTC-IC, expanded cells from each scaffold condition in the *ex vivo* hematopoietic expansion cultures and freshly thawed HSPCs, which serve as controls, were plated onto irradiated M2-10B4 murine fibroblast feeder cells in 35mm culture dishes and cultured in MyeloCult H5100 medium as instructed in the procedure manual by StemCell Technologies. After 5 weeks, all the cells from each dish were harvested, and cultured according to the CFC assay as described above. LTC-IC numbers were then calculated and normalized according to instructions in the procedure manual.

6.3.2.6 Mouse Engraftment Assay

Non-obese diabetic/severe combined immunodeficient (NOD/SCID) mice (Animal Resource Center, Perth, Australia) were maintained at the Biological Resource Center (BRC), Biopolis, Singapore. All animals were handled according to BRC regulations. 6-8 weeks old mice were irradiated at 350 cGy. Cells harvested

from 10-day *ex vivo* expansion cultures were mixed with 4×10^5 irradiated (1,500 cGy) CD34-depleted human bone marrow cells (carrier cells) and injected into the mice via the tail vein. For positive controls, 2 mice groups of 600 or 20,000 injected unexpanded HSPCs / 4×10^5 irradiated carrier cells mix were also examined. Finally, un-irradiated mice, irradiated mice and irradiated mice with 4×10^5 injected irradiated carrier cells groups were also included to serve as negative controls in this study.

Mice were sacrificed 6 weeks after cell transplantation. After euthanasia, bilateral femora and tibia were harvested from each animal and bone marrow cells were flushed out with 2% FBS, 5% human serum Hanks' buffer. The cells were subsequently stained with fluorescently labeled human CD45 antibody and the red blood cells lysed using FACS lysing solution (BD Biosciences). The percentage of human hematopoietic cells in the mouse bone marrow was quantified by flow cytometry. At least 40,000 gated events were acquired. Successful human hematopoietic stem cell engraftment was defined by the presence of at least 0.1% of human $CD45^+$ cells in the NOD/SCID mouse bone marrow cell population.

6.3.3 Statistical Analysis

All data were presented as mean ± standard deviation (SD). The statistical significance of the data obtained was analyzed by non-parametric Mann-Whitney test for mouse engraftment results and Student's t-test for all other results. Probability values of $p < 0.05$ were interpreted as denoting statistical significance.

6.4 Experimental Results

6.4.1 Surface Characterization of Aminated Nanofiber Scaffolds

Nonwoven PES nanofiber meshes with an average diameter of 529 ± 114 nm were prepared by electrospinning process. The PES nanofiber meshes were first

carboxylated by UV-initiated PAAc grafting and subsequently conjugated with diamines with 2, 4, or 6 alkane spacers (EtDA, BuDA or HeDA respectively) using carbodiimide cross-linking method (Fig. 6.1). XPS analysis showed the surface elemental concentration of nitrogen on the aminated fibers to be between 11.6% – 13.4% (Table 6.1), which indicated the similar conjugation efficiencies of the different diamines on the nanofiber surface. The unmodified and PAAc-grafted fibers on the other hand showed background nitrogen concentrations of <0.2%.

Table 6.1: XPS elemental analysis of PES nanofiber surfaces modified with different functional groups.

PES nanofiber surface	C atomic ratio (%)	O atomic ratio (%)	N atomic ratio (%)	S atomic ratio (%)
Unmodified	74.2	20.2	0.2	5.4
AAc	68.6	27.7	0.1	3.6
EtDA	65.2	19.8	13.4	1.6
BuDA	67.9	17.5	13.2	1.4
HeDA	71.8	14.9	11.6	1.7

In addition, the carbon XPS spectra (C_{1s}) showed that after PAAc grafting, the $\pi \rightarrow \pi^*$ shake-up satellite region at 291.7 eV (caused by aromatic carbon species in PES) was absent in PES AAc fiber surface, and replaced with the PAAc characteristic O–C=O region (Fig. 6.2). Subsequently, the XPS C_{1s} spectra also showed absence of O–C=O species for all amine conjugated fibers, indicating the complete conversion of the surface PAAc carboxylic acid groups to amide groups during the amine conjugation reaction.

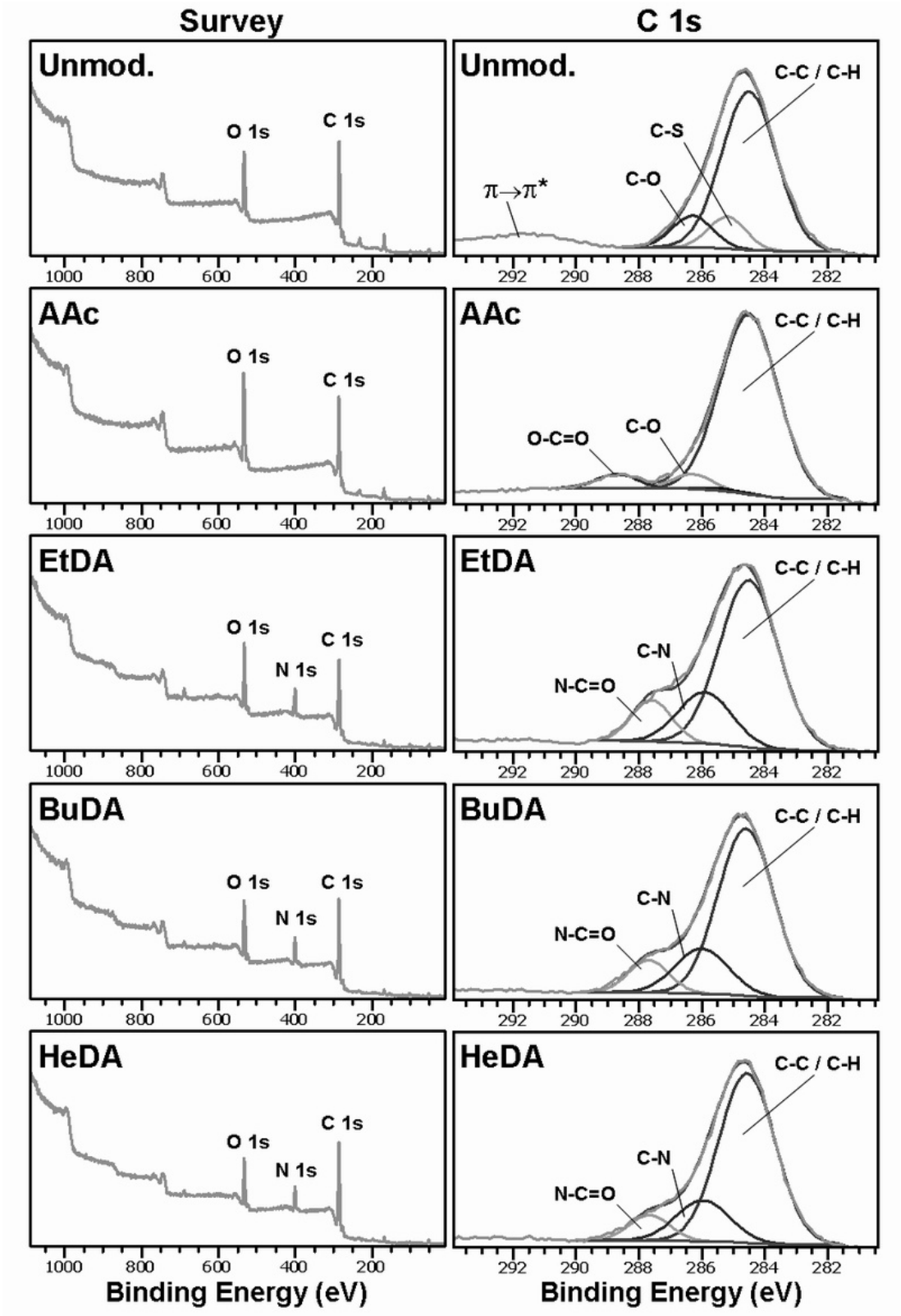

Figure 6.2: The XPS spectra of various modified PES nanofiber surfaces. Left panel: Survey spectra showing the relative abundance of O, N and C elements. Right panel: C1s spectra showing the relative abundance of the different carbon bonds.

6.4.2 *Ex Vivo* HSPC Expansion on Aminated Nanofiber Scaffolds

The efficiency of the various nanofiber scaffolds for supporting HSPC expansion was evaluated through 10-day expansion cultures. Fig. 6.3 showed the total nucleated cell fold expansion and $CD34^+CD45^+$ cell fold expansion after a 10-day expansion culture on different spacer amine nanofiber and control surfaces. Cells harvested from the expansion cultures showed >95% viability in all culture conditions. In general, HSPCs culture on Unmod and AAc surfaces yielded the lowest proliferation of total nucleated cells (85- and 152-fold, respectively); the $CD34^+CD45^+$ cell fraction was 13.3% and 26.1% of total cells, respectively, as analyzed by flow cytometry, which corresponded to a low 11- and 40-fold $CD34^+CD45^+$ cell expansion respectively. Although HSPCs cultured on TCPS surface proliferated extensively (895-fold), the $CD34^+CD45^+$ cell fraction was only 5.9% of total cells, corresponding to a 53-fold $CD34^+CD45^+$ cell expansion.

In contrast, the expansion of $CD34^+CD45^+$ cells on EtDA, BuDA and HeDA nanofiber mesh was significantly better than other test groups: EtDA and BuDA nanofiber mesh showed similar expansion profiles ($p > 0.05$) and yielded 773- and 805-fold expansion of total cells respectively (Fig. 6.3), with 25.9% (200-fold) and 29.2% (235-fold) of total cells expressing the $CD34^+CD45^+$ phenotype, respectively (Fig. 6.4). Interestingly, although HSPCs proliferation on HeDA surface was significantly lower as compared with EtDA and BuDA surfaces (210-fold, $p < 0.05$), the $CD34^+CD45^+$ cell fraction was the highest at 41.1% of total cells (86-fold $CD34^+CD45^+$ cell expansion).

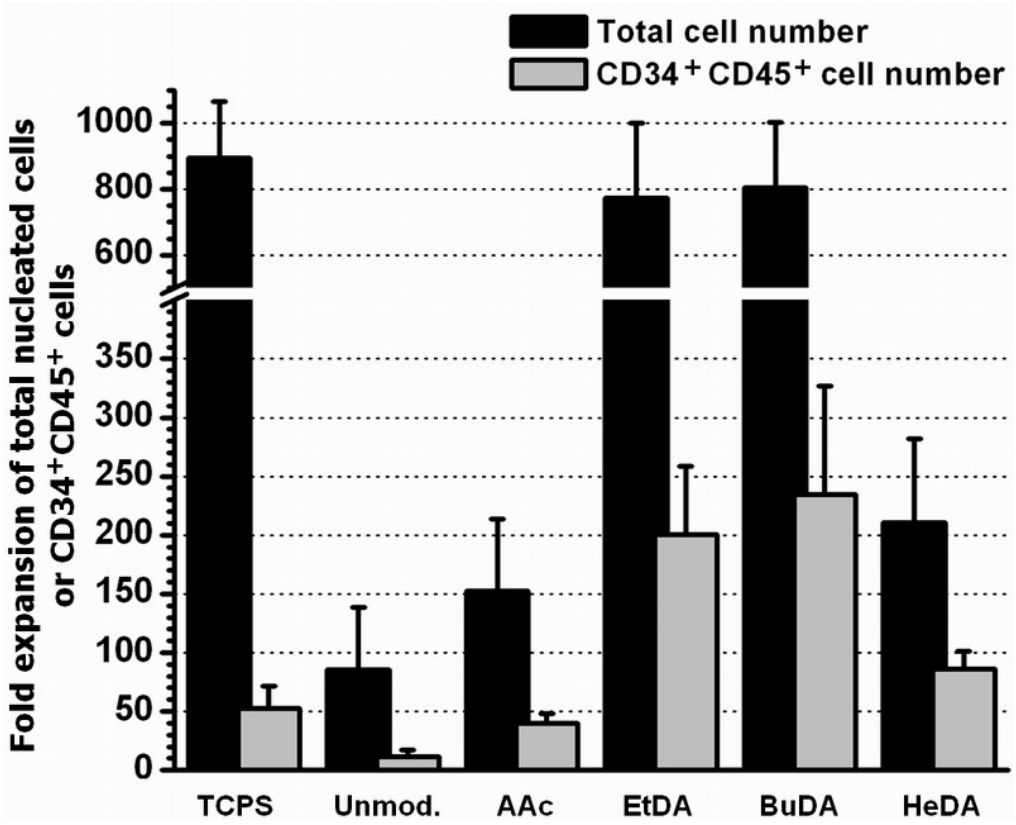

Figure 6.3: Fold expansion of total nucleated cells and $CD34^+$ cells following a 10-day culture of 600 human cord blood HSPCs on different substrates. Total cell and $CD34^+$ cell numbers were determined by hematocytometer cell counting and FACS analysis respectively at the end of culture. Data are means ± SD of 3-8 independent experiments, each conducted in triplicates.

In addition, we also observed that the $CD34^+CD45^+$ cell population expanded from HeDA nanofiber scaffolds co-expressed significantly lower levels of the myeloid CD13 marker (60.3 ± 7.3 % of expanded $CD34^+CD45^+$ cell population) compared to EtDA and BuDA nanofiber scaffolds (94.2 ± 3.5 %, $p < 0.05$ and 92.8 ± 3.8 %, $p < 0.05$ of expanded $CD34^+CD45^+$ cell population respectively (Fig. 6.4D).

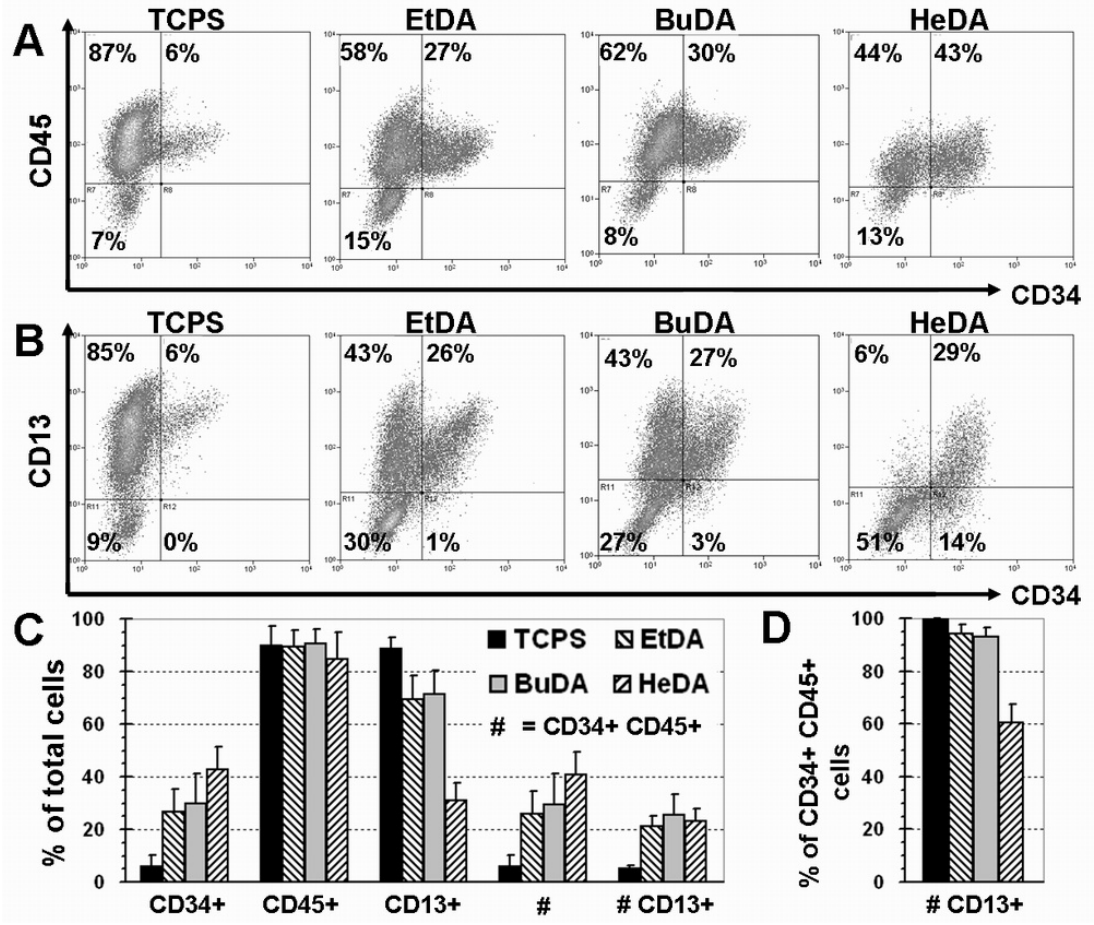

Figure 6.4: Representative FACS profiles (A, B) and surface marker expression summary (C, D) of cells after 10-day *ex vivo* expansion on TCPS and EtDA, BuDA and HeDA nanofiber scaffolds. (A) CD45 *vs.* CD34. (B) CD13 *vs.* CD34. (C) Percentage of total cells expressing one or multiple CD markers. (D) Percentage of the $CD34^{+}CD45^{+}$ cell population that are $CD34^{+}CD45^{+}CD13^{+}$. Data shown are mean ± SD of 5-8 experiments, each conducted in duplicates.

6.4.3 Morphology of Adherent Cells on Aminated Scaffolds

SEM imaging was used to monitor the proliferation kinetics of the adherent HSPC population on the nanofiber scaffolds. At selected time points during the 10-day expansion culture, samples were processed for SEM to image the presence of any adherent cells on the nanofiber scaffolds. We noted that expanded cells adhered weakly to TCPS, Unmod, and AAc surfaces, and most of these cells could easily be

washed off with very gentle rinsing. As such, only sparsely scattered cells remained adherent for SEM imaging.

In contrast, on both EtDA and BuDA modified PES nanofiber mesh, HSPC interaction and adhesion on the nanofiber surfaces were clearly evident. When SEM imaging was performed on day 3 cultures, small pockets of adherent HSPCs could already be observed interacting and proliferating on the aminated nanofiber mesh (Fig. 6.5A & 6.5B). The adherent HSPCs were anchored to the aminated nanofibers via numerous uropodia radiating from the cell surface (Fig. 6.5C). Cells undergoing division were also evident on the nanofiber surface (Fig. 6.5D). By day 8 of expansion culture, the adherent HSPCs proliferated to form distinct, densely populated circular cell colonies on the aminated nanofiber mesh (Fig. 6.5E & 6.5F). The distinct circular cell colonies most likely arose from single or small clusters of HSPCs proliferating outwards in a radial manner along the nanofiber surface. The cell colonies ranged from 0.1 to 1.3 mm in diameter, with cells numbering between 50 to a few thousand.

Adherent HSPCs proliferated well on EtDA (Fig. 6.6A & 6.6B) and BuDA (Fig. 6.6C & 6.6D) nanofiber surfaces to form densely populated cell colonies after 10 days of culture, and this was mirrored by the high mononucleated cell counts (Fig. 6.3). Conversely, the considerably lower proliferation rate on HeDA modified nanofiber surface (210-fold; Fig. 6.3) was reflected by smaller colony size, each containing less than 50 cells (Fig. 6.6E & 6.6F). Besides differences in adherent cell density and colony size, no obvious morphological differences could be discerned among the adherent cells expanded on the EtDA, BuDA, or HeDA nanofiber surfaces.

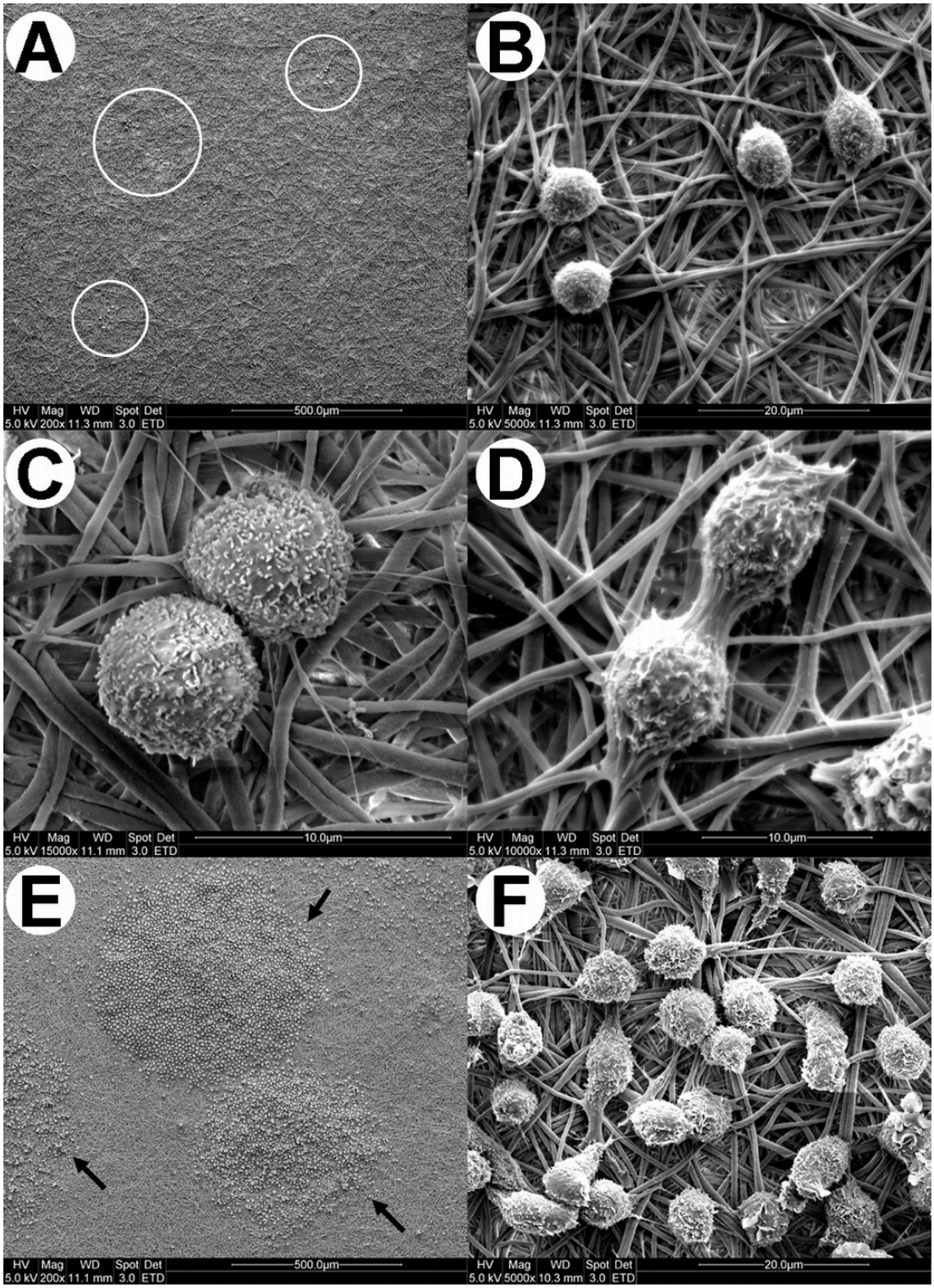

Figure 6.5: SEM images of HSPCs after (A-D) 3-day and (E, F) 8-day cultures on PES BuDA nanofiber mesh at various magnifications. (A, B) Pockets of adherent HSPCs were observed (white circles) proliferating on the aminated nanofiber surface. (C) Cells exhibited numerous filopodia which were interacting with the aminated nanofibers. (D) Cell division was also observed occurring on the nanofiber surface. (E, F) Towards day 8, HSPCs proliferated to form circular colonies (black arrows) on the nanofiber surface.

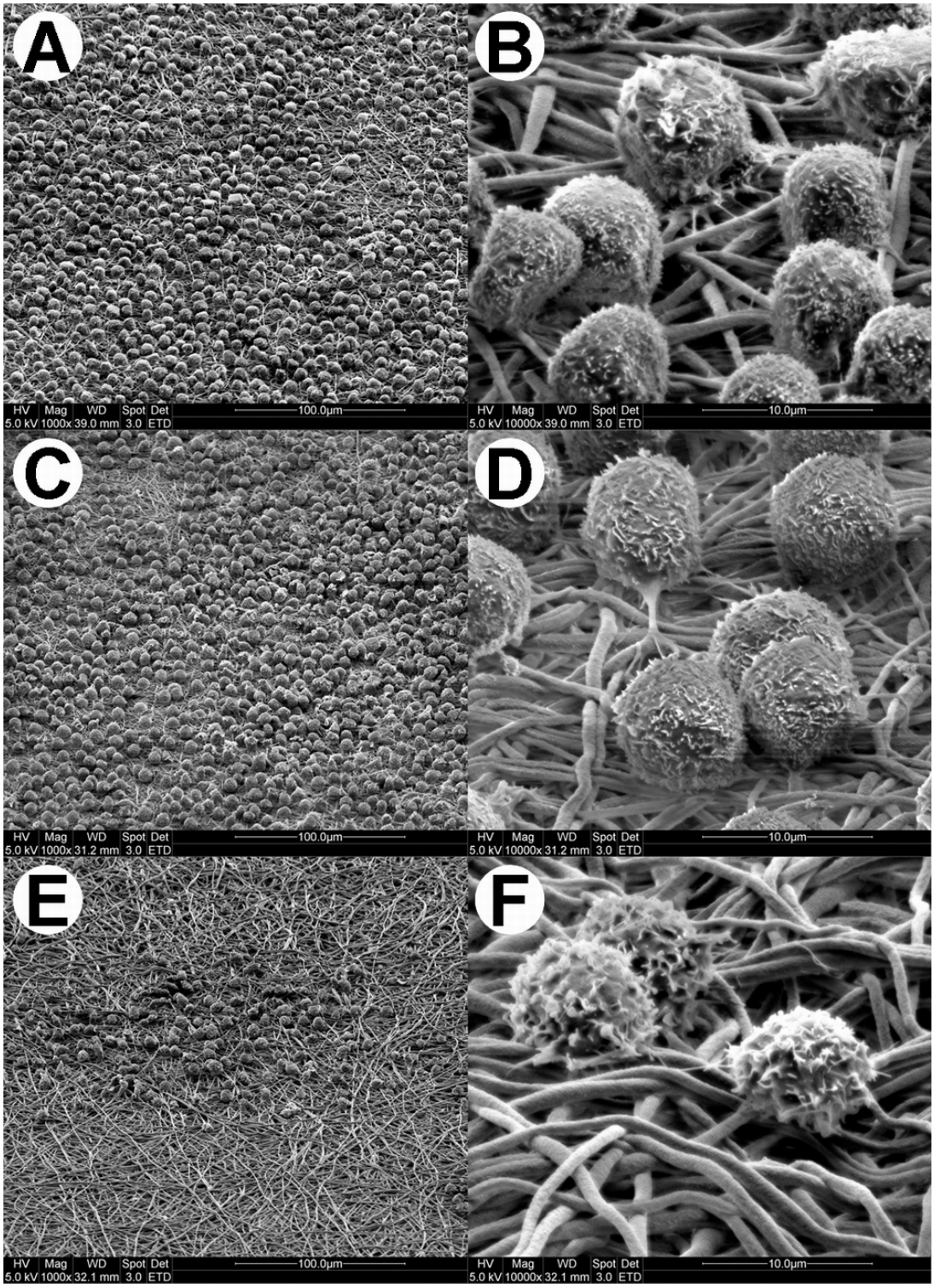

Figure 6.6: SEM images of adherent cell colonies after 10 days of expansion on PES (A, B) EtDA, (C, D) BuDA and (E, F) HeDA nanofiber mesh at various magnifications. Colonies of densely packed adherent cells were observed on EtDA and BuDA nanofiber surfaces. On HeDA nanofiber surfaces, adherent cells were sparsely located.

6.4.4 HSPC Clonogenic Potential from Various Scaffolds

CFC and LTC-IC assays were conducted to evaluate the fraction of primitive progenitor cells in the expanded cultures. The CFC results (Fig. 6.7) showed that cells expanded from Unmod and AAc nanofiber meshes yielded lower total CFU counts (1199 and 1609 respectively) as compared to TCPS control (2890, $p < 0.05$). Conversely, cells expanded from EtDA, BuDA and HeDA nanofiber meshes yielded significantly higher total CFU counts (3996, 4208 and 3742 respectively) compared to TCPS control ($p < 0.05$). In addition, significant differences were also observed in the number of primitive CFU-GEMM units generated by cells expanded on EtDA, BuDA and HeDA nanofiber mesh with 28.1% (1124/3995), 27.6% (1163/4207) and 28.4% (1064/3742) of total colony counts respectively, compared to cells expanded on TCPS (15.0%, 433/2890, $p < 0.05$). TCPS, on the other hand, generated higher percentages of CFU-GM units (63%), indicating differentiation commitment of the TCPS-expanded cells towards the myeloblast / monoblast lineage.

Results from LTC-IC assays (Fig. 6.8) suggested that HSPCs expanded from EtDA-, BuDA- and HeDA-scaffolds may be more primitive than those cultured on control surfaces. More importantly, the LTC-IC numbers generated from these conditions were significantly higher than that from unexpanded cells control ($p < 0.05$), suggesting higher degree of HSPC self-renewal on the aminated nanofiber scaffolds.

Interestingly, cells expanded from HeDA nanofiber scaffolds generated comparatively high numbers of colony units similar to EtDA and BuDA conditions (Fig. 6.7 & 6.8), even though the total cell expansion (Fig. 6.3) was shown to be low. We propose that the relatively high $CD34^+$ phenotype expression of cells expanded from HeDA nanofiber scaffolds may have contributed to this result.

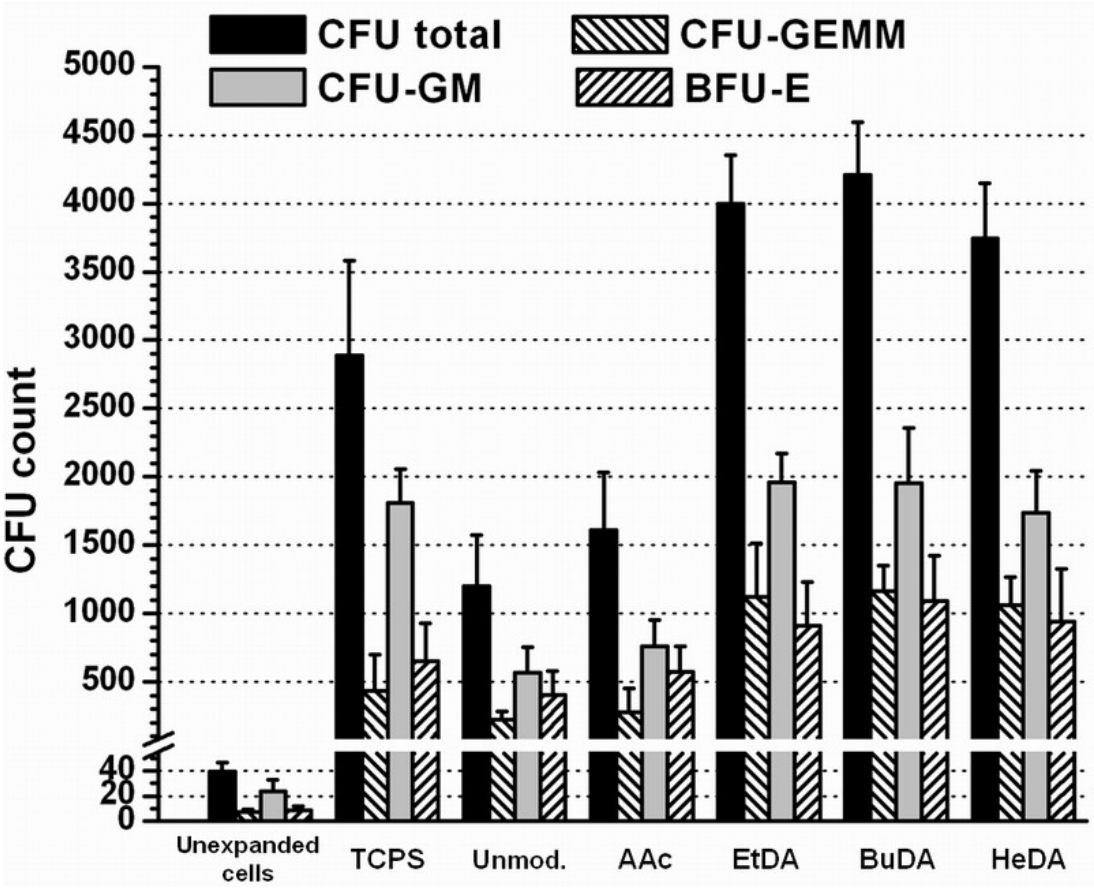

Figure 6.7: CFU counts after 14 days of culture, using the cells from the 10-day expansion cultures on various substrates and unexpanded HSPCs, normalized to CFU per 100 initial unexpanded HSPCs. Data are means ± SD of 3-8 experiments, each conducted in triplicates.

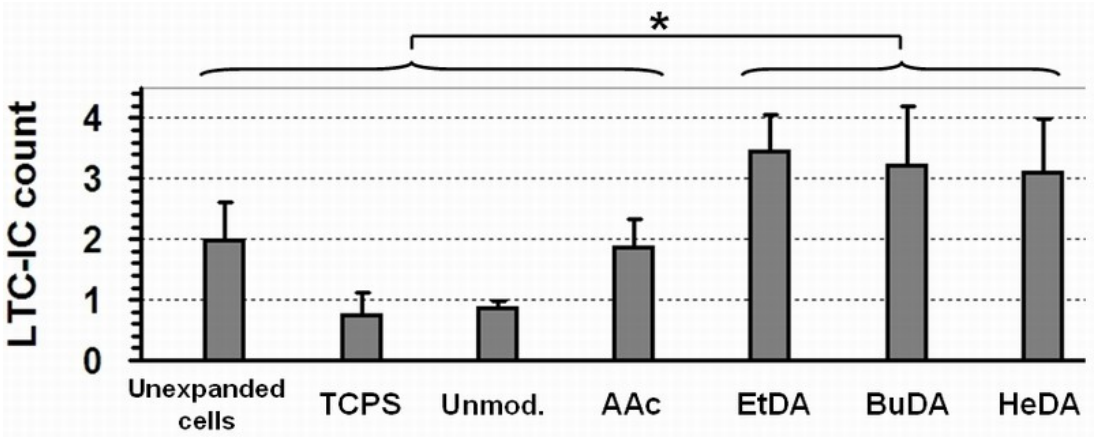

Figure 6.8: LTC-IC counts after 7 weeks of culture, using the cells from the 10-day expansion cultures on various substrates and unexpanded HSPCs, normalized to LTC-IC per 100 initial unexpanded HSPCs. Data are means ± SD of 2 experiments, each conducted in triplicates. * indicates $p < 0.05$.

6.4.5 HSPC NOD/SCID Repopulation Potential from Various Scaffolds

To access the effect of surface modified nanofiber scaffolds on the maintenance of HSPCs and their engraftment potential, cells harvested from 10-day expansion cultures were injected intravenously into sub-lethally irradiated NOD/SCID mice together with 4×10^5 irradiated carrier cells. As positive controls, 600 and 20,000 ("20k" group in Fig. 6.9) unexpanded $CD34^+$ cells were also injected into 2 groups of mice. The presence of > 0.1% human $CD45^+$ cells among the murine bone marrow cells after 6 weeks was used as a criterion for successful primary engraftment in the bone marrow of NOD/SCID mice.

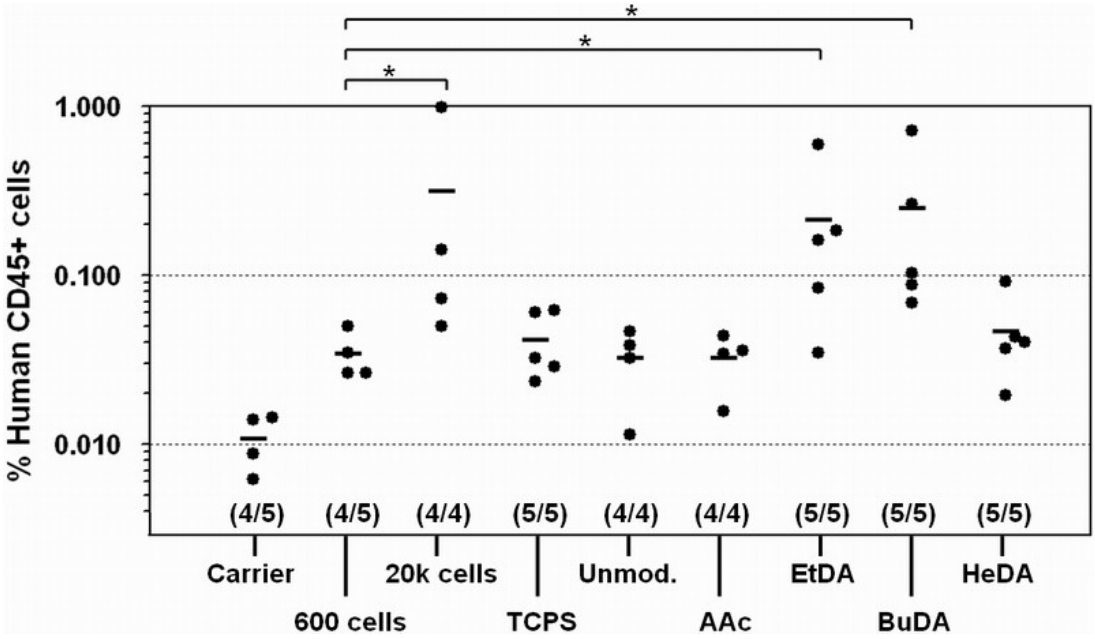

Figure 6.9: Engraftment efficiency of human $CD45^+$ cells in bone marrow of sub-lethally irradiated NOD/SCID mice transplanted with unexpanded HSPCs, cells from the 10-day expansion cultures on various substrates, and irradiated carrier cells alone. Numbers in parentheses indicate mice survival in the different experimental groups. * indicates $p < 0.05$.

Based on this criterion, only cells expanded on EtDA and BuDA scaffolds, along with 20,000 freshly thawed uncultured cells showed positive engraftment (Fig. 6.9). Moreover, there was statistical significance between EtDA *vs.* 600 cells and BuDA *vs.*

600 cells groups ($p < 0.05$), indicating improvement of HSPC engraftment potential following *ex vivo* expansion on EtDA and BuDA nanofiber scaffolds (600 cells was the initial cell seeding number for the expansion cultures). However, the HeDA group failed to show positive engraftment, even though its corresponding CFC and LTC-IC results were comparable to that of EtDA and BuDA groups.

6.5 Discussion

The present study investigates the effects of covalently grafted primary amine functional groups in conjunction with spacer chain length and surface nanofiber topography on *ex vivo* expansion and multipotency maintenance of human umbilical cord HSPC in serum-free culture.

We have shown in the previous chapter that both chemical and topographical cues can modulate HSPC-substrate interaction. On top of supporting total nucleated cell proliferation of the cultured HSPCs at rates highly comparable to that of commercial TCPS surface, aminated (EtDA) nanofiber scaffolds and films also demonstrated additional benefit of enriching $CD34^+CD45^+$ cell proportion to several fold higher than that on TCPS. Specifically, enhanced HSPC-scaffold interaction and adhesion was observed on aminated (EtDA) nanofiber scaffolds, compared with aminated film conditions. In addition, cells expanded from aminated nanofiber scaffolds exhibited better multipotency maintenance by supporting higher percentages of CFU-GEMM cells as compared to aminated film conditions.

Results in this chapter further confirmed the findings from Chapter 5. We showed that cells expanded on aminated nanofiber scaffolds generated significantly higher numbers of total CFU, CFU-GEMM units and LTC-IC counts, in contrast to the carboxylated nanofiber scaffold, unmodified nanofiber scaffold and TCPS

substrate conditions, which yielded various degree of reduction of these progenitor cells (Fig. 6.7 & 6.8).

More importantly, our results indicated that the spacer (ethylene, butylene and hexylene) linkages between amino groups and nanofiber surface influenced the expansion of HSPCs (Fig. 6.3). HSPCs cultured on BuDA-nanofiber scaffold showed similar expansion efficiency to that on EtDA-nanofibers. However, increasing the amine spacer length to 6-carbon alkyl chain (HeDA-nanofibers) reduced total cell expansion by 3.8 times but increased $CD34^+CD45^+$ cell percentage by 1.5 times (41.1% of total cells). Therefore, it appears that HeDA nanofiber scaffold was most efficient at preserving the $CD34^+$ phenotype, but at the expense of overall cell proliferation. The outcomes of *ex vivo* expansion experiments are largely determined by the balance between self-renewal and differentiation of HSPCs in culture [138,142]: Differentiation and hence, depletion of stem and progenitor cell populations, are often accompanied by rapid proliferation of differentiated cells.

Because of this reduced total cell expansion (4-times lower than that on BuDA-nanofibers, Fig. 6.3), and hence lower total cell transplantation dose, the engraftment efficiency of cells expanded on HeDA-nanofibers in NOD/SCID mice was lower than that expanded on BuDA- and EtDA-nanofiber scaffolds. This result confirmed that HSPC transplantation dose is one of the critical parameters for successful engraftment [132-136,141-145]. In addition, we also observed that the $CD34^+CD45^+$ cell population expanded from HeDA nanofiber scaffolds expressed significantly lower levels of the myeloid CD13 antigen compared to EtDA and BuDA nanofiber scaffolds (Fig. 6.4D). We believe that this lower $CD34^+CD45^+CD13^+$ / $CD34^+CD45^+$ expression was also a possible cause of low engraftment frequency for cells expanded on HeDA-nanofiber scaffold, given that a recently report suggests a highly positive

correlation between myeloid marker expression and the engraftment potential of human $CD34^+$ HSPCs [155].

SEM imaging analysis provided the direct evidence of HSPC adhesion on aminated nanofiber substrates (Fig. 6.5 & 6.6). Despite the varying degrees of proliferation, intimate binding of cells with nanofibers was evident for all three types of aminated nanofibers. The strikingly distinct circular colonies most likely arose from single or small clusters of HSPCs proliferating outwards in a radial manner along the nanofiber surface, suggesting that the sub-micron scale feature created by electrospun fibers provided traction and contact guidance for the dividing cells as they migrated away from the center of the colony. Numerous threadlike processes and uropodia emanating from the cell surface [201] apparently anchored the cells to the nanofibers and likely mediated the migration of the cells.

The distinct circular colony features that remained following several sample preparation steps prior to SEM imaging also clearly indicates the strong cell adhesion strength of the expanded cells on the aminated nanofiber mesh. In addition, the colony sizes and cell densities within the colonies correlated well with the total nucleated cell expansion data: HeDA-nanofiber scaffold yielded fewer and smaller colonies compared with EtDA- and BuDA-nanofiber scaffolds. Together with the results presented in the previous chapter, these SEM data suggested the importance of HSPC adhesion in regulating proliferation and self-renewal.

We again hypothesize that the adhesion of HSPCs on aminated nanofiber scaffolds may likely be mediated by CD34 antigen, the highly sialylated and negatively charged glycophosphoprotein, due to electrostatic charge-charge interaction. Recent evidences begin to unfold the important role of CD34 antigen in

regulating cell adhesion [147-150,152-154,156]. Under normal conditions, due to its halo of negatively charged sialic acid, CD34 antigen functions as antiadhesin, preventing cell-cell adhesion of HSPCs [147,148,150,156]. However, when CD34 is bound to antibodies [147,148,150,156] or to an extracellular ligand that is yet to be identified [148], cell-cell adhesion is enhanced, either through recruitment and "concentration" of CD34 to a cap region [150], and/or through antibody-CD34 (or ligand-CD34) mediated intracellular signaling [147,148,150,156], which may result in an up-regulation of cell adhesive molecules in HSPCs [148]. This latter suggests that it is likely that HSPCs interact with surface amino groups, either directly mediate or indirectly facilitate HSPC adhesion to the substrate. Nevertheless, the exact mechanism by which CD34 mediated HSPC adhesion and signaling plays on HSPC expansion and maintenance of pluripotency remains to be elucidated.

6.6 Concluding Remarks

In this chapter, we discussed the spacer effect of the surface-grafted amino groups. Nanofiber scaffolds amine-functionalized with different spacer-lengths modulate HSPC proliferation and phenotype maintenance differently, resulting in different HSPC proliferation kinetics, cell population phenotypic (CD34 and CD13 markers) expression, and also colony-forming and mouse engraftment ability. These observations further suggested the importance of nanofiber topography and amino functional group mediated cell-scaffold interactions in regulating HSPC proliferation and self-renewal.

CHAPTER SEVEN

Adhesive Cell-Scaffold Interaction through Aminated Nanofiber Scaffold Promotes Hematopoietic Stem/Progenitor Cell Maintenance and Lineage Commitment

7.1 Summary

We have shown in previous chapters that a combination of nanofiber topography and immobilized amine mediated cell-substrate interactions has enhanced HSPC adhesion on aminated nanofiber scaffolds, and generated a sub-population of highly adhesive HSPCs proliferating along nanofiber scaffold surface. In this present study, we compare the surface marker phenotypic and clonogenic differences of these adherent and non-adherent hematopoietic cell populations that arise after *ex vivo* expansion culture of $CD34^+$ human umbilical cord hematopoietic stem/progenitor cells (HSPCs) on aminated electrospun nanofiber scaffolds.

Detailed flow cytometry analysis and *in vitro* assay showed that the adherent cell population expressed significantly higher percentage of $CD34^+CD45^+$ cells (43.8%), compared with the non-adherent cell population (21.9%, $p < 0.05$). In addition, the adherent cell population also expressed higher percentage of CD13 myeloid marker (68.3% *vs.* 49.4%, $p < 0.05$) and lower percentage of erythroid marker ($CD71^{high}$, 14.1% *vs.* 46.2%, $p < 0.05$), compared with the non-adherent cell population. CFU assay also indicated significant commitment of the adherent population towards the myeloblast / monoblast lineage, while the non-adherent population showed skewed commitment towards the erythroid lineage.

This study highlights the importance of cell-scaffold interactions as a new approach in modulating HSPC multipotency maintenance and lineage commitment, other than cytokine modulation frequently described in literature.

7.2 Introduction

We have shown in Chapters 5 that both chemical cues and topographical cues synergistically regulate HSPC proliferation through cell-substrate interaction. Specifically, aminated nanofiber scaffolds are efficient in supporting total nucleated cell proliferation of cultured HSPCs at rates highly comparable to that of commercial TCPS surface, while concurrently enriching the $CD34^{+}CD45^{+}$ cell proportion to several times higher than that on TCPS.

Chapter 6 highlighted the spacer effect of the surface-grafted amino groups. Nanofiber scaffolds amine-functionalized with different spacer-lengths modulate HSPC proliferation and phenotype maintenance differently, resulting in different HSPC proliferation kinetics, cell population phenotypic (CD34 and CD13 markers) expression, and also colony-forming and mouse engraftment ability.

A direct consequence of these active cell-substrate interactions is the enhanced HSPC adhesion to aminated nanofiber scaffolds, compared with aminated films or other non-aminated surfaces (e.g. TCPS). The enhanced HSPC adhesion also resulted in sub-populations of highly adhesive HSPCs proliferating along nanofiber scaffold surface, forming unique circular cell colonies (Fig. 7.1). This is a unique growth pattern that is observed for the first time.

In this chapter, we will further investigate the phenotypic differences of these non-adherent and adherent hematopoietic cell populations expanded on aminated

(BuDA) nanofiber scaffolds, in an effort to further understand this HSPC-aminated nanofiber interaction.

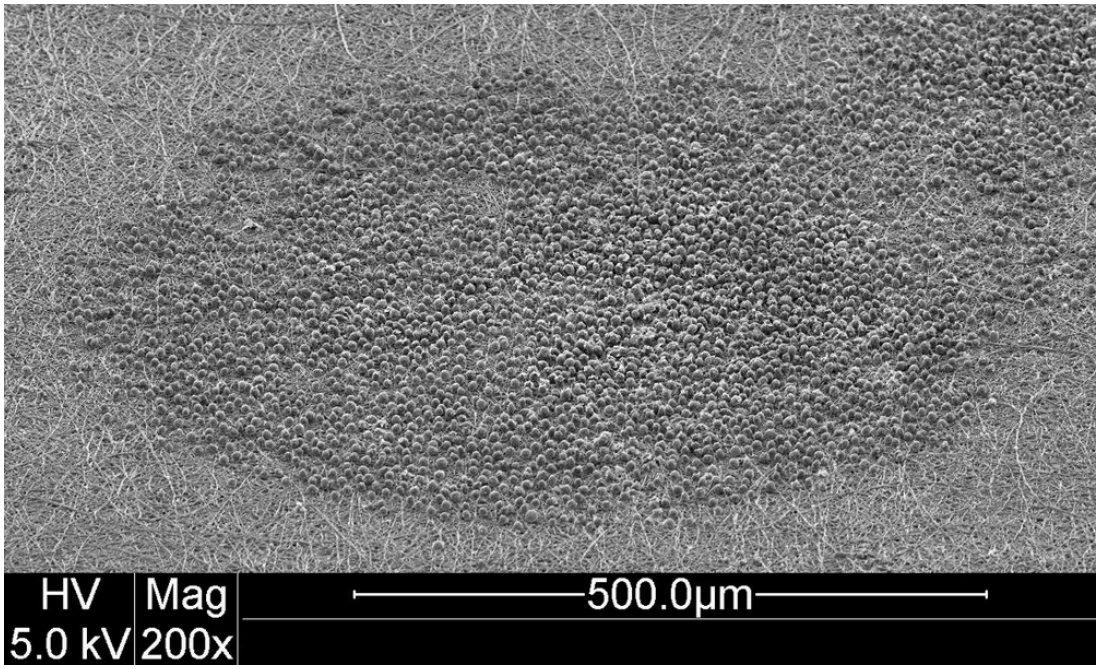

Figure 7.1: Image of a representative adherent cell colony formed on aminated (BuDA) nanofiber scaffold 10 days after *ex vivo* HSPC expansion.

7.3 Experimental Methods

All chemicals were purchased from Sigma-Aldrich unless otherwise stated.

7.3.1 Fabrication of PES Nanofiber Scaffolds

Detailed protocols for PES nanofiber scaffold fabrication can be found in Chapter 5.3.1.

7.3.1.1 Surface Amination of PES Nanofiber Scaffolds

The PES nanofibers were subsequently grafted with Poly(acrylic acid) (PAAc). Detailed protocols for PES nanofiber PAAc grafting can be found in Chapter 5.3.1.1.

The PAAc-grafted PES nanofiber meshes were further conjugated with 1,4-butanediamine (BuDA) using carbodiimide cross-linking method. Briefly, each

scaffold was first gently shaken in 2 mL acetonitrile containing 50 mM dicyclohexylcarbodiimide and 50 mM N-hydroxysuccinimide. After 6 h, the reaction solution was carefully aspirated and each scaffold was immediately immersed into 2 mL acetonitrile containing 0.03 mmol BuDA. After 12 h, the reaction solution was carefully aspirated and each scaffold was thoroughly washed in absolute ethanol to remove any dicyclohexyl urea, which is a by-product of the conjugation reaction. All substrates were subsequently sterilized in 70% ethanol, then loaded into 24-well tissue culture plates (Nunc) and stored in sterile PBS until use.

7.3.2 Hematopoietic Stem Cell Culture and Assays

Frozen human umbilical cord blood $CD34^+$ HSPCs were purchased from AllCells. The $CD34^+$ purity in the HSPC was determined to be 98% by flow cytometry and the viability was determined to be more than 97% by Trypan blue. Purified recombinant human stem cell factor (SCF), Flt-3 ligand (Flt3), thrombopoietin (TPO) and IL-3 was purchased from Peprotech Inc. Low density lipoprotein (LDL) was purchased from Athens Research & Technology Inc. The StemSpan™ serum-free expansion medium and MethoCult GF+ H4435 medium were all purchased from StemCell Technologies.

7.3.2.1 *Ex Vivo* Hematopoietic Expansion Culture

Six hundred HSPCs were seeded onto each BuDA-conjugated nanofiber scaffold. HSPCs were cultured in 0.6 mL StemSpan™ serum-free expansion medium supplemented with 0.04 mg/mL LDL, 100 ng/mL SCF, 100 ng/mL Flt3, 50 ng/mL TPO and 20 ng/mL IL-3 at 37°C, 5% CO_2 for 10 days. Similar cultures were also performed on tissue culture polystyrene surface (TCPS), which serve as a HSPC non-adhesive surface control in this study.

7.3.2.2 Cell Harvest

Cells were harvested after 10 days of expansion culture. Briefly, TCPS substrates and a portion of the BuDA-conjugated nanofiber scaffolds were washed once with non-trypsin cell dissociation solution and twice with 2% FBS Hanks' buffer at 5 min intervals between each wash; and the cell suspensions collected were designated as "TCPS' and "PES-BuDA" conditions respectively.

For the remainder of the BuDA-conjugated nanofiber scaffolds, the cells were harvested into 2 fractions. Briefly, the scaffolds were first gently washed twice with 2% FBS Hanks' buffer at 5 min intervals between each wash to harvest the non-adherent cells; and the cell suspensions collected were designated as "PES-BuDA 'sus' fraction". Subsequently, the scaffolds were washed once with non-trypsin cell dissociation solution and twice with 2% FBS Hanks' buffer at 5 min intervals between each wash to harvest the adherent cells; and the cell suspensions collected were designated as "PES-BuDA 'adh' fraction".

The cell suspensions collected were then concentrated through centrifugation at 500 ×g for 10 min. Aliquots of the concentrated cells were then used for cell counting by a hematocytometer, flow cytometry analysis and colony-forming cell assays.

7.3.2.3 Flow Cytometry

Fluorescently labeled antibodies for CD13, CD15, CD34, CD38, CD45, CD71 and GlyA cell surface markers were purchased from BD Biosciences. The cell samples were incubated with various antibody combinations at 4^{o}C for more than 30 min in 2% FBS Hanks' buffer. After antibody staining, the cells were washed twice using Hanks' buffer and fixed in 1% paraformaldehyde. Cells were analyzed by triple-color flow cytometry on a FACSCalibur analyzer (BD Biosciences). Relevant

isotype controls were also included to confirm specificity and for compensation setting. At least 20,000 gated events were acquired. The Milan-Mulhouse gating method was used for cell enumeration [151].

7.3.2.4 Colony-Forming Cell Assay

Detailed protocols for CFC assay can be found in Chapter 5.3.2.3.

7.3.3 Statistical Analysis

All data were presented as mean ± standard deviation (SD). The statistical significance of the data obtained was analyzed by the Student's t-test. Probability values of $p < 0.05$ were interpreted as denoting statistical significance.

7.4 Experimental Results

7.4.1 Lineage Analysis of Adherent and Non-Adherent HSPCs

After 10-day expansion culture using 600 initial $CD34^+$ HSPCs, cell proliferation on HSPC non-adhesive TCPS surface was 835 ± 196 folds, while cell proliferation on BuDA nanofiber scaffolds was comparatively similar at 702 ± 152 folds ($p > 0.05$). For BuDA nanofiber scaffold, the non-adherent cell population made up 54 ± 10 % of the total cell population, while the adherent cell population accounted for the remaining 46 ± 10 %.

Fig. 7.2 & 7.3 show the representative flow cytometry plots and surface marker expression summary of the *ex vivo* expanded cells. Consistent with previous observations in Chapters 5 & 6, expanded cells on BuDA condition expressed significantly higher percentages of $CD34^+CD45^+$ cells (33.1 ± 9.1 %) as compared to TCPS condition (7.1 ± 3.4 %, $p < 0.05$, Fig. 7.2A & 7.3A). Cells from BuDA

condition also expressed closer percentages of myeloid / erythroid (CD71 [61.2 ± 3.9 %]), erythroid (GlyA [21.1 ± 4.3 %]) and myeloid (CD13 [64.7 ± 8.9 %], CD15 [40.2 ± 5.7 %]) markers, as compared with TCPS condition (CD71 [52.6 ± 3.3 %], GlyA [10.7 ± 2.5 %], CD13 [90.2 ± 4.1 %], CD15 [51.8 ± 8.3 %]), suggesting balanced differentiation of HSPCs into both the erythroid and myeloid lineages on aminated nanofiber scaffolds (Fig. 7.2B, 7.2C & 7.3A). As discussed previously, cells from TCPS condition were more committed towards the myeloblast / monoblast lineage (Chapters 5 & 6). However, comparing between the adherent and non-adherent cell populations of BuDA scaffold condition, distinct differences were observed in surface marker distributions:

(1) The adherent cell population expressed higher percentage of the $CD34^{+}CD45^{+}$ primitive phenotype (43.8 ± 11.1 %), as compared to the non-adherent cell population (21.9 ± 6.5 %, $p < 0.05$, Fig. 7.2A & 7.3A).

(2) The adherent cell population expressed higher percentage of CD13 myeloid marker (68.3 ± 4.6 %), as compared to the non-adherent cell population (49.4 ± 5.7 %, $p < 0.05$, Fig. 7.2B & 7.3A).

(3) The non-adherent cell population expressed higher percentage of CD71 antigen (81.0 ± 3.1 %), as compared to adherent cell population (39.2 ± 8.2 %, $p < 0.05$, Fig. 7.2C & 7.3A). In particular, $CD71^{high}$ expression was significant in the non-adherent population (46.2 ± 3.2 %, $p < 0.05$), as compared to adherent population (14.1 ± 4.7 %, Fig. 7.2C). This indicated that cells in the non-adherent cell population were skewed towards erythroid lineage.

(4) The non-adherent cell population expressed higher percentage of late CD15 myeloid marker (44.4 ± 1.2 %, $p < 0.05$) and late GlyA erythroid marker (35.7 ± 7.4 % $p < 0.05$) as compared to adherent cell population (CD15 [33.5 ± 1.2 %], GlyA [12.4 ± 2.5 %], Fig. 7.3A). This indicates that cells in the non-adherent cell population were more differentiated.

(5) The $CD34^{+}CD45^{+}$ fraction of the non-adherent cell population expressed higher co-expression of CD71 (57.0 ± 9.4 % of $CD34^{+}CD45^{+}$ cells, $p < 0.05$) and $CD71^{high}$ (8.9 ± 2.3 % of $CD34^{+}CD45^{+}$ cells, $p < 0.05$) as compared to the corresponding adherent cell population (26.9 ± 6.5 % and 3.6 ± 2.1 % of $CD34^{+}CD45^{+}$ cells, respectively, Fig. 7.3B).

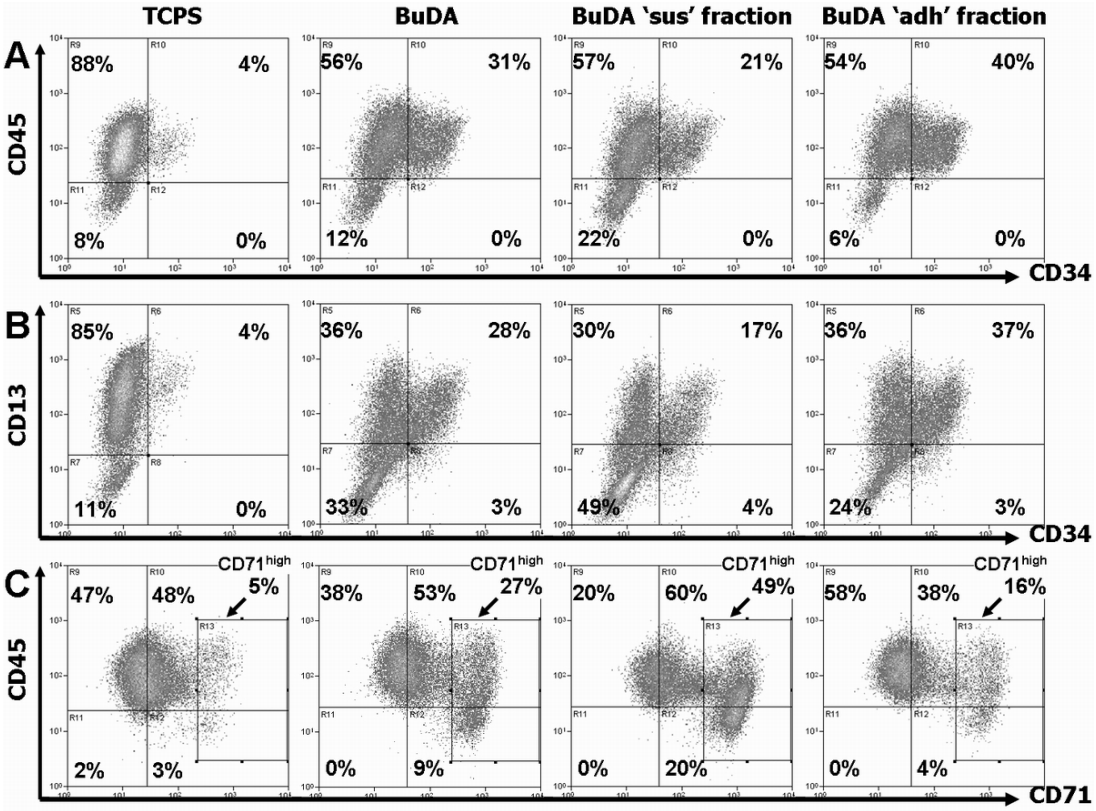

Figure 7.2: Representative FACS profiles of cells after 10-day *ex vivo* expansion on TCPS, PES-BuDA, and non-adherent ('sus') and adherent ('adh') fractions from PES-BuDA conditions. (A) CD45 *vs.* CD34. (B) CD13 *vs.* CD34. (C) CD45 *vs.* CD71.

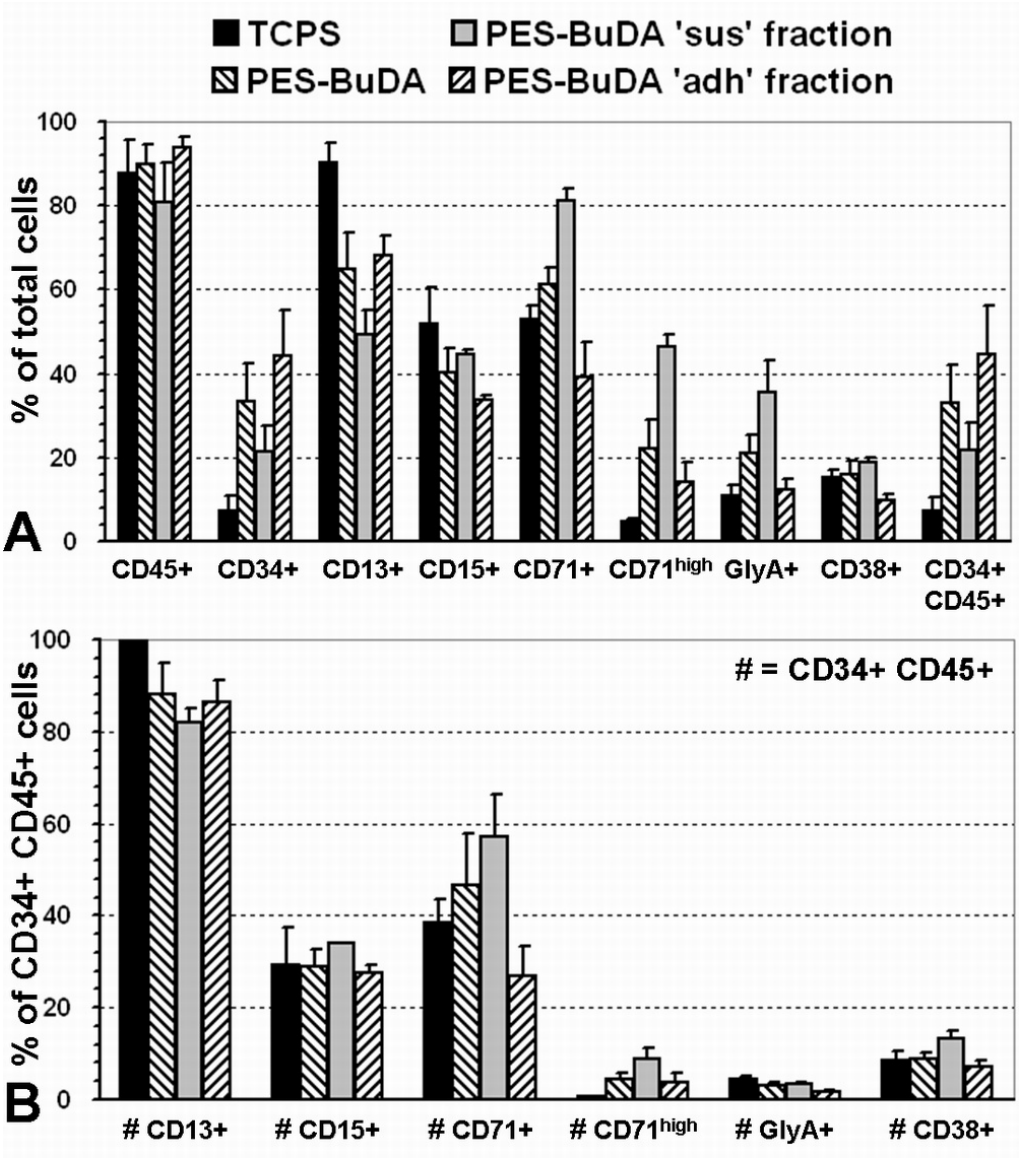

Figure 7.3: Surface marker expression summary of cells after 10-day *ex vivo* expansion on TCPS, PES-BuDA, and non-adherent ('sus') and adherent ('adh') fractions from PES-BuDA conditions. (A) Percentage of total cells expressing one or multiple CD markers. (B) Percentage of the $CD34^{+}CD45^{+}$ cell population that are also CDX^{+}, where CDX represents CD13, CD15, CD38, CD71 or GlyA. Data shown are mean ± SD of 3 experiments, each conducted in duplicates.

7.4.2 Clonogenic Differences of Adherent and Non-Adherent HSPCs

CFC assays were conducted to evaluate the fraction of primitive progenitor cells in the expanded cultures (Fig. 7.4). Cells expanded from BuDA-conjugated nanofiber scaffolds generated significantly higher percentages of the more primitive CFU-

GEMM units (23.8 ± 2.2 %, $p < 0.05$), as compared to cells expanded from TCPS condition (13.0 ± 3.6 %). TCPS condition, on the other hand, generated higher percentages of CFU-GM units (66.5 ± 9.1 %, $p < 0.05$), compared with BuDA condition (52.3 ± 6.8 %), indicating differentiation commitment of the TCPS-expanded cells towards the myeloblast / monoblast lineage.

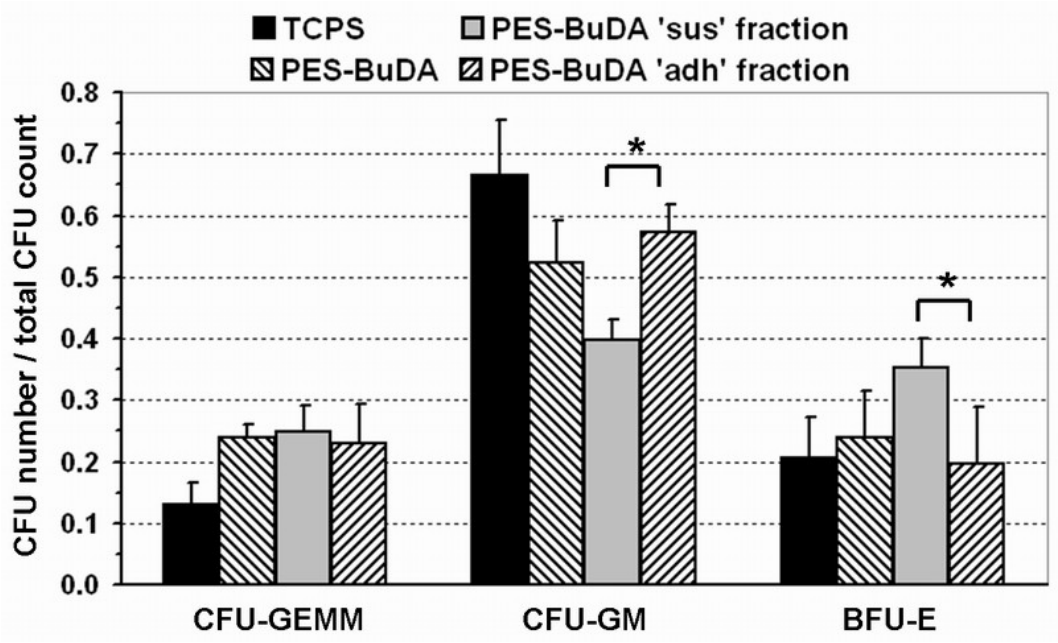

Figure 7.4: Specific CFU fractions after 14 days of culture, using the cells from 10-day expansion cultures on TCPS, PES-BuDA, and non-adherent ('sus') and adherent ('adh') fractions from PES-BuDA conditions, normalized to CFU type per total CFU generated. Data are means ± SD of 2 experiments, each conducted in triplicates. * indicates $p < 0.05$.

Comparing between the adherent and non-adherent cell populations of BuDA scaffold condition, we see that the adherent cell population yielded significantly higher percentages of CFU-GM units (57.4 ± 4.4 %, $p < 0.05$) and lower percentages of BFU-E units (19.6 ± 9.2 %, $p < 0.05$), as compared to the non-adherent cell population (CFU-GM [39.8 ± 3.2 %] and BFU-E [35.3 ± 4.6 %]). This result indicates differentiation commitment of the adherent population towards the myeloblast /

monoblast lineage, while for the non-adherent population differentiation commitment towards the erythroid lineage is significant.

7.5 Discussion

The phenomenon that aminated nanofibers can actively interact and modulate HSPC proliferation and phenotype maintenance underscores the importance of culture substrate properties in current stromal-free, cytokine-supplemented *ex vivo* HSPC expansion systems. A consequence of these interactions is the identification of a proliferative HSPC population subset that is highly adhesive to the aminated nanofiber surface. This study represents the first to identify such an adhesive population among HSPCs. Using BuDA-conjugated nanofiber scaffolds, we sought to investigate the phenotypic properties of this adherent hematopoietic cell population, as compared to the non-adherent hematopoietic cell population in the *ex vivo* HSPC expansion cultures.

The flow cytometry surface marker analysis results show that cells expressing $CD34^+$ were significantly enriched in the adherent cell population, compared with the non-adherent cell population, on aminated nanofiber scaffold cultures. The adherent cell population also exhibits a lesser degree of late differentiation markers (CD15 and GlyA), compared with the non-adherent cell population. This evidence suggests the important roles that cell-scaffold interactions play in maintaining HSPC proliferative capacity, as well as primitive phenotype maintenance, in cytokine-supplemented expansion cultures.

We have shown here and in Chapters 5 & 6 that in pure suspension cultures lack of any cell-substrate interaction signals (e.g. TCPS condition), the CD34 primitive phenotype maintenance of the cultured HSPCs is inefficient. In addition, we have also

shown that for scaffold cultures without the correct substrate signals (e.g. non-aminated scaffolds), the HSPC proliferative capacity in these scaffold cultures is poor. These observations suggest that the surface-immobilized amine molecules may be acting as a kind of "HSPC ligand" that mediates HSPC-scaffold interaction, and the nanofiber textured topography further enhances this cell-scaffold interaction [57-59].

As proposed earlier in Chapters 5 & 6, the results presented here further suggest that the CD34 surface marker likely serves as a receptor for the "amine-ligand". In the normal state, the highly sialylated and negatively-charged hematopoietic CD34 antigen acts as anti-adhesive molecule, preventing cellular adhesion in hematopoietic cells strongly expressing this marker (i.e. HSPCs) [147-150,152-154,156]. Furthermore, our observations have shown that cell-scaffold adhesion correlates well with $CD34^+$ expression, substantiating the hypothesis that the negatively-charged CD34 antigen could interact with the positively-charged immobilized amino groups.

An interesting finding that arises from comparing the surface marker phenotypes (Fig. 7.2 & 7.3) and clonogenic differences (Fig. 7.4) of the adherent and non-adherent hematopoietic cell populations is that the predominant lineage commitments of HSPCs within the 2 cell populations are different: The adherent HSPC population is prevalently committed towards the myeloblast / monoblast lineage, while the non-adherent HSPC population is significantly committed towards the erythroid lineage.

Currently, HSPC lineage commitment and differentiation is frequently modulated using soluble signals from recombinant cytokines in stromal-free *ex vivo* hematopoietic expansion cultures. Recombinant cytokines like IL, TPO, SCF, FL, etc. are used alone or in combination to regulate hematopoiesis in these suspension cultures [173-177,202,203]. For example, TPO, in combination with IL-1, IL-6, IL-11

and SCF has been shown to promote proliferation and differentiation of megakaryocytes from $CD34^+$ cells *in vitro* [202]; while FL, in combination with IL-7 and IL-12 has been shown to promote expansion of T- and B-lymphocyte progenitors [203]. FL and SCF are also important in regulating early hematopoiesis and it is frequently used in combination with GM-CSF, TPO or other cytokines to stimulate the proliferation of early hematopoietic progenitor cells [173-177].

However, the role of cell-substrate interaction signals has rarely been investigated in HSPC expansion cultures, maybe because of the lack of a suitable HSPC-adhesive substrate to investigate its effects. In this study, through the use of HSPC-adhesive aminated nanofiber scaffolds, we demonstrated the cell-scaffold interaction, as a new and convenient approach to regulate HSPC ($CD34^+$) multipotency maintenance as well as lineage commitment. Although the specific control of hematopoiesis is currently limited in our present scaffold system, we envision that by combining with potential factors like recombinant cytokines and other cell adhesion molecules [173-177,202-205], modulating HSPC-substrate interaction through nanofiber scaffold will become a highly useful method to regulate HSPC expansion.

7.6 Concluding Remarks

Aminated nanofibers enhance the interaction with HSPCs in *ex vivo* expansion culture; and the adherent hematopoietic cell population is enriched with $CD34^+CD45^+$ cells. In addition, different lineage commitment patterns are observed between the adherent and non-adherent cell populations. This study highlights the importance of cell-scaffold interactions in modulating HSPC maintenance and lineage commitment.

CHAPTER EIGHT

Conclusions

The success of scaffold-based cell cultures largely depends on the optimal events of attachment, proliferation, differentiation, and phenotypic maintenance, which in turn are governed by a host of signals provided by the cell-scaffold microenvironment. These signals include: (1) homotypic / heterotypic cell-cell interaction; (2) soluble signaling molecules; and (3) cell-substrate interaction signals. An ideal scaffold culture system should include all these interactive components. In this thesis, we have focused on cell-substrate interaction signals mediated by both substrate-bound signaling molecules and nanofiber scaffold topographical cues.

The general strategy of developing a scaffold that can provide both topographical and immobilized biochemical cues involves first nanofiber scaffold fabrication via the electrospinning technique, followed by nanofiber bio-functionalization. The bio-functionalization process involves the initial functionalization of the nanofiber surface with carboxylic acid groups using UV-initiated poly(acrylic acid) grafting method. This is followed by conjugation of bioactive molecules onto the functionalized nanofiber surfaces. In this thesis, we have presented the efficacy of this nanofiber bio-functionalization strategy on various cell culture systems like hepatocyte scaffold cultures and hematopoietic stem cell expansion cultures.

In Chapter 3, we have described the galactose bio-functionalization of electrospun PCLEEP nanofibers for liver cell cultures. Both galactosylated nanofiber scaffolds and galactosylated films supported the hepatic functions (albumin secretion, ammonia removal and cytochrome P450 activity) of the cultured primary hepatocytes

better than unmodified nanofiber scaffolds and films. Interestingly, galactosylated nanofiber scaffolds exhibit the unique property of promoting hepatocyte aggregates and cell infiltration within the mesh and around the fibers, forming an integrated spheroid-nanofiber construct. These results demonstrated that the nanofiber topography together with surface-immobilized galactose ligand synergistically enhance cell-substrate interaction as indicated by hepatocyte adhesion and infiltration, even though this enhanced cell-substrate interaction did not translate into significantly higher functional enhancement as compared to galactosylated film condition.

We subsequently demonstrated in Chapter 4 that hepatocyte cytochrome P450 activity enhancement can be brought about through further 3-Mc bio-functionalization of the galactosylated nanofiber scaffold. By taking advantage of the porous and layer-forming properties of electrospun nanofibers, we had designed a dual functional scaffold that induces two different biological responses from hepatocytes. Galactose bio-functionalization on nanofibers resulted in a scaffold that can induce hepatocyte adhesion and re-organization, while 3-Mc loading into the fiber, working together with fiber galactosylation, resulted in a hepatocyte bioactive scaffold that can also regulate the hepatocyte cytochrome P450 function.

In Chapter 5, we further presented the efficacy of this nanofiber bio-functionalization strategy on hematopoietic stem / progenitor cell expansion. Using amine molecule bio-functionalization, we have demonstrated the effectiveness of aminated electrospun PES nanofiber mesh as potential scaffolds for *ex vivo* HSPC expansion under serum-free conditions. Among the carboxylated, hydroxylated, and aminated PES substrates and TCPS, aminated PES substrates mediated the highest expansion efficiency of $CD34^{+}CD45^{+}$ cells and CFU potential. Aminated nanofiber mesh could further enhance the HSPC-substrate adhesion. In particular, aminated

nanofiber meshes supported a higher degree of cell adhesion, percentage of $CD34^+CD45^+$ cells and expansion of CFU-GEMM forming progenitor cells, as compared to aminated films. SEM imaging also revealed the discrete colonies of cells proliferating and interacting with the aminated nanofibers.

In Chapter 6, we showed that nanofiber scaffolds immobilized with amine functional groups of increasing 2-, 4-, 6-carbon spacer chain lengths could further modulate HSPC proliferation and phenotype maintenance, resulting in different HSPC proliferation kinetics, cell population phenotypic (CD34 and CD13 markers) expression, mouse engraftment potential and also short-term and long-term colony-forming ability. These observations further suggested the importance of nanofiber topography and amino functional group mediated cell-scaffold interactions in regulating HSPC proliferation and self-renewal.

Finally, in Chapter 7, we compared the surface marker phenotypic and clonogenic differences of the adherent and non-adherent hematopoietic cell populations that arise after *ex vivo* expansion culture of $CD34^+$ HSPCs on aminated electrospun nanofiber scaffolds. Detailed flow cytometry analysis showed that the adherent cell population expressed significantly higher percentage of $CD34^+CD45^+$ cells, compared with the non-adherent cell population. In addition, flow cytometry analysis and CFU assay also indicated significant commitment of the adherent population towards the myeloblast / monoblast lineage, while the non-adherent population showed skewed commitment towards the erythroid lineage. This study also highlights the importance of cell-scaffold interactions as a new approach in modulating HSPC multipotency maintenance and lineage commitment, other than cytokine modulation frequently described in literature.

In summary, this research has:

(1) Presented a nanofiber bio-functionalization strategy to develop polymeric nanofiber constructs that can serve as cell culture scaffolds.

(2) Demonstrated through primary hepatocyte cultures and hematopoietic stem / progenitor cell expansion cultures that these scaffolds can promote cell-substrate interactions and are bioactive in regulating cellular responses like cell adhesion, cell morphological reorganization, cell differentiated functions, cell proliferation, and cell phenotype maintenance.

(3) Demonstrated the synergistic effects that nanofiber topography and surface immobilized biochemical cues play in enhancing these cell-scaffold interactions and regulation of cellular functions.

APPENDIX

[1] Synthesis of 1-O-(6'-Aminohexyl)-D-galactopyranoside (AHG)

The galactose ligand AHG was synthesized according to procedures reported by Yin et al. [33]. The scheme is shown in Fig. 8.1.

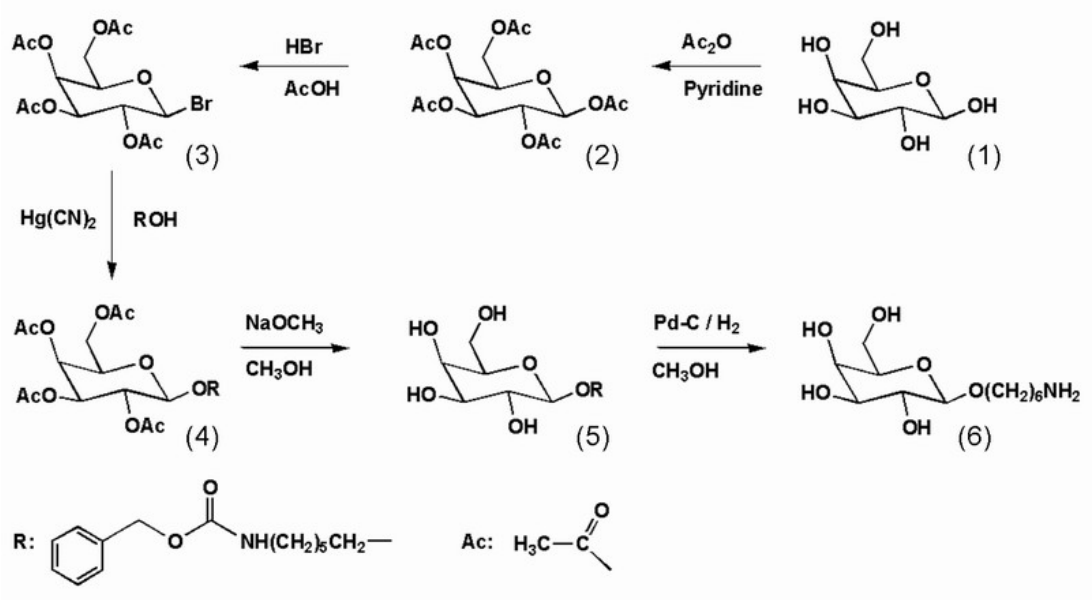

Figure 8.1: Synthesis scheme for AHG.

Benzyl *N*-(6-hydroxyhexyl) carbamate

Carbobenzoxy chloride solution (50% in toluene, 40 mL) and K_2CO_3 solution (8.3 g in 30 mL of H_2O) were added dropwise to an ice-cooled solution of 6-amino-1-hexanol (11.7 g, 0.1 mol) in 400 mL of ethyl acetate from two addition funnels simultaneously. After the addition, the mixture was further stirred at room temperature for 3 h, followed by washing with 1 N HCl (3×200 mL) and water (3×200 mL). The solution was dried over anhydrous $MgSO_4$ and evaporated to dryness. The residue was recrystallized from ethylacetate to yield a white powder (13.4 g, 53.4%), m.p. 80-82°C.

1,2,3,4,6-Penta-*O*-acetyl-D-galactopyranose (2)

β-D-galactose (1) (18.0 g, 0.10 mol) was dissolved in a mixture of dry pyridine (150 mL, 1.86 mol) and acetic anhydride (150 mL, 1.60 mol) and stirred at room temperature for 3 days. The mixture was concentrated by vacuum rotary evaporation to yield a yellow syrupy residue. The residue was dissolved in 200 mL of $CHCl_3$, extracted with 200 mL of cold 2 N H_2SO_4, and washed with saturated $NaHCO_3$ solution (200 mL) and water (2×200 mL). The organic phase was dried over anhydrous $MgSO_4$. The solution was filtered, concentrated, and vacuum dried. The residue was recrystallized from ethanol to yield a white powder (22.5 g, 57.7%). Thin-layer chromatography (TLC): ethylacetate-hexane (3:2), R_f = 0.54. ^{1}H-NMR ($CDCl_3$) δ: 1.99 (s, 3H, *Me*), 2.01 (s, 3H, *Me*), 2.03 (s, 3H, *Me*), 2.15 (d, 6H, 2*Me*), 4.10 (m, 2H, 2H^6), 4.34 (m, 1H, H^4), 5.33 (m, 2H, H^5 and H^3), 5.49 (t, 1H, H^2), 6.37 (s, 1H, H^1).

2,3,4,6-Tetra-*O*-acetyl-1-bromo-1-deoxy-D-galactopyranose (3)

Ten grams of (2) was dissolved in 50 mL of HBr solution (in glacial acetic acid, 11.5%, w/v) and diluted with 200 mL of $CHCl_3$. The resulted mixture was poured into 1.8 L of ice-water and thoroughly mixed. The organic layer was collected, washed with saturated $NaHCO_3$ solution (2×100 mL) and water (2×100 mL), dried over $MgSO_4$, and filtered. The filtrate was vacuum dried to syrup (3). Yield: 9.8 g (93.0%). TLC: ethylacetate-hexane (3:2), R_f = 0.65. ^{1}H-NMR ($CDCl_3$) δ: 1.89 (s, 3H, *Me*), 1.95 (s, 6H, 2*Me*), 2.05 (s, 3H, *Me*), 4.07 (m, 2H, 2H^6), 4.37 (m, 1H, H^4), 5.01 (m, 2H, H^5 and H^3), 5.11 (t, 1H, H^2), 5.30 (s, 1H, H^1).

1-O-[6'-(*N*-Benzyloxycarbonyl)aminohexyl]-2,3,4,6-tetra-*O*-acetyl-D-galactopyranoside (4)

(3) (9.6 g, 23.5 mmol) was mixed with benzyl *N*-(6-hydroxyhexyl) carbamate (6.52 g, 26 mmol), $Hg(CN)_2$ (6.55g, 26 mmol), Drierite (2.6 g) in a toluene-nitromethane mixture (1:1, v/v, 250 mL) and stirred for 24 h. The mixture was filtered and the filtrate was concentrated under reduced pressure. The residue was dissolved in $CHCl_3$ (200 mL), washed with 1M NaCl solution (2×200 mL) and 0.5M KBr solution (200 mL), dried over $MgSO_4$, and filtered. The filtrate was concentrated to syrup. The crude product was subjected to silica chromatography using ethylacetate-hexane (3:2, v/v, R_f = 0.39) as the eluent. (4) was obtained as white powder after evaporation of the solvent from the corresponding fractions (5.2 g, 38.2%). 1H-NMR (CDCl3) δ: 1.21-1.52 (m, 8H, 4CH_2), 1.95-2.18 (m, 12H, 4*Me*), 2.96 (t, 2H, CH_2-*N*), 3.54 (m, 2H, *O*-CH_2), 4.03 (m, 2H, 2H^6), 4.35 (m, 1H, H^4), 4.65 (m, 1H, H^5), 4.72 (d, 1H, H^2), 4.85 (d, 1H, H^2), 5.03 (d, 1H, H^1).

1-O-[6'-(*N*-Benzyloxycarbonyl)aminohexyl]-D-galactopyranoside (5)

One milliliter of sodium methoxide solution in methanol (5%, w/v) was added to a solution of (4) (5.0 g, 8.6 mmol) in methanol (100 mL). The mixture was stirred for 3 h, followed by adding Dowex 50WX8-200 ion-exchange resin (pretreated with 1N HCl and washed with methanol) until the pH value of the solution reached 5-6. The mixture was gently stirred for 0.5 h and filtered. The filtrate was evaporated to yield yellowish syrup (3.2 g, 90.0%). TLC: ethylacetate-acetic acid (9:1), R_f = 0.78. ^{1}H-NMR (D_2O) δ: 1.19 (m, 4H, 2CH_2), 1.34 (m, 2H, CH_2), 1.49 (m, 2H, CH_2), 2.98 (t, 2H, CH_2-*N*), 3.44 (m, 2H, *O*-CH_2), 3.55 (m, 2H, H^3 and H^4), 3.70 (d, 2H, H^6), 3.79 (m, 1H, H^5), 3.85 (d, 1H, H^2), 4.24 (d, 1H, H^1), 4.93 (s, 2H, CH_2-*Ph*), 7.20 (m, 5H, C_6H_5).

1-O-(6'-Aminohexyl)-D-galactopyranoside (6)

The deacetylated product (5) (3.2 g, 7.7 mmol) was dissolved in methanol (150 mL) with Pd-C catalyst (1.6 g). Hydrogen gas was bubbled into the stirred mixture until benzyloxycarbonyl group was completely removed as determined by TLC. Pd-C was filtered off and the filtrate was concentrated and vacuum dried to syrup. It was then dissolved in distilled water and lyophilized to obtain white powder (6) (1.8 g, 83.3%). TLC: ethanol-acetic acid (9:1), R_f = 0.23. ^{1}H-NMR (D_2O) δ: 1.32 (m, 4H, 2CH_2), 1.43 (m, 2H, CH_2), 1.59 (m, 2H, CH_2), 2.61 (t, 2H, *N*-CH_2), 3.43 (m, 2H, *O*-CH_2), 3.62 (m, 2H, H^3 and H^4), 3.73 (m, 2H, H^6), 3.88 (m, 2H, H^5 and H^2), 4.33 (d, 1H, H^1).

REFERENCES

[1] Hubbell JA. Biomaterials in tissue engineering. Biotechnology (NY) 1995;13(6):565-576.

[2] Griffith LG. Emerging design principles in biomaterials and scaffolds for tissue engineering. Ann N Y Acad Sci 2002;961:83-95.

[3] Peter SJ et al. Polymer concepts in tissue engineering. J Biomed Mater Res 1998;43(4):422-427.

[4] Chaikof EL et al. Biomaterials and scaffolds in reparative medicine. Ann N Y Acad Sci 2002;961:96-105.

[5] Yarlagadda PK et al. Recent advances and current developments in tissue scaffolding. Biomed Mater Eng 2005;15(3):159-177.

[6] Hammond JS et al. Scaffolds for liver tissue engineering. Expert Rev Med Devices 2006;3(1):21-27.

[7] Bottaro DP et al. Molecular signaling in bioengineered tissue microenvironments. Ann N Y Acad Sci 2002;961:143-153.

[8] Lutolf MP et al. Synthetic biomaterials as instructive extracellular microenvironments for morphogenesis in tissue engineering. Nat Biotechnol 2005;23(1):47-55.

[9] Dersch R et al. Nanoprocessing of polymers: applications in medicine, sensors, catalysis, photonics. Polymers for Advanced Technologies 2005;16(2-3):276-282.

[10] Huang ZM et al. A review on polymer nanofibers by electrospinning and their applications in nanocomposites. Composites Science and Technology 2003;63(15):2223-2253.

[11] Jayaraman K et al. Recent advances in polymer nanofibers. Journal of Nanoscience and Nanotechnology 2004;4(1-2):52-65.

[12] Subbiah T et al. Electrospinning of nanofibers. Journal of Applied Polymer Science 2005;96(2):557-569.

[13] Wang YK et al. Nanofibres and their influence on cells for tissue regeneration. Australian Journal of Chemistry 2005;58(10):704-712.

[14] Li WJ et al. Electrospun nanofibrous structure: A novel scaffold for tissue engineering. Journal of Biomedical Materials Research 2002;60(4):613-621.

[15] Li WJ et al. Biological response of chondrocytes cultured in three-dimensional nanofibrous poly(epsilon-caprolactone) scaffolds. J Biomed Mater Res 2003;67A(4):1105-1114.

[16] Li WJ et al. Multilineage differentiation of human mesenchymal stem cells in a three-dimensional nanofibrous scaffold. Biomaterials 2005;26(25):5158-5166.

[17] Li WJ et al. A three-dimensional nanofibrous scaffold for cartilage tissue engineering using human mesenchymal stem cells. Biomaterials 2005;26(6):599-609.

[18] Badami AS et al. Effect of fiber diameter on spreading, proliferation, and differentiation of osteoblastic cells on electrospun poly(lactic acid) substrates. Biomaterials 2006;27(4):596-606.

[19] Shin M et al. Contractile cardiac grafts using a novel nanofibrous mesh. Biomaterials 2004;25(17):3717-3723.

[20] Zong X et al. Electrospun fine-textured scaffolds for heart tissue construct. Biomaterials 2005;26(26):5330-5338.

[21] Mo XM et al. Electrospun P(LLA-CL) nanofiber: a biomimetic extracellular matrix for smooth muscle cell and endothelial cell proliferation. Biomaterials 2004;25(10):1883-1890.

[22] Xu C et al. Electrospun nanofiber fabrication as synthetic extracellular matrix and its potential for vascular tissue engineering. Tissue Eng 2004;10(7):1160-1168.

[23] Xu CY et al. In vitro study of human vascular endothelial cell function on materials with various surface roughness. Journal of Biomedical Materials Research Part A 2004;71A(1):154-161.

[24] Xu CY et al. Aligned biodegradable nanofibrous structure: a potential scaffold for blood vessel engineering. Biomaterials 2004;25(5):877-886.

[25] Yang F et al. Characterization of neural stem cells on electrospun poly(L-lactic acid) nanofibrous scaffold. J Biomater Sci Polym Ed 2004;15(12):1483-1497.

[26] Williamson MR et al. PCL-PU composite vascular scaffold production for vascular tissue engineering: attachment, proliferation and bioactivity of human vascular endothelial cells. Biomaterials 2006;27(19):3608-3616.

[27] Sun T et al. Self-organization of skin cells in three-dimensional electrospun polystyrene scaffolds. Tissue Eng 2005;11(7-8):1023-1033.

[28] Reneker DH et al. Nanometre diameter fibres of polymer, produced by electrospinning. Nanotechnology 1996;7(3):216-223.

[29] Li D et al. Electrospinning of nanofibers: Reinventing the wheel? Advanced Materials 2004;16(14):1151-1170.

[30] Zhu Y et al. Surface modification of polycaprolactone membrane via aminolysis and biomacromolecule immobilization for promoting cytocompatibility of human endothelial cells. Biomacromolecules 2002;3(6):1312-1319.

[31] Oehr C et al. Plasma grafting - a method to obtain monofunctional surfaces. Surface & Coatings Technology 1999;119:25-35.

[32] Uchida E et al. A Novel Method for Graft-Polymerization Onto Poly(Ethylene-Terephthalate) Film Surface by Uv Irradiation Without Degassing. Journal of Applied Polymer Science 1990;41(3-4):677-687.

[33] Yin C et al. High density of immobilized galactose ligand enhances hepatocyte attachment and function. J Biomed Mater Res 2003;67A(4):1093-1104.

[34] Ying L et al. Immobilization of galactose ligands on acrylic acid graft-copolymerized poly(ethylene terephthalate) film and its application to hepatocyte culture. Biomacromolecules 2003;4(1):157-165.

[35] Tan WJ et al. Adhesion contact dynamics of primary hepatocytes on poly(ethylene terephthalate) surface. Biomaterials 2005;26(8):891-898.

[36] Nakajima N et al. Mechanism of amide formation by carbodiimide for bioconjugation in aqueous media. Bioconjug Chem 1995;6(1):123-130.

[37] Reneker DH et al. Bending instability of electrically charged liquid jets of polymer solutions in electrospinning. Journal of Applied Physics 2000;87(9):4531-4547.

[38] Yarin AL et al. Taylor cone and jetting from liquid droplets in electrospinning of nanofibers. Journal of Applied Physics 2001;90(9):4836-4846.

[39] Yarin AL et al. Bending instability in electrospinning of nanofibers. Journal of Applied Physics 2001;89(5):3018-3026.

[40] Deitzel JM et al. The effect of processing variables on the morphology of electrospun nanofibers and textiles. Polymer 2001;42(1):261-272.

[41] Fong H et al. Beaded nanofibers formed during electrospinning. Polymer 1999;40(16):4585-4592.

[42] Zong XH et al. Structure and process relationship of electrospun bioabsorbable nanofiber membranes. Polymer 2002;43(16):4403-4412.

[43] Luong-Van E et al. Controlled release of heparin from poly(epsilon-caprolactone) electrospun fibers. Biomaterials 2006;27(9):2042-2050.

[44] Huang CB et al. Electrospun polymer nanofibres with small diameters. Nanotechnology 2006;17(6):1558-1563.

[45] Li D et al. Electrospinning of polymeric and ceramic nanofibers as uniaxially aligned arrays. Nano Letters 2003;3(8):1167-1171.

[46] Dersch R et al. Electrospun nanofibers: Internal structure and intrinsic orientation. Journal of Polymer Science Part A-Polymer Chemistry 2003;41(4):545-553.

[47] Teo WE et al. Electrospun fibre bundle made of aligned nanofibres over two fixed points. Nanotechnology 2005;16(9):1878-1884.

[48] Theron A et al. Electrostatic field-assisted alignment of electrospun nanofibres. Nanotechnology 2001;12(3):384-390.

[49] Katta P et al. Continuous electrospinning of aligned polymer nanofibers onto a wire drum collector. Nano Letters 2004;4(11):2215-2218.

[50] Sun ZC et al. Compound core-shell polymer nanofibers by co-electrospinning. Advanced Materials 2003;15(22):1929-+.

[51] Li D et al. Nanofibers of conjugated polymers prepared by electrospinning with a two-capillary spinneret. Advanced Materials 2004;16(22):2062-+.

[52] Zhang YZ et al. Coaxial electrospinning of (fluorescein isothiocyanate-conjugated bovine serum albumin)-encapsulated poly(epsilon-caprolactone) nanofibers for sustained release. Biomacromolecules 2006;7(4):1049-1057.

[53] Kidoaki S et al. Mesoscopic spatial designs of nano- and microfiber meshes for tissue-engineering matrix and scaffold based on newly devised multilayering and mixing electrospinning techniques. Biomaterials 2005;26(1):37-46.

[54] Ding B et al. Fabrication of blend biodegradable nanofibrous nonwoven mats via multi-jet electrospinning. Polymer 2004;45(6):1895-1902.

[55] Curtis AS et al. Reactions of cells to topography. J Biomater Sci Polym Ed 1998;9(12):1313-1329.

[56] Flemming RG et al. Effects of synthetic micro- and nano-structured surfaces on cell behavior. Biomaterials 1999;20(6):573-588.

[57] Dalby MJ et al. In vitro reaction of endothelial cells to polymer demixed nanotopography. Biomaterials 2002;23(14):2945-2954.

[58] Barbucci R et al. Micro and nano-structured surfaces. J Mater Sci Mater Med 2003;14(8):721-725.

[59] Dalby MJ et al. Use of nanotopography to study mechanotransduction in fibroblasts--methods and perspectives. Eur J Cell Biol 2004;83(4):159-169.

[60] Nishimura S et al. Three-dimensional architecture and distribution of collagen components in the goat hypophysis. Anat Rec A Discov Mol Cell Evol Biol 2004;277(2):275-286.

[61] Ojeda JL et al. Evidence of a new transitory extracellular structure within the developing rhombencephalic cavity. An ultrastructural and immunoelectron-microscopic study in the chick. Anat Embryol (Berl) 2000;202(3):257-264.

[62] Nishida T et al. The network structure of corneal fibroblasts in the rat as revealed by scanning electron microscopy. Invest Ophthalmol Vis Sci 1988;29(12):1887-1890.

[63] He W et al. Fabrication and endothelialization of collagen-blended biodegradable polymer nanofibers: potential vascular graft for blood vessel tissue engineering. Tissue Eng 2005;11(9-10):1574-1588.

[64] Li M et al. Electrospun protein fibers as matrices for tissue engineering. Biomaterials 2005;26(30):5999-6008.

[65] Ji Y et al. Electrospun three-dimensional hyaluronic acid nanofibrous scaffolds. Biomaterials 2006;27(20):3782-3792.

[66] Rho KS et al. Electrospinning of collagen nanofibers: effects on the behavior of normal human keratinocytes and early-stage wound healing. Biomaterials 2006;27(8):1452-1461.

[67] Chew SY et al. Sustained release of proteins from electrospun biodegradable fibers. Biomacromolecules 2005;6(4):2017-2024.

[68] Li C et al. Electrospun silk-BMP-2 scaffolds for bone tissue engineering. Biomaterials 2006;27(16):3115-3124.

[69] Liang DH et al. In vitro non-viral gene delivery with nanofibrous scaffolds. Nucleic Acids Research 2005;33(19):170.

[70] Ma ZW et al. Surface engineering of electrospun polyethylene terephthalate (PET) nanofibers towards development of a new material for blood vessel engineering. Biomaterials 2005;26(15):2527-2536.

[71] Ma ZW et al. Grafting of gelatin on electrospun poly(caprolactone) nanofibers to improve endothelial cell spreading and proliferation and to control cell orientation. Tissue Eng 2005;11(7-8):1149-1158.

[72] Robinette EJ et al. Synthesis of polymer-polymer nanocomposites using radiation grafting techniques. Nuclear Instruments & Methods in Physics Research Section B-Beam Interactions with Materials and Atoms 2005;236:216-222.

[73] Kim TG et al. Biomimicking extracellular matrix: cell adhesive RGD peptide modified electrospun poly(D,L-lactic-co-glycolic acid) nanofiber mesh. Tissue Eng 2006;12(2):221-233.

[74] Bismuth H et al. Orthotopic liver transplantation in fulminant and subfulminant hepatitis. The Paul Brousse experience. Ann Surg 1995;222(2):109-119.

[75] McCashland TM et al. The American experience with transplantation for acute liver failure. Semin Liver Dis 1996;16(4):427-433.

[76] Gridelli B et al. Strategies for making more organs available for transplantation. N Engl J Med 2000;343(6):404-410.

[77] Kaihara S et al. Tissue engineering: toward new solutions for transplantation and reconstructive surgery. Arch Surg 1999;134(11):1184-1188.

[78] Tzanakakis ES et al. Extracorporeal tissue engineered liver-assist devices. Annu Rev Biomed Eng 2000;2:607-632.

[79] Allen JW et al. Advances in bioartificial liver devices. Hepatology 2001;34(3):447-455.

[80] Allen JW et al. Engineering liver therapies for the future. Tissue Eng 2002;8(5):725-737.

[81] Chan C et al. Hepatic tissue engineering for adjunct and temporary liver support: critical technologies. Liver Transpl 2004;10(11):1331-1342.

[82] Dich J et al. Long-term culture of hepatocytes: effect of hormones on enzyme activities and metabolic capacity. Hepatology 1988;8(1):39-45.

[83] Waxman DJ. P450 gene induction by structurally diverse xenochemicals: central role of nuclear receptors CAR, PXR, and PPAR. Arch Biochem Biophys 1999;369(1):11-23.

[84] Liu J et al. Characterization and evaluation of detoxification functions of a nontumorigenic immortalized porcine hepatocyte cell line (HepLiu). Cell Transplant 1999;8(3):219-232.

[85] Kobayashi N et al. Establishment of a reversibly immortalized human hepatocyte cell line by using Cre/loxP site-specific recombination. Transplant Proc 2000;32(5):1121-1122.

[86] Roy P et al. Analysis of oxygen transport to hepatocytes in a flat-plate microchannel bioreactor. Ann Biomed Eng 2001;29(11):947-955.

[87] Bissell DM et al. Interactions of rat hepatocytes with type IV collagen, fibronectin and laminin matrices. Distinct matrix-controlled modes of attachment and spreading. Eur J Cell Biol 1986;40(1):72-78.

[88] Ben Ze'ev A et al. Cell-cell and cell-matrix interactions differentially regulate the expression of hepatic and cytoskeletal genes in primary cultures of rat hepatocytes. Proc Natl Acad Sci U S A 1988;85(7):2161-2165.

[89] Dunn JC et al. Long-term in vitro function of adult hepatocytes in a collagen sandwich configuration. Biotechnol Prog 1991;7(3):237-245.

[90] Hamilton GA et al. Regulation of cell morphology and cytochrome P450 expression in human hepatocytes by extracellular matrix and cell-cell interactions. Cell Tissue Res 2001;306(1):85-99.

[91] Vinken M et al. Rat hepatocyte cultures: collagen gel sandwich and immobilization cultures. Methods Mol Biol 2006;320:247-254.

[92] Carlisle ES et al. Enhancing hepatocyte adhesion by pulsed plasma deposition and polyethylene glycol coupling. Tissue Eng 2000;6(1):45-52.

[93] Chia SM et al. Hepatocyte encapsulation for enhanced cellular functions. Tissue Eng 2000;6(5):481-495.

[94] Yin C et al. Microcapsules with improved mechanical stability for hepatocyte culture. Biomaterials 2003;24(10):1771-1780.

[95] Bhatia SN et al. Effect of cell-cell interactions in preservation of cellular phenotype: cocultivation of hepatocytes and nonparenchymal cells. FASEB J 1999;13(14):1883-1900.

[96] Bhandari RN et al. Liver tissue engineering: a role for co-culture systems in modifying hepatocyte function and viability. Tissue Eng 2001;7(3):345-357.

[97] Lu HF et al. Three-dimensional co-culture of rat hepatocyte spheroids and NIH/3T3 fibroblasts enhances hepatocyte functional maintenance. Acta Biomater 2005;1(4):399-410.

[98] Peshwa MV et al. Mechanistics of formation and ultrastructural evaluation of hepatocyte spheroids. In Vitro Cell Dev Biol Anim 1996;32(4):197-203.

[99] Tzanakakis ES et al. The role of actin filaments and microtubules in hepatocyte spheroid self-assembly. Cell Motil Cytoskeleton 2001;48(3):175-189.

[100] Abu-Absi SF et al. Structural polarity and functional bile canaliculi in rat hepatocyte spheroids. Exp Cell Res 2002;274(1):56-67.

[101] Ma M et al. Biochemical and functional changes of rat liver spheroids during spheroid formation and maintenance in culture: I. morphological maturation and kinetic changes of energy metabolism, albumin synthesis, and activities of some enzymes. J Cell Biochem 2003;90(6):1166-1175.

[102] Landry J et al. Spheroidal aggregate culture of rat liver cells: histotypic reorganization, biomatrix deposition, and maintenance of functional activities. J Cell Biol 1985;101(3):914-923.

[103] Hodgkinson CP et al. Fibronectin-mediated hepatocyte shape change reprograms cytochrome P450 2C11 gene expression via an integrin-signaled induction of ribonuclease activity. Mol Pharmacol 2000;58(5):976-981.

[104] Lin KH et al. Long-term maintenance of liver-specific functions in three-dimensional culture of adult rat hepatocytes with a porous gelatin sponge support. Biotechnol Appl Biochem 1995;21 (Pt 1):19-27.

[105] Ijima H et al. Formation of a spherical multicellular aggregate (spheroid) of animal cells in the pores of polyurethane foam as a cell culture substratum and its application to a hybrid artificial liver. J Biomater Sci Polym Ed 1998;9(7):765-778.

[106] Powers MJ et al. A microfabricated array bioreactor for perfused 3D liver culture. Biotechnol Bioeng 2002;78(3):257-269.

[107] Mizumoto H et al. Liver regeneration using a hybrid artificial liver support system. Artif Organs 2004;28(1):53-57.

[108] Koide N et al. Formation of multicellular spheroids composed of adult rat hepatocytes in dishes with positively charged surfaces and under other nonadherent environments. Exp Cell Res 1990;186(2):227-235.

[109] Koide N et al. Continued high albumin production by multicellular spheroids of adult rat hepatocytes formed in the presence of liver-derived proteoglycans. Biochem Biophys Res Commun 1989;161(1):385-391.

[110] Yagi K et al. Rapid formation of multicellular spheroids of adult rat hepatocytes by rotation culture and their immobilization within calcium alginate. Artif Organs 1993;17(11):929-934.

[111] Sakai Y et al. Large-scale preparation and function of porcine hepatocyte spheroids. Int J Artif Organs 1996;19(5):294-301.

[112] Cho CS et al. Galactose-carrying polymers as extracellular matrices for liver tissue engineering. Biomaterials 2006;27(4):576-585.

[113] Cho CS et al. Effect of ligand orientation on hepatocyte attachment onto the poly(N-p-vinylbenzyl-o-beta-D-galactopyranosyl-D-gluconamide) as a model ligand of asialoglycoprotein. J Biomater Sci Polym Ed 1996;7(12):1097-1104.

[114] Gutsche AT et al. Engineering of a sugar-derivatized porous network for hepatocyte culture. Biomaterials 1996;17(3):387-393.

[115] Weigel PH et al. Specific adhesion of rat hepatocytes to beta-galactosides linked to polyacrylamide gels. J Biol Chem 1978;253(2):330-333.

[116] Griffith LG et al. Microdistribution of substratum-bound ligands affects cell function: hepatocyte spreading on PEO-tethered galactose. Biomaterials 1998;19(11-12):979-986.

[117] Chung TW et al. Preparation of alginate/galactosylated chitosan scaffold for hepatocyte attachment. Biomaterials 2002;23(14):2827-2834.

[118] Park TG. Perfusion culture of hepatocytes within galactose-derivatized biodegradable poly(lactide-co-glycolide) scaffolds prepared by gas foaming of effervescent salts. J Biomed Mater Res 2002;59(1):127-135.

[119] Yang J et al. Galactosylated alginate as a scaffold for hepatocytes entrapment. Biomaterials 2002;23(2):471-479.

[120] Yoon JJ et al. Surface immobilization of galactose onto aliphatic biodegradable polymers for hepatocyte culture. Biotechnol Bioeng 2002;78(1):1-10.

[121] Wen J et al. Preparation and characterization of poly(D,L-lactide-co-ethylene methyl phosphate). Polym Int 1998;47(4):503-509.

[122] Mao HQ. Biodegradable polyphosphoesters. In: Mathiowitz E, editor. Encyclopedia of Controlled Drug Delivery. New York, NY: Johns Wiley & Sons, Inc., 1999.

[123] Wen J et al. Poly(D,L-lactide-co-ethyl ethylene phosphate)s as new drug carriers. J Control Release 2003;92(1-2):39-48.

[124] Friend JR et al. Formation and characterization of hepatocyte spheroids. In: Morgan JR, Yarmush ML, editors. Tissue engineering methods and protocols. Totowa, NJ: Humana Press Inc., 1999: 245-252.

[125] Jauregui HO et al. Xenobiotic induction of P-450 PB-4 (IIB1) and P-450c (IA1) and associated monooxygenase activities in primary cultures of adult rat hepatocytes. Xenobiotica 1991;21(9):1091-1106.

[126] Hansen T et al. Cytochrome P450 enzyme activity and protein expression in primary porcine enterocyte and hepatocyte cultures. Xenobiotica 2000;30(1):27-46.

[127] Behnia K et al. Xenobiotic metabolism by cultured primary porcine hepatocytes. Tissue Eng 2000;6(5):467-479.

[128] Xu J et al. Characterisation of some cytotoxic endpoints using rat liver and HepG2 spheroids as in vitro models and their application in hepatotoxicity studies. II. Spheroid cell spreading inhibition as a new cytotoxic marker. Toxicol Appl Pharmacol 2003;189(2):112-119.

[129] Shimada T et al. Dose-response studies on the induction of liver cytochromes P4501A1 and 1B1 by polycyclic aromatic hydrocarbons in arylhydrocarbon-responsive C57BL/6J mice. Xenobiotica 2003;33(9):957-971.

[130] Chen XQ et al. Prediction of aqueous solubility of organic compounds using a quantitative structure-property relationship. J Pharm Sci 2002;91(8):1838-1852.

[131] Rytting E et al. Aqueous and cosolvent solubility data for drug-like organic compounds. AAPS J 2005;7(1):E78-E105.

[132] Emerson SG et al. In vitro expansion of hematopoietic cells for clinical application. Cancer Treat Res 1995;76:215-223.

[133] Alcorn MJ et al. Ex vivo expansion of haemopoietic progenitor cells. Blood Rev 1996;10(3):167-176.

[134] Collins PC et al. Ex vivo culture systems for hematopoietic cells. Curr Opin Biotechnol 1996;7(2):223-230.

[135] McAdams TA et al. Hematopoietic cell culture therapies (Part II): Clinical aspects and applications. Trends Biotechnol 1996;14(10):388-396.

[136] Bremers AJ et al. Immunology and immunotherapy of human cancer: present concepts and clinical developments. Crit Rev Oncol Hematol 2000;34(1):1-25.

[137] Noll T et al. Cultivation of hematopoietic stem and progenitor cells: biochemical engineering aspects. Adv Biochem Eng Biotechnol 2002;74:111-128.

[138] Bonnet D. Biology of human bone marrow stem cells. Clin Exp Med 2003;3(3):140-149.

[139] Robinson S et al. Ex vivo expansion of umbilical cord blood. Cytotherapy 2005;7(3):243-250.

[140] Takagi M. Cell processing engineering for ex-vivo expansion of hematopoietic cells. J Biosci Bioeng 2005;99(3):189-196.

[141] Migliaccio AR et al. Cell dose and speed of engraftment in placental/umbilical cord blood transplantation: graft progenitor cell content is a better predictor than nucleated cell quantity. Blood 2000;96(8):2717-2722.

[142] Eridani S et al. Cytokine effect on ex vivo expansion of haemopoietic stem cells from different human sources. Biotherapy 1998;11(4):291-296.

[143] Stewart DA et al. Factors predicting engraftment of autologous blood stem cells: CD34+ subsets inferior to the total CD34+ cell dose. Bone Marrow Transplant 1999;23(12):1237-1243.

[144] Wagner JE et al. Ex vivo expansion of umbilical cord blood hemopoietic stem and progenitor cells. Experimental Hematology 2004;32(5):412-413.

[145] Sorrentino BP. Clinical strategies for expansion of haematopoietic stem cells. Nature Reviews Immunology 2004;4(11):878-888.

[146] Holyoake TL et al. CD34+ positive haemopoietic cells: biology and clinical applications. Blood Rev 1994;8(2):113-124.

[147] Majdic O et al. Signaling and induction of enhanced cytoadhesiveness via the hematopoietic progenitor cell surface molecule CD34. Blood 1994;83(5):1226-1234.

[148] Healy L et al. The stem cell antigen CD34 functions as a regulator of hemopoietic cell adhesion. Proc Natl Acad Sci U S A 1995;92(26):12240-12244.

[149] Krause DS et al. CD34: structure, biology, and clinical utility. Blood 1996;87(1):1-13.

[150] Tada J et al. A common signaling pathway via Syk and Lyn tyrosine kinases generated from capping of the sialomucins CD34 and CD43 in immature hematopoietic cells. Blood 1999;93(11):3723-3735.

[151] Gratama JW et al. Flow cytometric enumeration and immunophenotyping of hematopoietic stem and progenitor cells. J Biol Regul Homeost Agents 2001;15(1):14-22.

[152] Lanza F et al. Structural and functional features of the CD34 antigen: an update. J Biol Regul Homeost Agents 2001;15(1):1-13.

[153] Prosper F et al. Regulation of hematopoiesis through adhesion receptors. J Leukoc Biol 2001;69(3):307-316.

[154] Drew E et al. CD34 and CD43 inhibit mast cell adhesion and are required for optimal mast cell reconstitution. Immunity 2005;22(1):43-57.

[155] Taussig DC et al. Hematopoietic stem cells express multiple myeloid markers: implications for the origin and targeted therapy of acute myeloid leukemia. Blood 2005;106(13):4086-4092.

[156] Tan PC et al. Na+/H+ Exchanger Regulatory Factor-1 Is a Hematopoietic Ligand for a Subset of the CD34 Family of Stem Cell Surface Proteins. Stem Cells 2006;24(5):1150-1161.

[157] Giebel B et al. Segregation of lipid raft markers including CD133 in polarized human hematopoietic stem and progenitor cells. Blood 2004;104(8):2332-2338.

[158] Goussetis E et al. In vitro identification of a cord blood CD133+CD34-Lin+ cell subset that gives rise to myeloid dendritic precursors. Stem Cells 2006;24(4):1137-1140.

[159] Bhatia M et al. A newly discovered class of human hematopoietic cells with SCID-repopulating activity. Nat Med 1998;4(9):1038-1045.

[160] Hogge DE et al. Enhanced detection, maintenance, and differentiation of primitive human hematopoietic cells in cultures containing murine fibroblasts engineered to produce human steel factor, interleukin-3, and granulocyte colony-stimulating factor. Blood 1996;88(10):3765-3773.

[161] Denning-Kendall P et al. Cobblestone area-forming cells in human cord blood are heterogeneous and differ from long-term culture-initiating cells. Stem Cells 2003;21(6):694-701.

[162] Fibbe WE et al. Ex vivo expansion and engraftment potential of cord blood-derived CD34+ cells in NOD/SCID mice. Ann N Y Acad Sci 2001;938:9-17.

[163] Lewis ID et al. Umbilical cord blood cells capable of engrafting in primary, secondary, and tertiary xenogeneic hosts are preserved after ex vivo culture in a noncontact system. Blood 2001;97(11):3441-3449.

[164] Dexter TM et al. Regulation of haemopoietic stem cell proliferation in long term bone marrow cultures. Biomedicine 1977;27(9-10):344-349.

[165] Thalmeier K et al. Establishment of two permanent human bone marrow stromal cell lines with long-term post irradiation feeder capacity. Blood 1994;83(7):1799-1807.

[166] Tsuji T et al. A murine stromal cell line promotes the expansion of CD34high+-primitive progenitor cells isolated from human umbilical cord blood in combination with human cytokines. Growth Factors 1999;16(3):225-240.

[167] da Silva CL et al. A human stromal-based serum-free culture system supports the ex vivo expansion/maintenance of bone marrow and cord blood hematopoietic stem/progenitor cells. Exp Hematol 2005;33(7):828-835.

[168] Breems DA et al. Stroma-conditioned media improve expansion of human primitive hematopoietic stem cells and progenitor cells. Leukemia 1997;11(1):142-150.

[169] Bhatia R et al. A clinically suitable ex vivo expansion culture system for LTC-IC and CFC using stroma-conditioned medium. Exp Hematol 1997;25(9):980-991.

[170] Verfaillie CM et al. Macrophage inflammatory protein 1 alpha, interleukin 3 and diffusible marrow stromal factors maintain human hematopoietic stem cells for at least eight weeks in vitro. J Exp Med 1994;179(2):643-649.

[171] Kadereit S et al. Expansion of LTC-ICs and maintenance of p21 and BCL-2 expression in cord blood CD34(+)/CD38(-) early progenitors cultured over human MSCs as a feeder layer. Stem Cells 2002;20(6):573-582.

[172] Baksh D et al. Adult human bone marrow-derived mesenchymal progenitor cells are capable of adhesion-independent survival and expansion. Exp Hematol 2003;31(8):723-732.

[173] Miller CL et al. Ex Vivo Expansion of Human and Murine Hematopoietic Stem Cells. In: Klug CA, Jordan CT, editors. Hematopoietic Stem Cell Protocols. Totowa, New Jersey: Humana Press Inc., 2002: 189-208.

[174] Brandt J et al. Role of c-kit ligand in the expansion of human hematopoietic progenitor cells. Blood 1992;79(3):634-641.

[175] Piacibello W et al. Extensive amplification and self-renewal of human primitive hematopoietic stem cells from cord blood. Blood 1997;89(8):2644-2653.

[176] Ohmizono Y et al. Thrombopoietin augments ex vivo expansion of human cord blood-derived hematopoietic progenitors in combination with stem cell factor and flt3 ligand. Leukemia 1997;11(4):524-530.

[177] Keil F et al. Effect of interleukin-3, stem cell factor and granulocyte-macrophage colony-stimulating factor on committed stem cells, long-term culture initiating cells and bone marrow stroma in a one-step long-term bone marrow culture. Ann Hematol 2000;79(5):243-248.

[178] Kawada H et al. Rapid ex vivo expansion of human umbilical cord hematopoietic progenitors using a novel culture system. Exp Hematol 1999;27(5):904-915.

[179] Li Y et al. Human cord cell hematopoiesis in three-dimensional nonwoven fibrous matrices: in vitro simulation of the marrow microenvironment. J Hematother Stem Cell Res 2001;10(3):355-368.

[180] Okamoto T et al. Effect of heparin addition on expansion of cord blood hematopoietic progenitor cells in three-dimensional coculture with stromal cells in nonwoven fabrics. J Artif Organs 2004;7(4):194-202.

[181] LaIuppa JA et al. Culture materials affect ex vivo expansion of hematopoietic progenitor cells. J Biomed Mater Res 1997;36(3):347-359.

[182] Rosenzweig M et al. Enhanced maintenance and retroviral transduction of primitive hematopoietic progenitor cells using a novel three-dimensional culture system. Gene Ther 1997;4(9):928-936.

[183] Astori G et al. Evaluation of ex vivo expansion and engraftment in NOD-SCID mice of umbilical cord blood CD34+ cells using the DIDECO 'Pluricell System'. Bone Marrow Transplant 2005;35(11):1101-1106.

[184] Jiang XS et al. Surface-immobilization of adhesion peptides on substrate for ex vivo expansion of cryopreserved umbilical cord blood CD34(+) cells. Biomaterials 2006;27(13):2723-2732.

[185] Feng Q et al. Expansion of engrafting human hematopoietic stem/progenitor cells in three-dimensional scaffolds with surface-immobilized fibronectin. J Biomed Mater Res A 2006. In press.

[186] Hann E et al. Development of a delivery system for the continuous endogenous release of an anti-idiotypic antibody against ovarian carcinoma. Hybridoma (Larchmt) 2005;24(3):133-140.

[187] Unger RE et al. Growth of human cells on polyethersulfone (PES) hollow fiber membranes. Biomaterials 2005;26(14):1877-1884.

[188] Yamagishi H et al. Development of A Novel Photochemical Technique for Modifying Poly(Arylsulfone) Ultrafiltration Membranes. Journal of Membrane Science 1995;105(3):237-247.

[189] Keselowsky BG et al. Surface chemistry modulates focal adhesion composition and signaling through changes in integrin binding. Biomaterials 2004;25(28):5947-5954.

[190] Kakabakos SE et al. Colorimetric determination of reactive solid-supported primary and secondary amino groups. Biomaterials 1994;15(4):289-297.

[191] Fujihara K et al. Guided bone regeneration membrane made of polycaprolactone / calcium carbonate composite nano-fibers. Biomaterials 2005;26(19):4139-4147.

[192] Bico J et al. Rough wetting. Europhysics Letters 2001;55(2):214-220.

[193] Wang R et al. Light-induced amphiphilic surfaces. Nature 1997;388(6641):431-432.

[194] Donaldson C et al. The CD34(+)CD38(neg) population is significantly increased in haemopoietic cell expansion cultures in serum-free compared to serum-replete conditions: dissociation of phenotype and function. Bone Marrow Transplant 2001;27(4):365-371.

[195] Wilson CJ et al. Mediation of biomaterial-cell interactions by adsorbed proteins: a review. Tissue Eng 2005;11(1-2):1-18.

[196] Calvi LM et al. Osteoblastic cells regulate the haematopoietic stem cell niche. Nature 2003;425(6960):841-846.

[197] Zhang J et al. Identification of the haematopoietic stem cell niche and control of the niche size. Nature 2003;425(6960):836-841.

[198] Wright DE et al. Physiological migration of hematopoietic stem and progenitor cells. Science 2001;294(5548):1933-1936.

[199] Bakowsky U et al. Cooperation between lateral ligand mobility and accessibility for receptor recognition in selectin-induced cell rolling. Biochemistry 2002;41(14):4704-4712.

[200] Houseman BT et al. The microenvironment of immobilized Arg-Gly-Asp peptides is an important determinant of cell adhesion. Biomaterials 2001;22(9):943-955.

[201] Francis K et al. Murine Sca-1(+)/Lin(-) cells and human KG1a cells exhibit multiple pseudopod morphologies during migration. Exp Hematol 2002;30(5):460-463.

[202] Williams JL et al. Thrombopoietin requires additional megakaryocyte-active cytokines for optimal ex vivo expansion of megakaryocyte precursor cells. Blood 1998;91(11):4118-4126.

[203] Piacibello W et al. Extensive amplification and self-renewal of human primitive hematopoietic stem cells from cord blood. Blood 1997;89(8):2644-2653.

[204] Gupta P et al. Stromal fibroblast heparan sulfate is required for cytokine-mediated ex vivo maintenance of human long-term culture-initiating cells. Blood 1996;87(8):3229-3236.

[205] Dao MA et al. Adhesion to fibronectin maintains regenerative capacity during ex vivo culture and transduction of human hematopoietic stem and progenitor cells. Blood 1998;92(12):4612-4621.